Crust-mantle boundary in eastern North America, from the (oldest) craton to the (youngest) rift.

Vadim Levin[1], Andrea Servali[1], Jill VanTongeren[1], William Menke[2], Fiona Darbyshire[3]

1. Department of Earth and Planetary Sciences, Rutgers University
610 Taylor Road, Piscataway, NJ, 08854-8066 USA
2. Department of Earth and Environmental Sciences, Columbia University
P.O. Box 1000, 61 Route 9W, Palisades, NY 10964-1000 USA
3. Geotop, Université du Québec à Montréal, C.P. 8888, Succ. Centre-Ville
Montréal, Qc, H3C 3P8

ABSTRACT

The North American continent consists of a set of Archean cratons, Proterozoic orogenic belts and a sequence of Phanerozoic accreted terranes. We present an ~1250 km long seismological profile that crosses the Superior craton, Grenville province, and Appalachian domains, with the goal of documenting the thickness, internal properties and the nature of the lower boundary of the North American crust using uniform procedures for data selection, preparation and analysis to ensure compatibility of the constraints we derive.

Crustal properties show systematic differences between the three major tectonic domains.

The Archean Superior Province is characterized by thin crust, sharp Moho and low values of Vp/Vs ratio. The Proterozoic Grenville Province has some crustal thickness variation, near-uniform values of Vp/Vs, and consistently small values of Moho width. Of the three tectonic domains in the region the Grenville Province has the thickest crust. Vp/Vs ratios are systematically higher than in the Superior Province. Within the Paleozoic Appalachian Orogen all parameters (crustal thickness, Moho width, Vp/Vs ratio) vary broadly over distances of 100 km or less, both across the strike and along it. Internal tectonic boundaries of the Appalachians do not appear to have clear signatures in crustal properties.

Of the three major tectonic boundaries crossed by our transect, two have clear manifestations in the crustal structure. The Grenville Front is associated with a change in crustal thickness and crustal composition (as reflected in Vp/Vs ratios). The Norumbega Fault Zone is at the apex of the regional thinning of the Appalachian crust. The Appalachian Front is not associated with a major change in crustal properties, rather it coincides with a zone of complex structure resulting from prior tectonic episodes, and thus presents a clear example of tectonic inheritance over successive Wilson Cycles.

1. INTRODUCTION

The overall chemistry and structure of the Earth's continental crust requires a complex, multistage process of formation (Rudnick and Gao, 2003). How that process operated over the course of Earth's history is still a matter of debate. Properties of the continental crust such as its vertical extent, the nature of its boundary with the underlying mantle, and the lateral variability in those parameters, are essential for informing the debate. In order to place better constraints on the formation, evolution, and growth of the continental crust, we have constructed a profile of seismological properties across eastern North America, stretching ~1250 km, from James Bay in central Quebec to the Fundy basin in New Brunswick (Figure 1).

The North American continent provides an ideal setting to probe Earth's crustal structure and composition in the context of nearly 3 Ga of geological history. The Superior Province of North America has not experienced major internal deformation for nearly 2.6 Ga, preserving crust that was last modified during the Archean. The oldest of the post-Archean terranes is the Grenville Province, formed at ~1 Ga and associated with the closure of an ocean basin and supercontinent assembly (Moore, 1986; Whitmeyer and Karlstrom, 2007; Hynes & Rivers, 2010). The Grenville Province contains accreted sections as well as reworked material from the Superior Craton and from Paleoproterozoic-age orogens. The Grenville Province separates the cratonic core of the continent from the younger (0.3−0.4 Ga) Appalachian terranes, which were accreted during the closure of the Iapetus ocean in the Paleozoic (Taylor, 1989; Hibbard et al, 2007). Our study crosses the Superior, Grenville and Appalachian domains. Its northwestern end is close to the area of the thickest lithosphere in North America (and globally, e.g. Artemieva, 2006) and some of the oldest rocks (3.8 Ga; David et al., 2009). The southeastern end of our transect is within the Fundy Basin formed during the opening of the Atlantic in the middle-late Triassic (Withjack et al., 1995).

The seismological profile presented here combines the lateral coverage of continent-scale studies with spatial resolution on the order of 10s of km. Uniform procedures used in data selection, preparation and analysis ensure compatibility of the constraints we derive for the thickness, internal properties and the nature of the lower boundary of the North American crust. Our primary objectives are to explore whether first-order properties of the continental crust have systematic differences for areas with significantly different age of consolidation (e.g., Thompson et al., 2010; Yuan, 2015), and to investigate the way tectonic boundaries seen at the surface extend to depth. The latter goal is facilitated by the denser spatial sampling of regions in the vicinity of the Grenville Front, the Appalachian Front, and the Norumbega Fault Zone, discussed in more detail below.

2. GEOLOGIC SETTING AND TECTONIC HISTORY

2.1 Tectonic units

2.1.1 The Superior Craton

The Superior craton is the largest of the Archean cratons (Card, 1990). It is made up of several distinct terranes with origin dates as early as 3.8 Ga (David et al., 2009). The northern and southern portions of the Superior craton are dominated by high grade gneisses, whereas the center of the craton is characterized by granite-greenstone and metasedimentary belts (Card, 1990). It is widely considered that the assembly of the

Superior craton from these distinctive cratonic blocks occurred mainly during 2.72 Ga and 2.68 Ga collisional events (Percival et al., 2007), though debate exists over the exact style and timing of these events. Amalgamation of the craton occurred by north-south compression and dextral transpression (Card, 1990) with younger terranes more common in the southernmost portions. The transect presented here constrains seismic properties of the La Grande terrane, the Opinaca subprovince, and the Abitibi granite-greenstone belt. In his comprehensive review of Superior craton geology, Card (1990) suggests that the final accretion of the craton occurred by "subduction-driven oblique accretion of oceanic and continental volcanic arcs, accretionary sedimentary wedges, older microcontinental fragments, etc. in a convergent margin setting". Such a scenario is similar to that proposed for the accretion of the Appalachians to the Laurentian margin approximately 2 billion years later (see below).

2.1.2 The Grenville Province

The Grenville Province exposes a region of intense tectonism associated with the assembly of the supercontinent Rodinia between 1.1 and 0.9 Ga. Surface exposures indicate peak metamorphism of metaigneous and metasedimentary units in the upper amphibolite to granulite facies (6 – 8 kbar; Annovitz and Essene, 1990). Assembly of Rodinia in this region began with accretion of island arc terranes during the Elseviran and Shawiningan Orogenies, followed by continent-continent collision during the later Grenville Orogeny (e.g., Rivers, 2015).

2.1.3 The Appalachians

During the lead up to the assembly of the supercontinent Pangea in the early Paleozoic, four distinct island arc terranes and continental fragments were accreted to the Laurentian margin in eastern North America (van Staal et al., 2009). These accretionary episodes (the Taconic, Salinic, Acadian, and Neoacadian orogenies) are now what define the present day Appalachians. In contrast to that observed throughout the Grenville Province, the majority of surface exposures in the Appalachians correspond to shallow crustal levels (e.g. limestones, shales, upper island arc crust) and are not deeply eroded remnants. Our transect crosses all but one of the classic northern Appalachian terranes: Humber, Dunnage, Gander and Avalon (Hibbard et al., 2007; van Staal et al., 2009).

2.1.4 Rifting of eastern North America

In the region covered by our study, in the Central Segment of the eastern North American rift system, the breakup of Pangea and opening of the Atlantic Ocean took place during the middle Jurassic to late Triassic. Rifting proceeded by a series of asymmetric half-grabens and basement-involved border faults (Withjack et al., 2012). The strike of border faults throughout the eastern North American rift system suggests that faulting was accommodated along previous suture zones associated with the prior orogenesis (Withjack et al., 2012).

2.2 Major tectonic boundaries

2.2.1 The Grenville Front

The continent-scale Grenville Front (GF) separates the exposure of the Archean Superior province from the Grenville Orogen (Irving et al., 1972; Moore, 1986). Initially believed to be the locus of the continent-continent collision, and thus a quintessential "continental suture" (Dewey and Burke, 1973), the GF has been later interpreted as a major contractional fault system (e.g., Rivers et al., 1989) acting on the former passive margin of the Archean-age continent. In some places the GF accommodates 10 km or more of vertical displacement resulting from northwest thrusting of Grenville Orogen rocks over the foreland to their present-day position (Rivers et al., 1989). Since the end of Mezoproterozoic (~1 Ga, Hynes and Rivers, 2010) there has been little tectonic activity on the GF. Seismic studies (e.g. Green et al., 1988; Martignole et al., 2000; White et al., 2000) showed the GF to extend through the middle crust, and in many reconstructions (Rivers et al., 1989; Ludden and Hynes, 2000; Hynes and Rivers, 2010) it is shown to cut the crust and sole into the Moho. Associations of the GF with systematic changes in seismic properties of the lithospheric upper mantle have been proposed by Aktas and Eaton (2006), Frederiksen et al. (2006), and Zhang and Frederikson (2013).

2.2.2 The Appalachian Front

The Appalachian Front (AF), a boundary between the Appalachians and the Grenville Province, follows the St. Lawrence river northeast of Quebec City (e.g., Tremblay et al., 2013). Historically referred to as Logan's Line (Alcock, 1945; Thomas, 2006), it is a clear case of tectonic inheritance (Thomas, 2006), as two episodes of rifting (one successful and one not), and a contractional tectonic front all took place broadly along this boundary. A locus of faulting associated with the opening of the Iapetus ocean in earliest Paleozoic time (Kumarapeli, 1985), and subsequently a northwestern-most reach of the Taconic nappes, the Appalachian Front (AF) is a good example of the mismatch between surface geology and deep crustal lithology as Grenville-age rocks are known to extend east of the AF (Hynes and Rivers, 2010).

2.2.3 Other boundaries

In addition to boundaries demarcating distinct terranes within it, the Appalachian Orogen hosts a number of more enigmatic structures with complex history. The Mesozoic-age St. Lawrence rift is nearly coincident with the AF. The St. Lawrence rift is a site of failed continental separation, and one of the most seismically active areas of Eastern North America (e.g. Lamontagne et al., 2003). Most of the seismicity is localized within a ~350 Ma old impact structure (the Charlevoix crater, Rondot, 1971), of which only the northwestern half exists at present, the rest having been destroyed during the formation of the Appalachians.

The Norumbega Fault Zone (NFZ) of coastal Maine (Figure 1) is a dextral shear zone approximately 40 km wide and over 400 km long with evidence of motion from mid-Paleozoic to Cretaceous time (Wang and Ludman, 2004; West and Roden-Tice, 2003). The NFZ has since been eroded down to mid-crustal depths (Ludman and West, 1999). In earlier reconstructions of the Appalachian terrane mosaic (e.g. Williams and Hatcher, 1982) the boundary between two major terranes, Gander(ia) and Avalon(ia), was traced along the NFZ, although most recent compilations (e.g. van Staal et al., 2009; Hibbard et al., 2007) draw this boundary offshore. As argued by Ludman (1986) the NFZ started as a suture between elements of the future Gander terrane, but subsequently acted as a transcurrent boundary, with possible modern analogs being the San Andreas, Anatolian or Denali faults.

3. DATA

We use publicly available data from continuously recording seismic observatories in the region (Figure 1), including long-term nodes of the Canadian POLARIS network and the Canadian National Seismic Network, permanent sites of the US Advanced National Seismic System, and temporary stations placed in the region by the Transportable Array (TA) of the Earthscope project. The key additional dataset comes from the Earthscope FlexArray operated by Levin, Menke and Darbyshire in Quebec and Maine from 2012 to 2015. These data are embargoed until the Fall of 2017. All data are stored and accessible via IRIS Data Management Center (ds.iris.edu).

The large and diverse set of observing instruments shares general characteristics, such as the broad-band sensitivity to the seismic signal (all sensors have uniform response up to 40 s period, most have uniform responses up to 100 s), recording at 40 samples per second or higher, and a large dynamic range. Some sites have been recording continuously for over a decade. The shortest observing periods in our dataset are those of the Earthscope TA sites that operated for 18-24 months.

We utilize three-component records of first-arriving compressional (P) waves from earthquakes at teleseismic distances (over 2000 km or 20°). The typical frequency range of the seismic records we use is between 5Hz and 0.05Hz, well within the recording parameters of our instruments. We use catalogs of global seismic activity to select time intervals of P, Pdiff, and PKP wave arrivals from earthquakes with magnitudes over 5.7 anywhere on Earth. Timeseries for these intervals from all sites in our combined array are visually inspected, and those with a recognizable earthquake signal present are selected. To increase the directional coverage and the overall number of observations, for some stations we also used clear observations of P waves from events with magnitudes between 5 and 5.7 at distances smaller than 50°.

4. METHODS

4.1 Receiver Function Analysis

We probe crustal properties using receiver function (RF) methodology (Ammon, 1991) that takes advantage of shear (S) waves present in the coda of first-arriving compressional (P) waves from distant earthquakes. Arriving within seconds after the onset of the P wave, these S wave have to originate near the point of observation. Both direct and multiply reflected phases are expected (Figure 2).

We use a multitaper spectral correlation variant of the RF technique that affords an exceptional resolution of higher frequency components within the converted-wave time series (Park and Levin, 2000). We are interested in the architecture of the crust, and thus restrict our attention to the P-to-SV (radial) component of the receiver function that is primarily sensitive to the isotropic properties of the medium (Levin and Park, 1997; Bostock 1998). We bin observed seismograms according to their epicentral distance and backazimuth, and construct bin-averaged RFs for directional and epicentral bins of chosen width. Details of the spectral-domain weighted stacking in the multitaper-correlation RFs are given in Park and Levin (2000) and Park and Levin (2016).   Park and Levin (2001) show the feasibility of using P waves from relatively small (10°-25°)

epicentral distances. However, sources at such distances form a small fraction of the data set we have assembled.

For each site, we produce RF gathers organized by backazimuth and epicentral distance (Figure 3ab), and use them to identify the phase most likely representing a conversion from the Moho. In choosing the target phase we use the following criteria, derived from the expected behavior of the P-to-S wave converted at a horizontal boundary (Cassidy, 1992): (1) We anticipate an increase in seismic velocity downward across the Moho, and thus we look for the prominent positive phase. (2) We require directional consistency of this phase (designated P_{mS}), in terms of both its appearance and its timing. (3) We also ensure that the target phase has a correct epicentral moveout (i.e., arrives earlier for more distant sources, Gurolla and Minster, (1998)). Inclusion of the relatively short epicentral distances is especially helpful for the last criterion.

Figure 3 shows an example of a near-ideal wavefield for the northernmost site of our array (WEMQ). For the backazimuth gather (Figure 3A) individual records falling within a 20° backazimuth bin are combined into a common RF. Bins are set up with 50% overlap so that each earthquake observed influences two adjacent bins. All bins with 2 or more events recorded are shown. We have the least amount of data from the East (Figure 3C), and the arrangement of backazimuths (starting from 90° rather then 0°) improves the apparent continuity of the presented wavefield pattern. At WEMQ we see a positive converted phase at ~4.5 s delay. It is observed from all directions, and has a nearly-constant timing (Figure 3A). Most of the changes that do appear for different directions are within a range expected given the variability of the source distances. The omni-directional epicentral gather (Figure 3B) documents its proper moveout, and also shows likely multiple phases at times 12-16 s.

4.2 Measure of the Moho Width

We are interested in the details of the change in seismic properties at the crust-mantle transition (Moho). To investigate them we construct receiver function time series with different frequency content (Figure 4A), and examine resulting pulse shapes of the P_ms phases. As shown by Bostock (1999), P_{mS} phases will have significant amplitude when the vertical extent of a smooth velocity gradient is smaller than the wavelength of the incident P wave. For a case of a thin layer bound by two sharp boundaries, Levin et al. (2016) show that individual conversions from the top and the bottom may be distinguished if the vertical distance between them is larger than $M = \frac{\lambda_S}{4}\left(\frac{k}{k-1}\right)$, where k = Vp/Vs, and λ_S is the wavelength of the P_{mS} phase. For a typical crustal value of k=1.75 this relationship yields M=0.58λ_S, meaning that boundaries separated by a distance less than M cannot be distinguished from a single abrupt (sharp) contrast in seismic properties.

To avoid distortions of the P_{mS} pulse from differences in incidence angle and/or small-scale lateral changes of the near-surface structure beneath the site we construct RF time series for a group of sources with very similar epicentral distance and backazimuth values (Figure 3C). The resulting RFs do not require additional processing as all rays included have near-identical incidence parameters. Examination of the data set showed that earthquake sources in Central America (backazimuth ~200°SE, epicentral distance 30°-40°; Figure 3C) yield especially good results. Using the same source region for all sites in the ~1250 km long array provides an extra level of consistency in the resulting time series, and makes comparisons between sites more straightforward. RF time series for the Central American group of earthquakes are constructed for a set of maximum frequencies (Figure 4A), representing different wavelengths of P_{mS} waves. Our data make it possible to construct such RF beams up to 3 Hz.

A visual inspection of the frequency-dependent RF time series leads to a choice of the highest frequency where the shape of the P_{mS} pulse is still "simple": the pulse shape resembles a Gaussian, and there is a single peak. As discussed above, we assume that the departure from the simple shape takes place when the vertical extent of the crust-mantle transition is commensurate with the wavelength of the corresponding P_{mS} phase. This wavelength provides a measure of the Moho width for a chosen site.

4.3 Average crustal properties: seismic velocity and thickness

The delay time of the P_{mS} wave provides a measure of the depth to the Moho. Experience with synthetic P-to-S converted waves (e.g., Cassidy, 1992; Levin and Park, 1997) suggests that in band-limited time series the delay from a specific boundary corresponds to a peak of the P_{mS} pulse. For known crust-averaged values of P and S wave speeds, the Moho depth may be estimated as $h = \frac{t}{\left(\sqrt{\frac{1}{V_s{}^2} - p^2} - \sqrt{\frac{1}{V_p{}^2} - p^2}\right)}$, where *t* is the delay of the P_ms phase, Vp and Vs are velocities of P and S waves, and *p* is the ray parameter. We take *t* to be the time of the peak in the "simple" P_{mS} phase in the highest frequency RF time series. For earthquakes at epicentral distances 30° – 40° the value of *p* is ~0.07 s/km.

Tesauro et al. (2014) present a detailed Vp model for the crust of the North American continent. We have interpolated their 1°x1° grid of crust-averaged values in our region (Supplementary Figure 1) and sampled the resulting distribution at the locations of our sites. In the region crossed by our array, Vp values range from 6.45 to 6.55 km/s. In all subsequent analyses we adopt a value of Vp=6.5 km/s.

To determine crust-averaged Vs values, we employ an H-*k* stack algorithm (Zhu and Kanamori, 2000) that assumes the crust to be a uniform layer of thickness H with constant Vp and Vs values, and takes advantage of the differences in epicentral distance moveout curves for direct and multiply-reflected P-to-S converted waves (Figure 2). The essence of the method is in selecting a combination of the crustal thickness H and wavespeed ratio *k*=Vp/Vs that would best predict the timing of both direct and multiply reflected waves. A successful combination should yield a large positive value in the stack. Figure 4b shows examples of such analysis applied to the omni-directional epicentral RF gathers. All combinations of H and *k* falling into a dark-shaded region yield acceptable matches for the observed wavefield. The best match is marked, and the outline of the area within 5% of the maximum stack value is shown, offering an estimate of the likely uncertainty in the result of the search.

Values of shear wave speed corresponding to the maximum in the H-*k* stack surface are used to evaluate the wavelength of the highest-frequency P_{mS} phase necessary for the analyses of Moho thickness. Together with Vp=6.5 km/s these values are used to compute crustal thickness on the basis of the time *t* corresponding to the peak of the highest frequency P_{mS} phase.

For site WEMQ, these estimates are: crustal thickness from the H-*k* stack 39 km, Vs = 3.77 km/s; delay of the P_{mS} phase at the highest frequency 4.5 s; thickness estimate using the P_{mS} delay *h* = 37.77 km; highest frequency *f*=3 Hz; shortest wavelength λ = Vs/f=1.26 km; Moho width using a formula from Levin et al. (2016) is M~0.75 km. For site D60A, the estimates are: Vs = 3.57 km/s, H= 41.5 km, *h*=45.38 km, *f*=0.5 Hz, λ = 7.14 km, M~3.95 km.

Two estimates of crustal thickness, *H* and *h*, differ in the amount of data included in them, and consequently in the volume of the crust that they represent. The H-*k* stack measure is based on the analysis of the full RF wavefield. An assumption inherent for this measure is that the crust is an infinite uniform layer with a horizontal boundary. Consequently, we construct an omni-directional epicentral gather of all RFs (e.g., Figure 3B), and search for H and *k* values that would best predict positions of positive and negative pulses within it. To insure stability of the stacking procedure, the frequency range of RFs used in this analysis is relatively low, up to 0.5Hz. Because of the directional averaging, the H-k stack measure represents a sample of the crust-mantle boundary depth in a cone circumscribed by all incoming waves. For typical values of incidence angles of direct P-to-S converted waves (Figure 2) this area is approximately

30 km in diameter when the crustal thickness is on the order of 35 km, and larger for thicker crust. Multiply-reflected waves included in the H-k stack sample a region approximately twice as wide. Significantly, the stacking procedure is not guided to recognize specific phases in the RF wave field, treating all values as meaningful. As we will discuss in the following section, RF wavefields may be quite complex, with additional phases present in the time interval searched the H-*k* stack algorithm. This inevitably leads to broad ranges of *k* values yielding very similar solutions.

The crustal thickness measure *h* using a narrow beam of RFs for a chosen direction samples an area of the crust-mantle boundary a few km across. The use of the same earthquake source region for all estimates using the P_{mS} phase ensures that results are compatible between different locations along our transect. This measure also assumes the crust to be uniform in properties, although the assumption only needs to be true along the RF beam. The estimate of the P_{mS} phase timing is done using the highest frequency of the RF beam that displays a pulse with the shape expected from a simple boundary. In most cases this frequency is much higher than the 0.5Hz used in the H-*k* stack analysis, and consequently the positioning of the peak of the P_{mS} pulse is clearer (e.g., Figure 4A, sites WEMQ and DMCQ). The P_{mS} estimate of crustal thickness relies on the value of Vp/Vs obtained using the H-k stack, and thus in cases where *k* is poorly constrained by the H-*k* stack method, the P_{mS} based estimate is also less reliable. Such instances are discussed individually in the following sections.

4.4 Glossary of crustal parameters

Vp, Vs – average velocities of P wave and S wave in the crust;

H – an estimate of the crustal thickness based on the stacking of direct and multiply-reflected P-to-S converted waves;

k – an estimate of the Vp/Vs ratio based on the stacking of direct and multiply-reflected P-to-S converted waves;

h – an estimate of the crustal thickness based on the delay time of the P-to-S converted wave P_{mS} and average crustal velocities Vp and Vs;

t - the value of the delay time is measured from the hjghest frequency receiver functions preserving a simple shape of the P_{mS} phase.

M – Moho width, the vertical distance over which values of seismic velocities change at that bottom of the crust.

5. RESULTS

We present a summary of our results in Figure 5, in the form of a composite transect projected onto a line with end points at 79W, 52N and 65.285W, 44.633N. The line is chosen to coincide with the trace of our array where it crosses the Grenville Province, to pass through the Charlevoix region of intense seismic activity in and close to St. Lawrence River, and to be as perpendicular as possible to major tectonic boundaries in the region, such as the Appalachian Front and the Grenville Front (Figure 1). Arguably, our transect traces the shortest path from the oldest rocks in the core of the North American craton to the region of the most recent deformation in the Fundy Basin. Our sites are within ~200 km of the transect trace, resulting in a 400 km wide swath through the continent. All values used to produce Figure 5 are presented in Table 1.

5.1 Crustal Thickness.

Averaged over the length of the profile, our estimates of crustal thickness using the H-*k* stacking technique yield 37.1+/-2 km, while estimates using picked delay times of P_{mS} phases have an average of 37.0+/-4.6 km. This is very close to 38.3+/-2 km value we obtain by averaging values sampled from the database of Tesauro et al. (2014).

5.1.1 Grenville Front

An increase in crustal thickness relative to the near-constant thickness of the Archean (Levin et al., 2016) and Proterozoic crust is seen on both sides of the GF (Figure 5). From north to south, an abrupt thickening of the crust at the GF is followed by a gradual decrease over a distance of ~150 km (Figure 6). Figure 7 illustrates datasets from three locations adjacent to the GF. An increase in P_{mS} phase delay in excess of 1.5 s takes place between sites QM70 (north of GF, delay of 4 s) and QM66 (very close to the trace of GF, delay of 5.6 s). Delay of 5.3 s is seen at site QM62 south of the GF. All delay values reported here are measured for the chosen highest frequency RF bin (see Methods). At site QM70 an additional positive phase at ~8 s is present, suggesting an additional deeper boundary with strong velocity contrast. Estimates of the crustal thickness are 34.98, 38.9 and 43.78 km for sites QM70, QM66, QM62, respectively. We note that the constraints on the value of *k* are especially weak at site QM66, with nearly all values searched yielding comparable level of “fit”. This is likely due to the poor excitation of crustal multiples that are a key ingredient in the H-*k* stack. In contrast, at site QM70 multiply reflected P-to-S converted waves may be clearly seen at delays ~13 s (Figure 7), and yield a stable estimate of *k*. If we choose *k*=1.75 instead of *k*=1.88 for site QM66, the estimate of crustal thickness increases to 45.5 km. This estimate would be more consistent with this site having the largest value of P_{mS} phase delay in this part of the transect.

5.1.2 ***Appalachian Front***

The area adjacent to the AF shows a regional increase in the mean crustal thickness. Averaging Moho depth values falling within ~100 km on either side of the AF (between coordinates 700 and 900 km on our transect, Figure 8), we get crustal thickness estimates of 41.44+/3.9 from H-*k* stacks, and 41.21 +/-4.3 from P_{mS} delay times. An average of values extracted from Tesauro et al. (2014) for the corresponding sites is 39 +/- 0.7 km.

Resonances in unconsolidated sediments like those filling parts of the St. Lawrence River valley tend to produce reverberations in RFs (Cassidy, 1992) that complicate their interpretation. Fortunately, sites we use to develop crustal structure constraints in the vicinity of the AF do not display these characteristic features (Figures 9, 10, and Supplement).

Figure 9 shows examples of H-k stacking surfaces and waveforms for two long-running seismic sites on the northern and southern banks of St. Lawrence River (and thus on the opposite sides of the AF). Both sites show evidence for additional structures in the uppermost mantle lithosphere. Site A64 on the northern shore (and thus within the Grenville Province) has a P_{mS} delay of 5.2 s (Figure 9). Combined with the well-constrained low value of *k*=1.71, this results in a crustal thickness estimate of 44.36 km. An additional positive phase at ~8 s implies a presence of another converting boundary

15-20 km beneath the Moho (60-65 km total depth). At site A21 within the Appalachian Orogen the value of P_{mS} delay is larger (5.4 s) while the estimate of the crustal thickness is smaller (37.5 km) due to a very high preferred value of k=1.88. Figure 9 shows that this estimate is not very tight. If k=1.78 (at the lower end of the 5% contour) is chosen for the crustal thickness calculation, we get H=44 km and h=41.75 km. Site A21 also has clear converted phases, positive and negative, at delay times 8-10 s, implying complex structure of the uppermost mantle.

While at most sites close to the AF our estimates of crustal thickness approach (or exceed) 40 km, two sites yield very small estimates of crustal thickness (Figure 8). At site A61, on the northern shore of the St. Lawrence River, RF waveforms are complex, and H-k stacking result is poorly constrained. P_{mS} delay value of 5 s was chosen. It is the weaker of the two positive pulses (Figure 10), selected for the proper sense of moveout it displays. It is, however, followed closely by a more energetic pulse at ~6 s, which likely dominates the H-k stack. Consequently, crustal thickness estimates based on the H-k stack (42 km) and the P_{mS} delay (34.5 km) diverge considerably. On the other hand, site E60A displays a simpler wavefield and a well-constrained H-k stack. An estimate of thin crust, H= 32.5 and h=33.3 km, is thus reliable even though this site is an exception for the broad region on both sides of the AF. Notably, this site is near the limit (~200 km) of inclusion into the transect, and thus exemplifies along-strike variability in complex tectonic units crossed by it.

5.1.3 *Eastern Maine*

An area with exceptionally small crustal thickness is observed in eastern Maine, between coordinates 1010 and 1130 of the transect (Figure 11). Average values obtained in this section of the transect are 32.2 +/-1.3 km from the H-*k* stacks, and 31.6 +/- 1.8 km using P_{mS} delays. For comparison, the average of values sampled from the much more widely spaced grid nodes of Tesauro et al. (2014) are 39.21+/-2.6 km. In Figure 12 we present representative examples of H-*k* stacks and waveforms for sites within this region, QM16 and G64A, that both have thin crust, and also site QM10 where crustal thickness is closer to the regional average. Site QM16 shows clear evidence for thin crust. While the number of records available at this temporary seismic site is relatively small, the H-*k* stack result is very well constrained, yielding a crustal thickness value of 31 km. The P_{mS} delay of 3.8 s yields crustal thickness estimate of 31.9 km. Similarly, site QM10 shows a very well-constrained H-*k* stack result, with a crustal thickness estimate of 34 km. A P_{mS} delay of 4.2 s results in crustal thickness estimate of 34.7 km. Sites QM16 and QM10 have near-identical best-fitting values of *k* (Figure 12), thus the change in P_{mS} delay value likely reflects true change in crustal thickness. Site G64A presents a more complicated wavefield, and its H-*k* stack pattern is less well constrained. There appear to be two patches of near-identical high values on it. The automatically determined best fitting combination is H=26.5 km, *k*=1.89. Inspection of the H-*k* diagram (Figure 12) suggests that values of *k* in 1.7 - 1.8 range offer data fits that are nearly as good. Establishing a maximum value of H-*k* stack for this range yields a combination H=32, *k*=1.76 that is more consistent with findings at other nearby sites. A P_{mS} delay value of 3.8 s results in a crustal thickness estimate of 30.51 km. RF waveforms at site G64A contain a clear positive pulse at ~11 s that likely causes a disruption of the H-*k* stack pattern. The moveout of this pulse in the epicentral RF gather (Figure 12) is consistent with it being a direct converted phase from an interface in the upper mantle.

5.1.4 Differences between H-k stack crustal thickness and P_{mS} crustal thickness

In our dataset and analysis, the values of *h* and H are almost always different. This is expected as the H obtained by the H-*k* stack method represents a broader spatial average than *h* obtained from the P_{mS} value (see Methods section). However, in most cases the difference is within 2 km, and likely reflects the natural uncertainty of these relatively simplistic measures. In instances where H and *h* estimates agree, we suggest that the similarity is a qualitative measure of simplicity of the crustal structure. Conversely, instances where these values diverge signify crustal and/or upper mantle complexity. Site CHGQ next to the GF is a good example of significant crustal heterogeneity implied by the divergence of H and *h* (Figure 6). The H-*k* stack yields a rather unsurprising value of 35 km. However (as discussed in considerable detail in Levin et al., 2016) there is more than one candidate for the P_{mS} pulse in the RF wavefield, and choosing the pulse at 3.5 s delay yields *h*=29 km.

Over the course of our transect we find no systematic relationship between the difference in H and *h* and any of the other parameters we have constrained (such as Moho width, *k*), or the tectonic unit. This local nature of complexity reflected in the occasional divergence of simple measures of crustal thickness offers a cautionary note, especially for the extensively used H-*k* stacking method. Consequently, the summary map showing all crustal thickness values along the transect (Figure 14) depicts *h*. We believe it to be a more reliable indicator of lateral changes in crustal thickness.

5.2 Vp/Vs ratio

A vast majority of sites yields estimates of Vp/Vs ratio (*k)* that fall between 1.7 and 1.8 (Figures 5, 15). Averaging over the entire data set, we obtain *k*=1.77+/-0.06. A number of solitary outliers are seen, as well as a region of consistently elevated values in the vicinity of the AF.

Within the Superior Province two prominent outliers are sites QM66 and MATQ. Both display H-*k* stack patterns that allow a broad range of values for *k* that would yield similarly good fits to the waveforms (see Figure 7 for QM66 data). Similarly, site QM39 in the Grenville province, and sites QM34 and QM31 in the Appalachian Orogen (see Table 1) have high values of *k* chosen by the algorithm out of a broad range of nearly-identical data fit results.

In the vicinity of the AF we also find a number of sites with high, but poorly constrained *k* values, such as A61 (Figure 10). Better-constrained results are seen at A21 on the southern shore of St. Lawrence (Figure 9). Site A54 across the river from it has a very similar pattern. However, in both cases, the range of *k* values within 5% of the maximum is quite broad, and reaches transect-average value of 1.77.

A number of sites display error surfaces that suggest bi-modal distributions of preferred H-*k* combinations. Figure 13 shows data for two such sites. In both cases there are two regions with stack value within 5% of absolute maximum. RF wave fields are complex, especially at site A11 where, like at all other St. Lawrence River sites, deeper interfaces in the upper mantle are likely. The choice of the best-fitting H-*k* combination is likely influenced by these additional signals, and ends up being very low (1.70) at A11, and relatively high (1.86) at QM36. Error surfaces suggest, however, that alternative choices are possible for both sites.

One location where the high value of *k* appears to be required by the data is site E60A (Figure 10) where the RF wavefield is simpler, and the shape of the H-*k* stack surface suggests good constraints on the preferred value. This site, however, is unique in the region, and is located nearly 200 km off of our transect line.

5.3 Moho Width

An estimate of the vertical extent of Moho width on the basis of the wavelength of PmS phases depends on both the frequency of the pulse and the value of *k*. Given the range of plausible values for *k*, the wavelength influence dominates. A choice of the wavelength is done on the basis of inspection of frequency-dependent RF beams. As discussed in the Methods section, we seek the highest frequency for which the appearance of the P_{mS} pulse still resembles a converted wave from a single boundary. Figure 4A illustrates the range of observations. In the ideal data set from site WEMQ within the Superior Province we observe a progressive narrowing of the pulse for each successive increase in frequency, and choose the highest frequency our data contain, 3 Hz. Most locations in the Superior Province show similar results, yielding estimates of the Moho width not exceeding 1.5 km (Levin et al., 2016). One exception is the area just north of the GF.

A major change takes place within the Grenville Province, a short distance north of the St. Lawrence River (Figure 6). A large fraction of sites in the southern half of our transect have estimates of the Moho width in the 3 – 4.5 km range. This is due to observed complexity of P_{mS} pulses at high frequencies, which makes it necessary to choose longer wavelength for estimating the width of the Moho. Figure 4a shows examples of choices made for sites with different degree of complexity in the P_{mS} pulse.

Figure 14 shows estimates of crustal thickness and Moho width on a map of the region. There is no obvious correlation between crustal thickness and Moho width in our dataset. There is, however, a strong trend of increasingly variable Moho width with distance away from the Superior Craton (Figure 6, and discussion below).

5.4 Summary of key results

- We find locally thickened crust beneath the GF (Figure 6), a region of complex crust and upper mantle on both sides of the AF (Figure 8), and a region of significantly thinned crust in eastern Maine (Figure 11).

- Throughout the region the ratio of compressional and shear wave speeds *k* largely stays within the range 1.71 to 1.83 (Figures 5, 15). Close inspection of locations where it exceeds 1.85 reveals broad ranges of acceptable *k* values at most of them, making this value less reliable.

- Superior and Grenville Provinces have uniformly small values of Moho width, mostly less than 1.5 km (Figures 5, 14). The few exceptions include regions of intense tectonism: the GF, and the St. Lawrence rift. Within the Appalachian

Orogen, the Moho width varies considerably. While instances of sub-km Moho boundary are present, many sites show much wider transitions, up to 4.5 km.

- In a number of locations, especially close to the boundaries of major tectonic domains (GF, AF) we find compelling evidence for discontinuities in seismic properties that reside below the one that we interpret as the crust-mantle boundary (Figures 6, 8). Commonly observed within the lithospheric upper mantle of Earth's continents, these features likely reflect its complex history.

6. DISCUSSION

6.1 Comparison of our results with other estimates of crustal thickness in the region

6.1.1 Match and mismatch with Tesauro et al. (2014)

We used the continent-wide compilation of Tesauro et al. (2014) as a reference for the value of Vp in our region. To compare the crustal thickness estimates we have obtained with those contained in the 1°x1° grid of Tesauro et al., (2014), we interpolated the values and sampled the resulting surface (Supplementary Figure 1, Table 1) at locations of our sites. Perhaps unsurprisingly, we find significant differences between our estimates of crustal thickness and the interpolated values of Tesauro et al. (2014). We also found a number of locations where our results match well.

In the central Superior Province, our estimates of crustal thickness are considerably smaller, while in the southern part (250-400 km along the profile, Figures 5,

6) our estimates and those of Tesauro et al. (2014) are similar. South of the GF, where we document a local thickening of the crust, our results diverge again. In most locations where we have reliable results in the vicinity of the St. Lawrence river our estimates of the crustal thickness differ from Tesauro et al. (2014). Finally, almost all sites in the Appalachians have crustal estimates considerably smaller (up to 8 km) than those in the Tesauro et al. (2014) compilation.

The differences we see are expected, as the values in a Tesauro et al. (2014) database are compiled from studies using P waves in the crust and the upper mantle immediately beneath it. Most of the observations used are from central and western parts of the North American continent, and their extrapolation into eastern North America is performed on the basis of similarity between tectonic units. Notably, there are data points in Tesauro et al. (2014) for the southern Superior Province region crossed by our profile, and the agreement with our results is best here.

The disagreement in crustal thickness values raises the question of the viability of using Vp estimates from Tesauro et al. (2014) as the basis for our own measurements. However, the value we adopt (Vp=6.5 km/s) is a commonly assumed average continental crust value, similar to a global average (Vp=6.45, Christensen and Mooney, 1995). Levin et al. (2016) document tests of the influence of significantly larger and smaller values of Vp on the outcomes of H-*k* stacking analysis. Changes in Vp on the order of 5% (e.g., from 6.5 km/s to 6.2 km/s for the whole crust) result in systematic changes to H on the order of 2 km. Changes in *k* are less systematic, and range from negligible to ~0.02 (e.g., from 1.75 to 1.73).

6.1.2 Other studies employing the **H-*k*** *method*

Some of the sites examined in this study are included in the Earthscope Automated Receiver Survey (EARS, IRIS DMC (2010)), a routine data analysis product that uses a version of the H-*k* stack algorithm (Crotwell and Owens, 2005). Two sites (MATQ and CHGQ) are in the Superior Province, while the rest are in the southernmost Grenville Province around the St. Lawrence River, and in the Appalachians. With few exceptions, our results on the crustal thickness agree with those in the EARS database to within 3 km. Given the likely tradeoffs associated with choices of Vp (a uniform value in our study, a site-specific value in EARS) we feel that this is an expected level of mismatch. A few sites show crustal thickness differences in excess of 10 km. All of them are close to the St. Lawrence River, an area where we see highly complex RF wave fields. Another site with a mismatch of 8 km is on the shore of the Fundy Basin. Similarly, most sites where comparisons are possible have values of *k* that match to within 0.05. Exceptions once again include sites next to St. Lawrence River, and also site MATQ in the Superior Province (Figure 6) where our result is highly uncertain.

A study by Thompson et al., (2015) using another variant of the H-*k* methodology included three sites we have investigated (WEMQ, MATQ and CHGQ, Figure 6). Near-identical results were obtained at WEMQ and MATQ, while for site CHGQ, where we noted considerable complexity in the RF wavefield, Thompson et al. (2015) find a significantly higher value of *k.*

Finally, a recent study by Petrescu et al. (2016) included a limited subset of data used here, and also employed a variant of the H-*k* stack method to probe average crustal properties. Comparing the values for all locations where Petrescu et al. (2016) had more than 20 records in their analysis, we find very similar results everywhere except at site MATQ in the Superior Province and site A64 on the shore of the St. Lawrence River. In both instances, Petrescu et al. (2016) report ~3 km thicker crust, and smaller values of *k*.

6.2 Variability of Moho Width

Based on a subset of the data used here, Levin et al. (2016) noted that all stations within the Superior Craton display uniformly sharp (<1.5 km vertical thickness) Moho transitions regardless of the age of the tectonic terrane or the surface lithology. In the significantly expanded dataset presented here, we observe a similar "baseline" Moho width of less than 1.5 km throughout all tectonic regimes investigated (Superior Province, Grenville Province, and Appalachians), however, there is significantly more variability within the Appalachian terranes as compared with the others (Figures 5, 14, 16). Below we highlight two regions where Moho width is seen to deviate significantly from the <1.5 km baseline value: at the Grenville Front and throughout the Appalachians.

6.2.1 The Grenville Front

As noted above, the 1.1 – 0.9 Ga Grenville orogeny is considered to be a period of intense mountain building and deformation due to continent-continent collision, similar to that of the modern-day Himalaya. Despite this tectonic history and surface exposure, there is only a small, laterally restricted, cluster of stations that display slightly more diffuse Moho boundaries, up to 2.5 km thick (Figures 5, 6) immediately adjacent to the Grenville Front in both the Superior Craton and within the parautocthonous Grenville terranes. Away from this small region, Moho width returns to the baseline of <1.5 km throughout the remainder of the Grenville Province, despite the larger mean crustal thickness (as described above).

There are two potential causes for this small, laterally-restricted, perturbation of the Moho boundary at the Grenville Front:

(1) The accretionary style of the Grenville orogeny. While the Grenville Front was previously suggested to be a vertical tectonic suture (e.g. Dewey and Burke, 1973), there is considerable evidence that the parautochthonous and allochthonous terranes of the Grenville Province may have been thrust at low angle on top of the existing passive margin of the Superior Craton (see Rivers et al., 2015 for a detailed discussion). In this case, the Moho boundary may not be indigenous to the Grenville, but is rather the Archean-age Moho of the pre-existing lithosphere. As such, it would not be expected to have a radically different signature from that of the Superior Craton to the northwest.

The small perturbation of ~+1.0 km in Moho thickness at the Grenville Front may be due to the transition from thin Superior Craton crust (average ~35 km) to the relatively thicker crust in the Grenville Province (average ~40 km). The Moho at this transition between thinner and thicker crust may be more diffuse due to lithospheric flow or tectonic suturing at this boundary.

(2) An additional explanation of the smaller-than-expected perturbation in Moho width at the Grenville Front may lie in its age. The uniform crustal thickness and sharp Moho transition seen throughout the data from the Superior Craton led Levin et al. (2016)

to conclude that the lower crust and lithosphere of the Superior Craton had experienced some degree of delamination and/or reorganization after amalgamation of the craton from numerous continental fragments (terranes). Levin et al. (2016) suggested that the high mantle potential temperatures (and therefore Moho and ambient mantle lithosphere temperature) present during the Archean significantly reduced the viscosity of the crust and lithosphere allowing for efficient reorganization to occur.

In the case of the 1.1-0.9 Ga Grenville orogeny, however, mantle potential temperatures are estimated to have been only 100-150°C hotter than the modern day, as compared with ~250°C in the Archean. It is possible that the lower mantle potential temperature, and the limited amount of time since orogenesis, have resulted in the preservation of the Moho perturbation at the Grenville Front today. It is certainly clear when comparing with the more recent deformation history of the Appalachians that there is a strong correlation between increasing Moho width and the timing of tectonism. Fischer (2002) noted the age dependence of the ratio between surface topography and the underlying crustal thickness in continental collision belts, hypothesizing that long-term cooling and attendant metamorphic reactions lead to the loss of buoyancy in the crustal root of the mountains. Age-dependent variations in Moho width documented here likely reflect similar processes.

6.2.2 Appalachian Front

In contrast to the Superior Craton-Grenville Province transition, the transition between the Grenville Province and the accreted terranes of the Appalachians is associated with a large variability in Moho width. As before, the baseline of <1.5 km

Moho width is recorded throughout the Appalachian continental crust; however, many stations have Moho width in excess of 4.5-5 km (Figure 8).

The ribbon continents of Dashwoods, Ganderia, Avalonia, and Meguma accreted to the Laurentian margin during the Taconic, Salinic, Acadian, and Neoacadian orogenies, causing an eastward migration of the continent boundary. The Dashwoods crustal block is likely underlain by Grenvillian basement (van Staal et al., 2007); whereas Ganderia and Avalonia likely have the Gondwana continental margin at the base (van Staal et al., 1996). Meguma is preserved only in southern Nova Scotia, to the northeast of our seismic profile.

Each of these continental fragments has arc-related geochemical affinities, and the accretion of Ganderia and Avalonia in particular led to significant subduction-related volcanism on the western edge of the growing Laurentian margin. Modern day arcs are characterized by highly diffuse Moho boundaries (e.g. Calvert et al., 2008), and thus it is perhaps unsurprising that the continental crust below the Appalachians retains this diffuse Moho signature in many locations.

Perhaps most significantly, however, the transition from a uniformly sharp Moho to a more diffuse and variable Moho occurs at locations immediately to the NW of the St. Lawrence River (Figures 8, 16), and is *not* exactly coincident with the Appalachian Front separating the Proterozoic Grenville Province lithologies from the Phanerozoic Appalachian terranes. The observation of diffuse Moho within the Grenville Province and extending within the Appalachians therefore suggests that the Moho in this region was disturbed *prior to* the formation of Pangea and the amalgamation of these tectonic fragments. Our results indicate that perhaps the Moho was disturbed during the initial rifting of Rodinia (approximately 765-680 Ma; Ernst and Bleeker, 2010) and the opening of the Iapetus ocean basin, and has since been unable to recover its original sharp structure.

6.2.3 Concluding statement

Our data suggest that the Moho width of 1.5 km or less is a common value within the continental crust, and deviations up to 4.5 or 5 km can result from a variety of tectonic processes affecting the deep crust and lithosphere. Our results suggest that the Moho will become significantly more diffuse during continental rifting episodes, both successful (such the opening of the Atlantic) and not (e.g., the St. Lawrence Rift). Instances of diffuse Moho in the Appalachians imply that in the last ~750 Ma of Earth's history other tectonic processes (e.g. subduction) may have acted to increase Moho width, and that the time since these episodes have not been sufficient to re-establish the "sharp" Moho seen in older terranes such as Grenville.

6.3 Crustal properties along a densely sampled continental transect – an overview.

Maps of our results presented in Figures 14 and 15 and an annotated cross-section (Figure 16) offer a broad overview of the crustal properties in three distinct tectonic domains.

The Superior Province is characterized by a thin crust, sharp Moho and low values of Vp/Vs ratio. While these are expected findings for a region of Archean crust, the uniformity of properties across a large area that includes terranes with distinct histories is notable. Relatively small lateral spacing of our observations, especially in the southern part of the Superior Province, excludes the possibility of local variations being missed. Our study supports the notion that the crust of the Archean continents is indeed very similar, and has a simple internal structure, almost everywhere. This in turn comports well with the narrative of the Archean crust formation involving repeated reworking by density sorting processes (Johnson et al., 2014; Jagoutz and Kelemen, 2015; Levin et al., 2016).

The Appalachian Orogen presents a dramatically different set of traits. All parameters (crustal thickness, Moho width, Vp/Vs ratio) vary broadly over distances of 100 km or less, however major tectonic boundaries of the Appalachians (marked in Figures 1, 15, 16) do not have a clear manifestation in the crustal properties. The variability of crustal thickness appears to be systematic, with areas beneath westernmost Appalachian terranes having thicker crust than those along the Atlantic coast. Western parts of the Appalachian Orogen are likely underlain by the Grenville-age passive margin (e.g., Hynes and Rivers, 2010), and thus thick crust beneath them may be at least partially inherited from the passive margin of Laurentia. The dramatic crustal thinning (from over 45 to under 30 km) appears to peak in the vicinity of the Norumbega Fault Zone, a complex deformation belt where large amounts of shear deformation took place in the late stages of the Appalachian Orogen formation (Wang and Ludman, 2004).

In contrast to the systematic changes in crustal thickness, measures of Moho width and Vp/Vs ratio vary as much across the strike of the Appalachian terranes as they do along it. An area of consistently elevated Vp/Vs ratios is observed adjacent to the St.

Lawrence River. Thick crust and complex structure of the crust-mantle transition (Figure 8) are consistent with consequences of the late-Proterozoic failed rifting episode (such as the crustal underplating by heavy residues of rifting-related melting, e.g., Ernst and Bleeker, (2010)).

The Grenville Province presents an intermediate picture, with some crustal thickness variation, and near-uniform values of Vp/Vs and Moho width (Figures 15, 16). Of the three tectonic domains in the region, the Grenville Province has the thickest crust. Vp/Vs ratios are systematically higher than in the Superior Province. Differences between the Grenville Province and the adjacent Superior Province follow the patterns documented by Thompson et al (2010) elsewhere in Canada, and by Yuan (2015) in Australia. The change in crustal thickness across the GF is abrupt on the Superior Province side and more gradual on the Grenville Province side.

Sites in the southernmost part of the Grenville Province, adjacent to the St. Lawrence River, display combinations of properties (especially thick crust, diffuse Moho, high Vp/Vs ratio) very similar to those seen on the other side of the Appalachian Front, and consistent with consequences of the failed rifting episode.

Taken together, our transect presents a view of the Earth's continental crust as fairly uniform within regions of common tectonic history (Superior, Grenville, Appalachians), with deviations largely limited to major tectonic boundaries. Significantly, of the three tectonic boundaries crossed by our transect, only two have clear manifestations in the crustal structure. The GF is associated with a change in crustal thickness and crustal composition (as reflected in Vp/Vs ratios), while the Norumbega Fault Zone is at the apex of the regional thinning of the Appalachian crust. Interestingly, the most clear tectonic boundary in the region, the Appalachian Front, appears to coincide with the locus of crustal complexity resulting from prior tectonic episodes, and thus presents a clear example of tectonic inheritance over successive Wilson Cycles.

ACKNOWLEDGEMENTS

This work was supported by the NSF Earthscope grant EAR-1147831 and the Aresty Center for Undergraduate Research, and made possible by the open data policies of the Canadian National Data Centre for Earthquake Seismology and Nuclear Explosion Monitoring, and IRIS DMC. Discussions with A. Hynes, and formal reviews by D. Eaton and A. Frederikson contributed greatly to the quality of the paper. Figures were drawn using GMT (Wessel and Smith, 1991).

REFERENCES CITED

Aktas, K., Eaton, D.W., 2006, Upper-mantle velocity structure of the lower Great Lakes region: Tectonophysics, 420, 267–281

Alcock, F.J., 1945. Logan's Fault: Journal of the Royal Astronomical Society of Canada, Vol. 39, p.213.

Ammon, C.J., 1991, The isolation of receiver effects from teleseismic P waveforms: Seismological Society of America Bulletin, v. 81, p. 2504–2510.

Anovitz, L. M., and E.J. Essene, 1990, Thermobarometry and pressure-temperature paths in the Grenville Province of Ontario: Journal of Petrology 31.1, pp.197-241.

Artemieva, I.M., 2006, Global 1°x1° thermal model TC1 for the continental lithosphere: implications for lithosphere secular evolution: Tectonophysics, 416, 245-277.

Bostock, M. G., 1998, Mantle stratigraphy and evolution of the Slave province: Journal of Geophysical Research: Solid Earth,103, B9 pp. 21183-21200.

Bostock, M. G., 1999, Seismic waves converted from velocity gradient anomalies in the Earth's upper mantle: Geophys. J. Int. 138, 747-756

Card, K.D., 1990, A review of the Superior Province of the Canadian Shield, a product of Archean accretion: Precambrian Res. 48, 99–156.

Calvert, A. J., S. L. Klemperer, N. Takahashi, and B. C. Kerr, 2008, Three-dimensional crustal structure of the Mariana island arc from seismic tomography: J. Geophys. Res., 113, B01406, doi:10.1029/2007JB004939.

Cassidy, J. F. ,1992, Numerical experiments in broadband receiver function analysis: *Bull. Seism. Soc. Am.* **82,** 1453–1474.

Christensen, N.I., Mooney, W.D., 1995, Seismic velocity structure and composition of the continental crust: a global view. J. Geophys. Res. 100, 9761–9788.

Crotwell, H. P., and T. J. Owens, 2005, Automated receiver function processing: Seism. Res. Lett., 76, 702-708.

David J., Godin L, Stevenson R, O'Neil J, Francis D., 2009, U–Pb ages (3·8–2·7 Ga) and Nd isotope data from the newly identified Eoarchean Nuvvuagittuq supracrustal belt, Superior Craton, Canada: Geological Society of America Bulletin;121:150-163.

Dewey, JF and K Burke, 1973, Hot Spots and Continental Break-up: Implications for Collisional Orogeny, Geology; v. 2; no. 2; p. 57-60; DOI: 10.1130/0091-7613

Ernst, R.E., W. Bleeker, 2010, Large igneous provinces (LIPs), giant dyke swarms, and mantle plumes: significance for breakup events within Canada and adjacent regions from 2.5 Ga to the Present: Canadian Journal of Earth Sciences, 47, pp. 695–739

Fischer, K. M., 2002, Waning buoyancy in the crustal roots of old mountains: J. Geophys. Res. 417 (6892) : 933-936

Frederiksen, A.W., I.J. Ferguson, D. Eaton, S.-K. Miong, E. Gowan, 2006, Mantle fabric at multiple scales across an Archean-Proterozoic boundary, Grenville Front, Canada: Physics of The Earth and Planetary Interiors, v. 158, pp. 240-263, DOI: 10.1016/j.pepi.2006.03.025.

Green, A.G., Milkereit, B., Davidson, A., Spencer, C., Hutchinson, D.R., Cannon, W.F., Lee, M.W., Agena, W.F., Behrendt, J.C., and Hinze, W.J. 1988, Crustal structure of the Grenville Front and adjacent terranes: Geology, **16**: 788–792.

Gurrola, H., and Minster, B.J., 1998, Thickness estimates of the upper-mantle transition zone from bootstrapped velocity spectrum stacks of receiver functions: Geophysical Journal Interna- tional, v. 133, p. 31–43, doi:10.1046/j.1365-246X .1998.1331470.x.

Hibbard, J.P., C.R. van Staal, and D.W. Rankin, 2007, A comparative analysis of pre-Silurian crustal building blocks of the northern and the southern Appalachian Orogen: American Journal of Science, 307, 23-45.

Hynes, A. and T. Rivers, 2010, Protracted continental collision — evidence from the Grenville Orogen: Canadian Journal of Earth Sciences, v. 47, pp. 591-620

IRIS DMC, 2010, Data Services Products: EARS EarthScope Automated Receiver Survey, doi:10.17611/DP/EARS.1.

Irving, E., J. K. Park & J. L. Roy, 1972, Palaeomagnetism and the Origin of the Grenville Front: Nature 236, 344 – 346, doi:10.1038/236344a0

Jagoutz, O. and P. Kelemen, 2015, Deep Petrological Processes and Structure of Island Arcs: Annual Review of Earth and Planetary Science, Vol 43, 12.1-12.42

Johnson, T. E., Brown, M., Kaus, B. J. P. and VanTongeren, J. A., 2014, Delamination and recycling of Archaean crust caused by gravitational instabilities: Nature Geoscience **7**, 47–52

Kumarapeli, P.S., 1985, Vestiges of lapetan Rifting in the Craton West of the Northern Appalachians: Geoscience Canada 12, 54-59.

Lamontagne M., Keating P., Perreault S., 2003, Seismotectonic characteristics of the Lower St. Lawrence Seismic Zone, Quebec: insights from geology, magnetics, gravity, and seismic: Canadian Journal of Earth Sciences, Volume 40, Number 2, February 2003 , pp. 317-336(20).

Levin, V. and J. Park, 1997, P-SH conversions in a flat-layered medium with anisotropy of arbitrary orientation: Geoph. Journ. Int., 131, pp 253-266.

Levin, V., J. A. VanTongeren, and A. Servali, 2016, How sharp is the sharp Archean Moho? Example from eastern Superior Province: Geophys. Res. Lett., 43, doi:10.1002/2016GL067729

Ludden, J. and Hynes, A., 2000, The lithoprobe Abitibi-Grenville transect: two billion years of crust formation and recycling in the Precambrian shield of Canada: Canadian Journal of Earth Sciences, **37**, 459–476.

Ludman, J., 1986, Timing of terrane accretion in eastern and east-central Maine: Geology 14, 411-414.

Ludman, A. and West, D.P.,1999, Norumbega fault system of the northern Appalachians: Boulder, Colorado, Geological Society of America Special Paper 331.

Martignole, J., A J Calvert, R Friedman, P Reynolds, 2000, Crustal evolution along a seismic section across the Grenville Province (western Quebec): Canadian Journal of Earth Sciences, 37:(2-3), 291-306, DOI: 10.1139/e99-123

Moore, J., 1986, Introduction, The Grenville province then and now: Canada Geol Soc. Special Paper 31, 1-11.

Park, J., and V. Levin, 2000., Receiver functions from multiple-taper spectral correlation estimates: BSSA, v90, pp. 1507-1520

Park, J. and V. Levin, 2001, Receiver functions from regional P waves: Geophysical Journal International, v. 147, 1-11

Park, J. and V. Levin, 2016, Statistics and Frequency-Domain Moveout for Multiple-Taper Receiver Functions: GJI, in press, doi:10.1093/gji/ggw291

Percival, J.A., 2007, Geology and metallogeny of the Superior Province, Canada, *in* Goodfellow, W.D., ed., Mineral Deposits of Canada: A Synthesis of Major Deposit-Types, District Metallogeny, the Evolution of Geological Provinces, and Exploration Methods: Geol. Assoc.Canada, Mineral Deposits Div., Spec. Pub. No. 5, p. 903-928.

Petrescu, L., I. D. Bastow, F. A. Darbyshire, A. Gilligan, T. Bodin, W. Menke, and V. Levin, 2016, Three billion years of crustal evolution in eastern Canada: Constraints from receiver functions, J. Geophys. Res. Solid Earth, 121, doi:10.1002/2015JB012348.

Rivers, T., J. Martignole, C. F. Gower, A. Davidson, 1989, New tectonic divisions of the Grenville Province, Southeast Canadian Shield: Tectonics, v. 8, pp. 63-84, doi:10.1029/TC008i001p00063.

Rivers, T., 2008, Assembly and preserva- tion of lower, mid and upper orogenic crust in the Grenville Province – Implications for the evolution of large hot long-duration orogens: Precambri- an Research, v. 167, p. 237–259, http://dx.doi.org/10.1016/j.precam-res.2008.08.005.

Rivers, T., 2015, Tectonic Setting and Evolution of the Grenville Orogen: An Assessment of Progress Over the Last 40 Years, Geoscience Canada, v. 42 p. 77-124. 48p.

Rondot, J., 1971, Impactite of the Chalevoix Structure, Quebec, Canada: Journ. Geoph. Res., v. 76, pp. 5414-5423

Rudnick, R. L. and Gao, S., 2003, The composition of the continental crust: In Treatise on Geochemistry, v. 3, ed. H. D. Holland and K. K. Turekian. Oxford: Elsevier, pp. 1–64.

Slagstad, T., Culshaw, N.G., Daley, J.S., and Jamieson, R.A., 2009, Western Grenville Province holds key to mid- continental Granite-Rhyolite Province enigma: Terra Nova, v. 21, p. 181–187, http://dx.doi.org/10.1111/j.1365- 3121.2009.00871.x.

Taylor, S, 1989, Geophysical framework of the Appalachians and adjacent Grenville province, in: Pakiser, L., Mooney, W., (Eds.) Geophysical framework of the United States, Geol. Soc. Am. Memoir 79, 317-348.

Tesauro, M., M. K. Kaban, W. D. Mooney, and S. Cloetingh, 2014, NACr14: A 3D model for the crustal structure of the North Ameri- can continent: Tectonophysics 631, 65–86,

Thomas, W.A., 2006, Tectonic inheritance at a continental margin: GSA Today, v. 16, no. 2, p. 4–11.

Thompson, D. A., I. D. Bastow, G. Helffrich, J.-M. Kendall, J. Wookey, D. B. Snyder, and D. W. Eaton, 2010, Precambrian crustal evo- lution: Seismic constraints from the Canadian shield: Earth Planet. Sci. Lett. 297, pp. 655–666,

Thompson D. A., J.-M. Kendall, G. R. Helffrich, I. D. Bastow, J. Wookey and D. B. Snyder, 2015, CAN-HK: An a Priori Crustal Model for the Canadian Shield: Seis. Res. Let., v 86, p 1-9.

Tremblay ,A., Long, B and M. Massé, 2003, Supracrustal faults of the St. Lawrence rift system, Québec: kinematics and geometry as revealed by field mapping and marine seismic reflection data: Tectonophysics Volume 369, pp. 231-252

Tremblay, A., M. K. Roden-Tice, J. A. Brandt, and T. W. Megan**,** 2013, Mesozoic fault reactivation along the St. Lawrence rift system, eastern Canada: Thermochronologic evidence from apatite fission-track dating: GSA Bulletin, v. 125, p. 794–810;

van Staal, C.R., Sullivan, R.W., and Whalen, J.B., 1996, Provenance and tectonic history of the Gander Margin in the Caledonian/Appalachian Orogen: implications for the origin and assembly of Avalonia, *in* Nance, R.D., and Thompson, M.D., eds., Avalonian and Related Peri- Gondwanan Terranes of the Circum-North Atlantic: Geological Society of America, Special Paper 304, p. 347-367.

van Staal, CR, JB Whalen, P Valverde-Vaquero, A Zagorevski and N Rogers, 2009, Pre-Carboniferous, episodic accretion-related, orogenesis along the Laurentian margin of the northern Appalachians: Geological Society, London, Special Publications, v. 327, p. 271-316, doi: 10.1144/SP327.13.

Wang, C., and Ludman, A., 2004, Deformation conditions, kinematics, and evolution of shallow crustal ductile shearing in the Norumbega Fault System in the Northern Appalachians, Eastern Maine: Tectonophysics, vol. 384, p. 129-148.

Wessel, P., and W. H. F. Smith, 1991, Free software helps map and display data: Eos Trans. AGU, 72, 441, doi:10.1029/ 90EO00319.

West, DP Jr and MK Roden-Tice, 2003, Late Cretaceous reactivation of the Norumbega fault zone, Maine: Evidence from apatite fission-track ages: Geology; July 2003; v. 31; no. 7; p. 649-652; DOI: 10.1130/0091-7613

Williams, H. and RD Hatcher, 1982, Suspect terranes and accretionary history of the Appalachian orogeny: Geology v. 10, pp. 530-536; DOI: 10.1130/0091-7613

White, D.J., Forsyth, D.A., Asudeh, I., Carr, S.D., Wu, H., Easton, R.M., and Mereu, R.F. 2000, A seismic-based cross-section of the Grenville orogen in southern Ontario and western Quebec: Canadian Journal of Earth Sciences, 37(2–3): 183–192.

Withjack, M. O., P. E. Olsen, and R. W. Schlische,1995, Tectonic evolution of the Fundy rift basin, Canada: Evidence of extension and shortening during passive margin development: Tectonics, 14(2), 390–405, doi:10.1029/94TC03087.

Withjack, M.O., Schlische, R.W., and Olsen, P.E., 2012, Development of the passive margin of eastern North America—Mesozoic rifting, igneous activity, and drifting, in Roberts, D.G., and Bally, A.W., eds., Regional Geology and Tectonics, Volume 1B—Phanerozoic Rift Systems and Sedimentary Basins: New York, Elsevier, p. 301-335.

Whitmeyer, S.J. and K.E. Karlstrom, 2007, Tectonic model for the Proterozoic growth of North America, Geosphere, 3, 220–259; doi:10.1130/GES00055.1

Yuan, H. 2015, Secular change in Archaean crust formation recorded in Western Australia: Nature Geoscience **8**, 808–813

Zhang, J. and A. W. Frederikson, 2013, 3-D crust and mantle structure in southern Ontario, Canada via receiver function imaging: Tectonophysics, v. 608, pp. 700–712

Zhu, L. & Kanamori, 2000, H. Moho depth variation in southern California from teleseismic receiver functions: J. Geophys. Res. **105,** 2969–2980

Table 1. Seismic observatories used in this study and values of various parameters of the crustal structure determined for them. Distances along and across the profile are computed with respect to the line from 79W, 52N to 65.285W, 44.633N (shown in Figures 1, 14,15). Values for crustal thickness H, Vp/Vs and Vs are obtained from the receiver function H-*k* stacking analysis assuming Vp=6.5 km/s. **Bold font** is used for sites where H-*k* stack analysis yields a stable result with a single clear maximum. Crustal thickness *h* is computed using Vp, Vs, and the *delay* of the P_{mS} phase, using a formula for a single homogeneous layer (see ***Methods***). Wavelength λ is evaluated using maximum frequency *f* of the RF beam and Vs, and the corresponding Moho width M is evaluated using Vp/Vs ratio (see text for details). Equipment used at all sites is documented in the IRIS Data Management System.

Dist. along	Dist. across	Station Lon.	Station Lat.	Station name	H, km	Vp/Vs	delay, s	Vs, km/s	*h, km*	max *f*, Hz	λ, km	M, km
-8.04	**135.93**	**-77.97**	**53.05**	**WEMQ**	**39**	**1.726**	**4.5**	**3.77**	**37.77**	**3**	**1.26**	**0.75**
88.76	**100.01**	**-77.10**	**52.29**	**QM90**	**35**	**1.714**	**3.9**	**3.79**	**33.27**	**3**	**1.26**	**0.76**
186.03	**90.48**	**-76.02**	**51.71**	**NMSQ**	**37.5**	**1.678**	**4.3**	**3.87**	**38.57**	**2.5**	**1.55**	**0.96**
219.07	-152.48	-77.64	49.76	MATQ	32.5	1.894	4.3	3.43	29.48	2.5	1.37	0.73
279.95	**56.17**	**-75.23**	**50.96**	**QM80**	**33.5**	**1.696**	**3.9**	**3.83**	**34.10**	**3**	**1.26**	**0.78**
299.27	**44.32**	**-75.11**	**50.78**	**QM78**	**33**	**1.75**	**4**	**3.71**	**32.53**	**3**	**1.24**	**0.72**
316.22	**55.48**	**-74.82**	**50.76**	**QM76**	**35**	**1.696**	**4.2**	**3.83**	**36.73**	**3**	**1.28**	**0.78**
342.45	**46.25**	**-74.60**	**50.56**	**QM74**	**36**	**1.696**	**4.3**	**3.83**	**37.60**	**1.75**	**2.19**	**1.33**
368.40	**38.31**	**-74.37**	**50.36**	**QM72**	**33.5**	**1.75**	**4.1**	**3.71**	**33.34**	**1.5**	**2.48**	**1.44**
379.51	**14.82**	**-74.45**	**50.13**	**QM70**	**34.5**	**1.696**	**4**	**3.83**	**34.98**	**1.25**	**3.07**	**1.87**
398.55	**-1.39**	**-74.37**	**49.91**	**CHGQ**	**34**	**1.732**	**3.5**	**3.75**	**29.14**	**1**	**3.75**	**2.22**
423.41	-41.52	-74.44	49.49	QM66	39.5	1.882	5.6	3.45	38.90	1.5	2.30	1.23
467.59	-32.36	-73.88	49.31	QM62	42.5	1.738	5.3	3.74	43.78	2	1.87	1.10
494.73	**-32.16**	**-73.58**	**49.16**	**QM61**	**41**	**1.768**	**5.2**	**3.68**	**41.32**	**2**	**1.84**	**1.06**
508.31	**-21.04**	**-73.34**	**49.17**	**QM60**	**40.5**	**1.768**	**5.3**	**3.68**	**42.12**	**1.75**	**2.10**	**1.21**
550.59	-4.63	-72.74	49.05	QM58	39.5	1.756	5	3.70	40.35	2	1.85	1.07
572.74	**-13.18**	**-72.58**	**48.86**	**QM56**	**38**	**1.768**	**4.9**	**3.68**	**38.94**	**3**	**1.23**	**0.71**
594.69	**18.79**	**-72.07**	**48.96**	**DMCQ**	**35.5**	**1.81**	**4.6**	**3.59**	**34.71**	**1.5**	**2.39**	**1.34**

656.92	-10.38	-71.66	48.41	QM50	40	1.738	4.9	3.74	40.48	2.25	1.66	0.98
677.30	**-181.32**	**-72.88**	**47.10**	**D58A**	**37**	**1.804**	**5.1**	**3.60**	**38.76**	**3**	**1.20**	**0.67**
745.63	8.42	-70.58	48.03	QM40	40	1.738	5.8	3.74	47.91	1	3.74	2.20
755.14	-34.89	-70.85	47.68	QM38	43	1.792	5.7	3.63	43.96	0.5	7.25	4.10
761.40	50.64	-70.05	48.23	QM39	39.5	1.852	5.3	3.51	38.08	0.75	4.68	2.54
796.08	**-32.21**	**-70.41**	**47.46**	**A54**	**39.5**	**1.876**	**5.7**	**3.46**	**39.86**	**1**	**3.46**	**1.86**
797.39	3.46	-70.09	47.69	A61	42	1.888	5	3.44	34.51	1	3.44	1.83
799.11	**24.36**	**-69.89**	**47.83**	**A64**	**41.5**	**1.714**	**5.2**	**3.79**	**44.36**	**1**	**3.79**	**2.28**
805.31	**-103.28**	**-70.92**	**46.91**	**D60A**	**41.5**	**1.822**	**6.1**	**3.57**	**45.38**	**0.5**	**7.14**	**3.95**
813.23	**-175.42**	**-71.45**	**46.37**	**E60A**	**32.5**	**1.846**	**4.6**	**3.52**	**33.28**	**2.5**	**1.41**	**0.77**
818.34	**-11.26**	**-70.01**	**47.47**	**A16**	**46**	**1.744**	**5.5**	**3.73**	**45.08**	**1.25**	**2.98**	**1.75**
819.49	**23.86**	**-69.69**	**47.70**	**A21**	**39.5**	**1.882**	**5.4**	**3.45**	**37.51**	**1.5**	**2.30**	**1.23**
823.83	-39.82	-70.20	47.24	A11	49.5	1.696	5.4	3.83	47.22	2	1.92	1.17
827.35	-42.80	-70.19	47.20	D61A	40.5	1.87	5.6	3.48	39.42	0.75	4.63	2.49
836.72	-7.18	-69.79	47.39	QM36	39.5	1.864	5.5	3.49	38.98	2	1.74	0.94
860.88	-40.68	-69.83	47.02	QM34	40.5	1.894	5.8	3.43	39.77	0.75	4.58	2.42
865.23	-123.07	-70.49	46.43	E61A	43.5	1.714	4.8	3.79	40.94	0.75	5.06	3.03
868.21	**-186.88**	**-70.99**	**45.97**	**F61A**	**44.5**	**1.72**	**5.1**	**3.78**	**43.15**	**0.5**	**7.56**	**4.51**
901.17	3.26	-69.05	47.08	D62A	35.5	1.864	5	3.49	35.44	1.5	2.32	1.25
907.79	**-59.07**	**-69.52**	**46.62**	**E62A**	**37.5**	**1.804**	**4.8**	**3.60**	**36.48**	**0.75**	**4.80**	**2.69**
921.53	-0.99	-68.89	46.93	QM31	34	1.864	4.7	3.49	33.31	2	1.74	0.94
934.40	**-142.28**	**-69.97**	**45.90**	**F62A**	**39**	**1.756**	**4.5**	**3.70**	**36.31**	**1.75**	**2.12**	**1.23**
935.92	**-3.09**	**-68.76**	**46.83**	**QM30**	**37.5**	**1.762**	**5**	**3.69**	**40.04**	**0.75**	**4.92**	**2.84**
957.96	46.94	-68.11	47.04	D63A	36.5	1.714	4.3	3.79	36.68	3	1.26	0.76
963.80	-7.74	-68.53	46.64	QM28	36	1.762	4.3	3.69	34.43	0.5	7.38	4.27
983.30	**-22.12**	**-68.46**	**46.42**	**E63A**	**34.5**	**1.738**	**4.2**	**3.74**	**34.69**	**1**	**3.74**	**2.20**
990.09	**21.14**	**-68.02**	**46.67**	**PQI**	**33.5**	**1.804**	**4.4**	**3.60**	**33.44**	**3**	**1.20**	**0.67**
990.18	**-59.73**	**-68.72**	**46.13**	**QM20**	**35**	**1.768**	**4.5**	**3.68**	**35.76**	**1**	**3.68**	**2.12**
999.13	**-114.78**	**-69.10**	**45.70**	**F63A**	**33.5**	**1.762**	**4.1**	**3.69**	**32.83**	**0.75**	**4.92**	**2.84**
1011.67	**-190.56**	**-69.62**	**45.11**	**G63A**	**35.5**	**1.69**	**4**	**3.85**	**35.27**	**1**	**3.85**	**2.36**
1019.75	**10.01**	**-67.83**	**46.42**	**E64A**	**32.5**	**1.786**	**3.8**	**3.64**	**29.53**	**1**	**3.64**	**2.07**
1020.12	**-161.19**	**-69.29**	**45.26**	**PKME**	**34**	**1.684**	**3.8**	**3.86**	**33.80**	**0.5**	**7.72**	**4.75**
1031.11	**-62.74**	**-68.35**	**45.86**	**F64A**	**31**	**1.804**	**4**	**3.60**	**30.40**	**1**	**3.60**	**2.02**
1052.52	-134.52	-68.76	45.25	G64A	32	1.76	3.8	3.69	30.51	1	3.69	2.14
1053.74	**171.38**	**-66.06**	**47.28**	**BATG**	**33.5**	**1.702**	**3.9**	**3.82**	**33.82**	**3**	**1.27**	**0.77**
1102.80	**-96.23**	**-67.95**	**45.21**	**QM16**	**31**	**1.726**	**3.8**	**3.77**	**31.89**	**0.5**	**7.53**	**4.48**
1117.84	**-99.89**	**-67.84**	**45.09**	**QM15**	**30.5**	**1.762**	**3.7**	**3.69**	**29.63**	**0.5**	**7.38**	**4.27**
1125.98	-76.52	-67.56	45.20	G65A	33	1.72	3.9	3.78	33.00	1.25	3.02	1.81
1137.61	**-107.20**	**-67.72**	**44.93**	**QM10**	**34**	**1.738**	**4.2**	**3.74**	**34.69**	**0.75**	**4.99**	**2.94**
1168.80	**-111.22**	**-67.46**	**44.71**	**EMMW**	**35.5**	**1.762**	**4.3**	**3.69**	**34.43**	**1**	**3.69**	**2.13**
1171.66	-97.20	-67.31	44.79	H66A	34	1.786	4.5	3.64	34.96	0.5	7.28	4.13

1173.78	-44.97	-66.84	45.12	GGN	35.5	1.738	4.5	3.74	37.17	1.25	2.99	1.76
1232.65	**123.49**	**-64.81**	**45.85**	**LMN**	**41**	**1.726**	**5.1**	**3.77**	**42.80**	**3**	**1.26**	**0.75**

FIGURE CAPTIONS

Figure 1 (A) Eastern North America tectonic terranes (blue – Archean, green – Grenville, orange – Appalachian, heavy grey – Norumbega Fault Zone) and locations of observatories used in the study. Red symbols: boxes – permanent sites; Inverted triangles – QMIII array; triangles – Earthscope TA. Open symbols – other sites in the region. Grey line shows a transect used for projecting data from individual sites onto a common plane. Solid boxes outline areas of special interest discussed in the Results section. (B) Enlarged maps for areas of special interest, with site names indicated.

Figure 2. A schematic depiction of the ray path geometry of the observed seismic waves.

Figure 3. (A) Backazimuthal gather of radial receiver functions (RFs) for site WEMQ (see Table 1), with 20° wide bins overlapped by 50%. (B) Epicentral gather for all observed data, with bins of 10° in distance, and 50% overlap. (C) Map of sources used to construct the gathers shown in (A) and (B). Directions (backazimuths) of sources with respect to the observing site (in the center of the map) are preserved by the projection. Red symbols show locations of earthquakes used to construct an RF beam for site WEMQ in Figure 4A.

Figure 4. (A) Receiver function beams constructed for groups of nearby earthquakes. Site names marked. Sources for site WEMQ shown by red dots in Figure 3c. Stars mark the time series we chose as those with the highest frequency of the P_{mS} phase. (B). Results of omnidirectional H-*k* (crustal thickness – Vp/Vs ratio) stacking of the entire data set (e.g.,

Figure 3B for site WEMQ). White dots mark maximum of the stack, the white contours show values at 95% of the maximum. Green lines show min/max values of that contour if they fall within the search box. Exact values of H and *k* corresponding to the white dot are given in Table 1.

Figure 5. A composite image combining all main findings of this study in a common reference frame of the transect plane (grey line in Figure 1). Locations of seismic observing sites are projected onto the line of the transect, and RF waveforms and corresponding values of P_{mS} delay, crustal thickness, and Moho width are plotted at respective locations along it. RF waveforms have a maximum frequency of 2Hz. Moho width is estimated using the highest frequency chosen for the site (see Table 1). Lowermost panel shows three estimates of crustal thickness at locations of our sites: values interpolated from results of Tesauro et al. (2014) (crosses), values obtained from the H-*k* stack (circles), and values obtained by converting the measured P_{mS} delay times (red dots in waveform plot) to depth on the basis of Vp and Vs values (squares). Top panel shows topography along the transect. Locations of the main tectonic boundaries are marked: G- Grenville Front, A – Appalachian Front, N – Norumbega Fault Zone.

Figure 6. The Grenville Front section of the transsect. Values of *k*=Vp/Vs that we consider unreliable are shown by shaded circles (cf. Table 1). All other symbols are as in Figure 5.

Figure 7. Crustal thickening associated with the Grenville Front (GF). H-*k* stacking surfaces and waveforms for sites located north of GF (QM70), next to GF (QM66), and south of GF (QM62) are shown.

Figure 8. The Appalachian Front section of the transect. Symbols are as in Figure 6.

Figure 9. Observations near the Appalachian Front. Sites on opposite sides of AF (A21 on the southern shore, A64 on the northern shore of St. Lawrence River) show evidence for thick crust, and also for complex structure in the uppermost mantle (extra phases at 8 s for site A64; at 10 s for site A21).

Figure 10. Two sites with exceptionally small estimates of crustal thickness in the viscinity of Appalachian Front. Site A61 has poorly constrained *k*, and thus the true thickness is likely larger.

Figure 11. The Norumbega Fault Zone section of the transect. Symbols are as in Figure 6.

Figure 12. Examples of H-*k* stacks and RF waveforms for a set of sites in the region of very thin crust in southern Maine.

Figure 13. Examples of data for sites with both high and low values of *k* favored by the data.

Figure 14. Map showing Moho width and crustal thickness. Colors denote depth, while symbol size scales with Moho width, as shown in the legend.

Figure 15. Map showing the distribution of Vp/Vs ratio in the region. Colors denote the value of k=Vp/Vs.

Figure 16. A summary of major results of our study showing topography (upper panel, vertical scale in meters) and estimates of crustal thickness (lower panel, symbols as in Figure 5, in km). Green horizontal line – average crustal thickness based on our new results. Ages of last significant tectonic activity are marked above corresponding regions of the transect.

[1]GSA Data Repository item 201Xxxx, showing an interpolated map of Vp values, as well as RF waveforms, H-*k* stacks and frequency-dependent RF beams for all sites, is available online at www.geosociety.org/pubs/ft20XX.htm, or on request

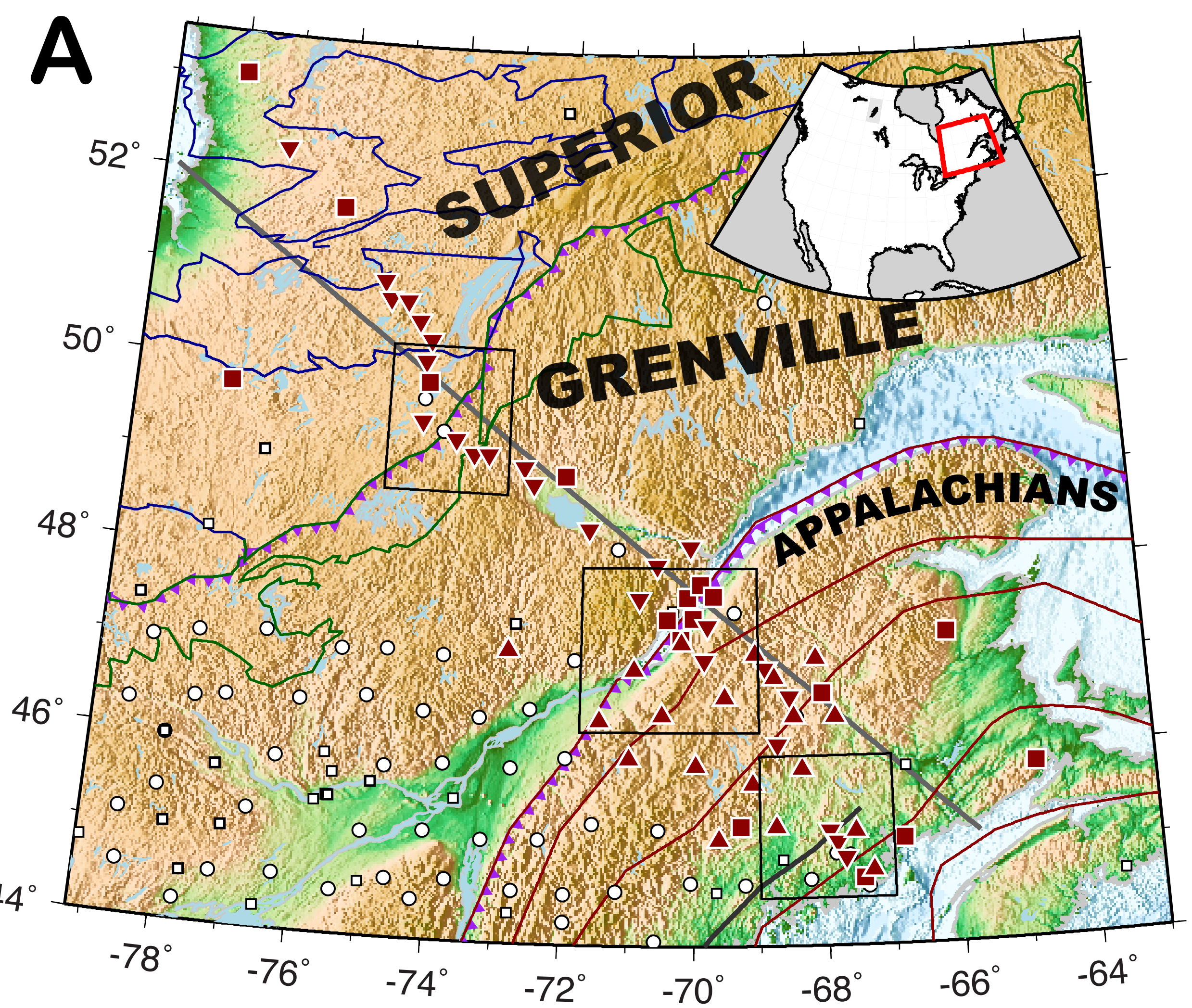
A
SUPERIOR
GRENVILLE
APPALACHIANS
52°
50°
48°
46°
44°
-78°
-76°
-74°
-72°
-70°
-68°
-66°
-64°

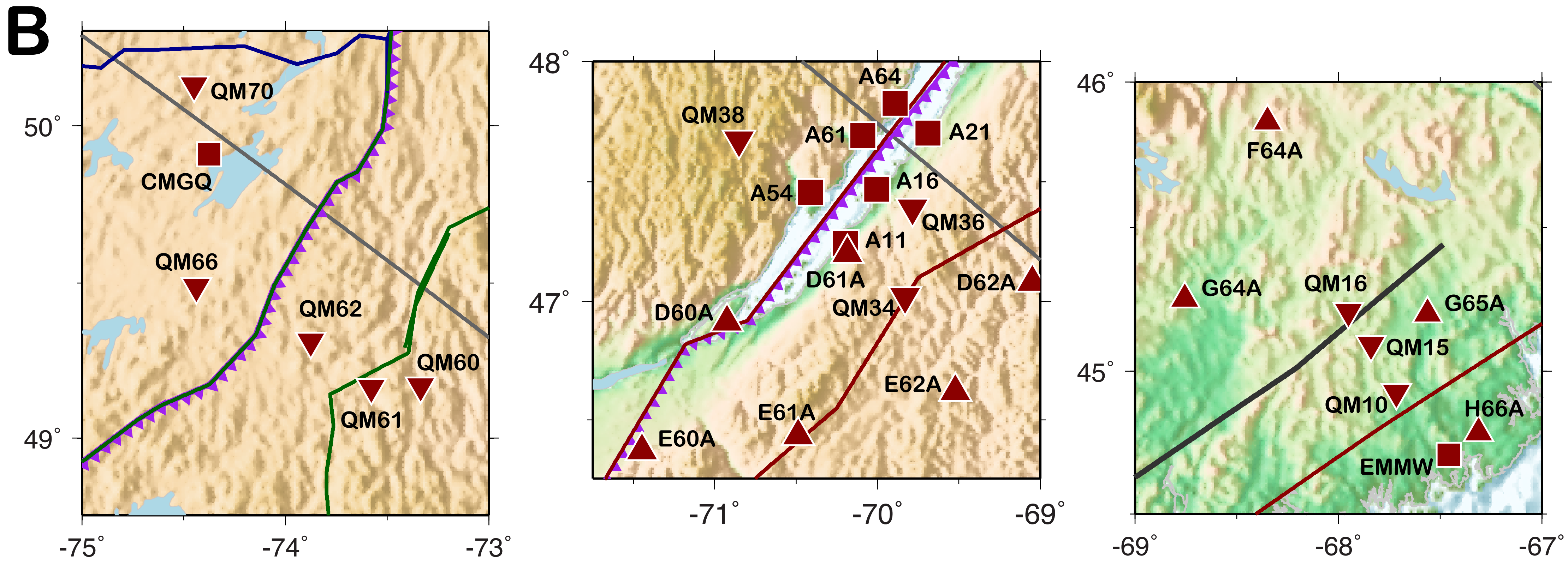
B
QM70
50°
CMGQ
QM66
QM62
QM60
QM61
49°
-75°
-74°
-73°
48°
47°
A64
QM38
A61
A21
A54
A16
QM36
A11
D61A
D62A
D60A
QM34
E62A
E61A
E60A
-71°
-70°
-69°
46°
45°
F64A
G64A
QM16
G65A
QM15
QM10
H66A
EMMW
-69°
-68°
-67°

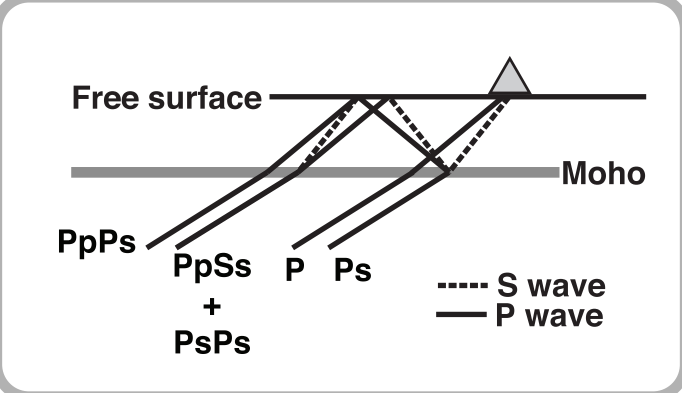
Free surface
Moho
PpPs
PpSs
+
PsPs
P
Ps
S wave
P wave

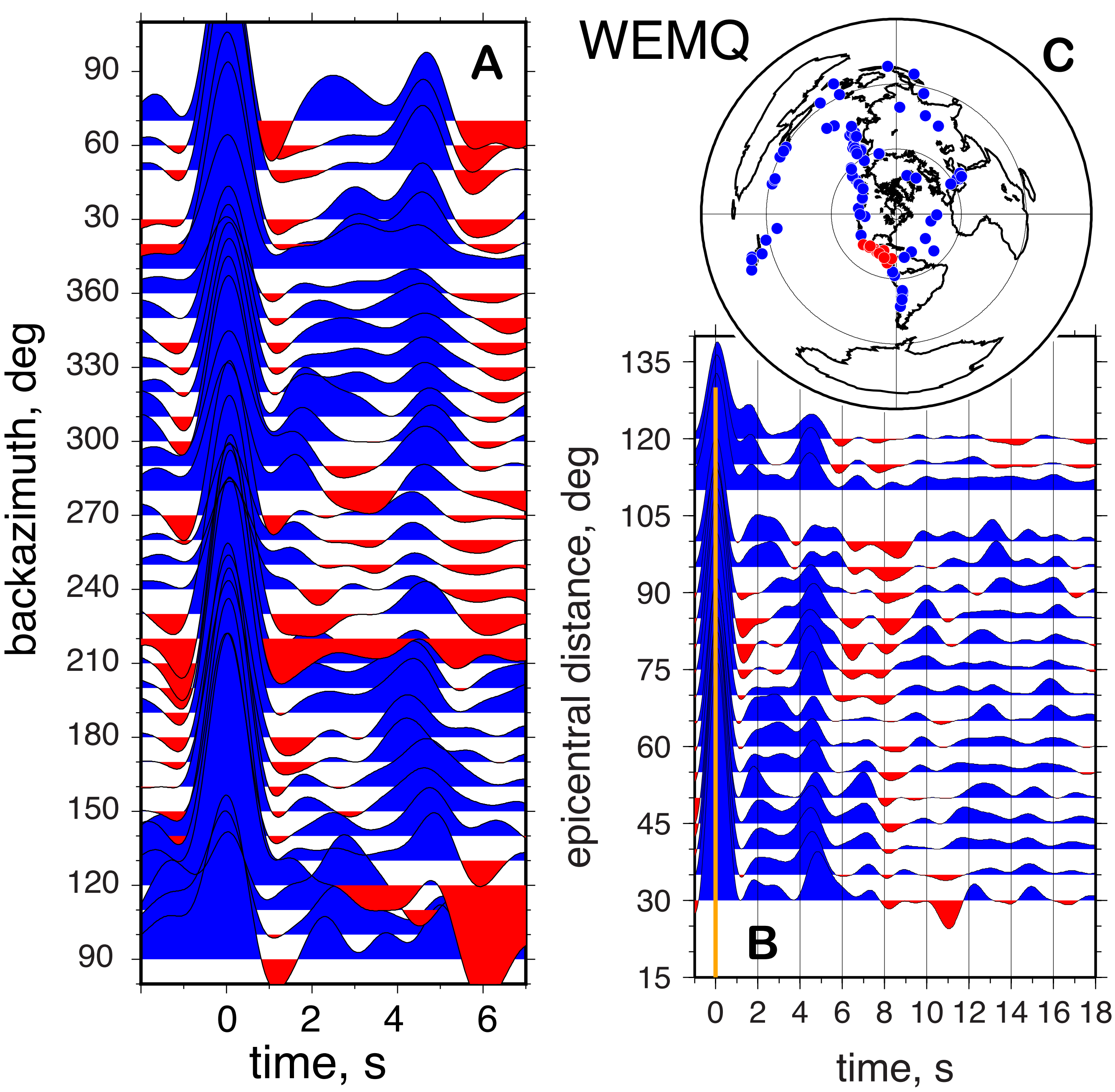
WEMQ
A
B
C
backazimuth, deg
90
60
30
360
330
300
270
240
210
180
150
120
90
0
2
4
6
time, s
epicentral distance, deg
135
120
105
90
75
60
45
30
15
0
2
4
6
8
10
12
14
16
18
time, s

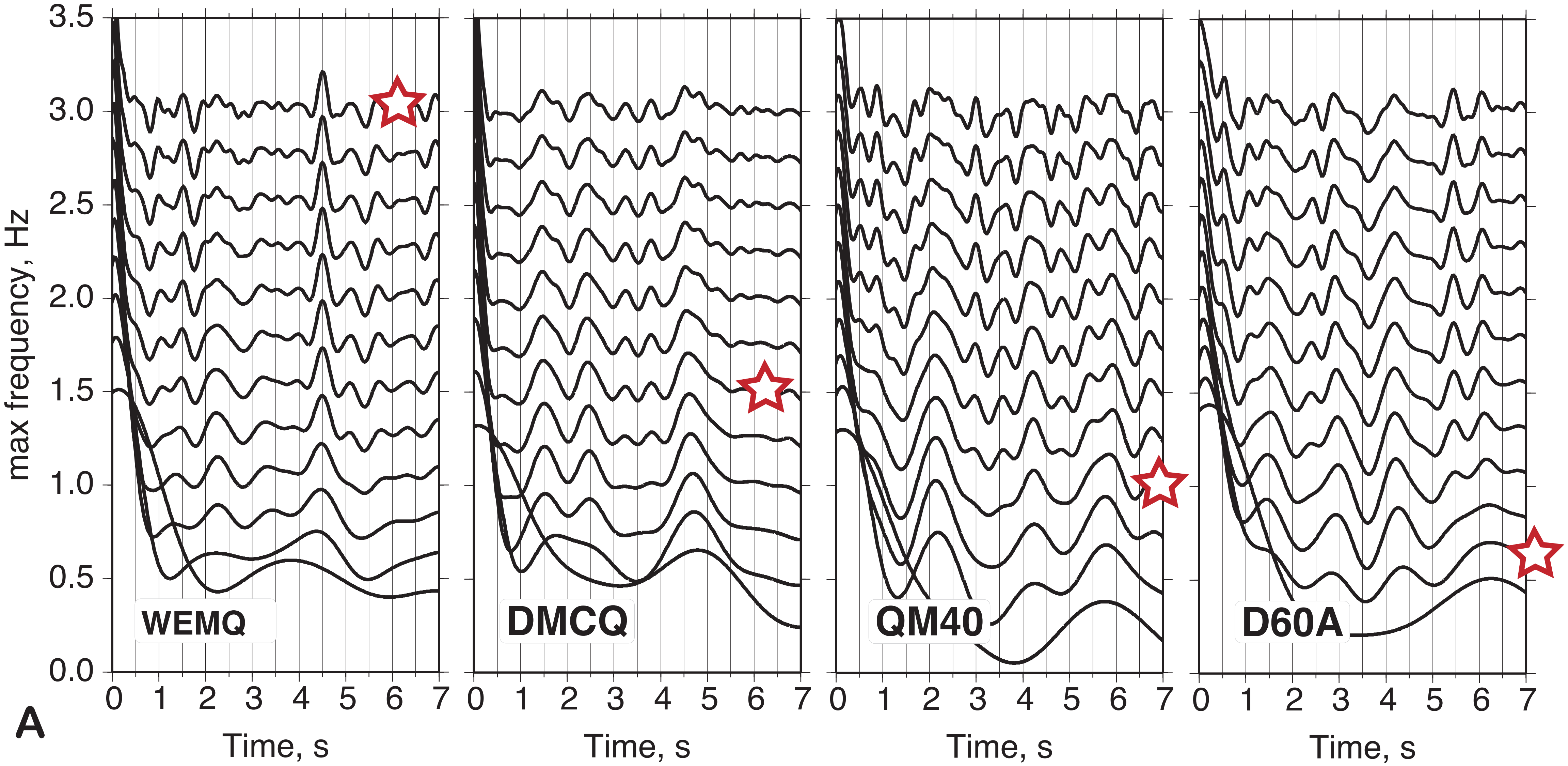

max frequency, Hz
3.5
3.0
2.5
2.0
1.5
1.0
0.5
0.0
WEMQ
DMCQ
QM40
D60A
0 1 2 3 4 5 6 7
Time, s
A

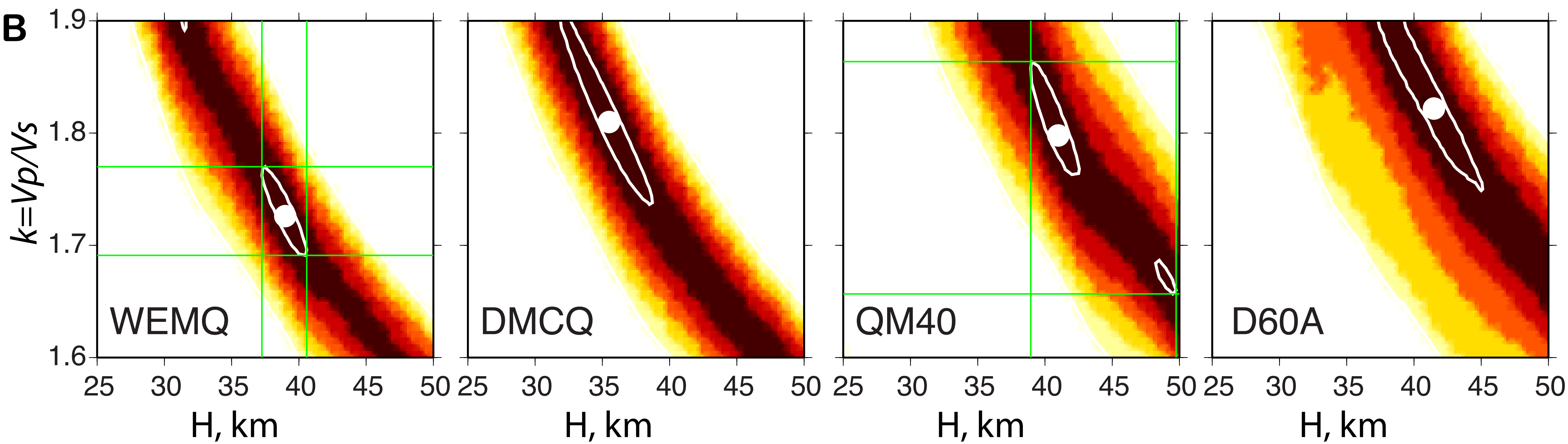
B
1.9
1.8
1.7
1.6
k=Vp/Vs
WEMQ
DMCQ
QM40
D60A
25
30
35
40
45
50
H, km

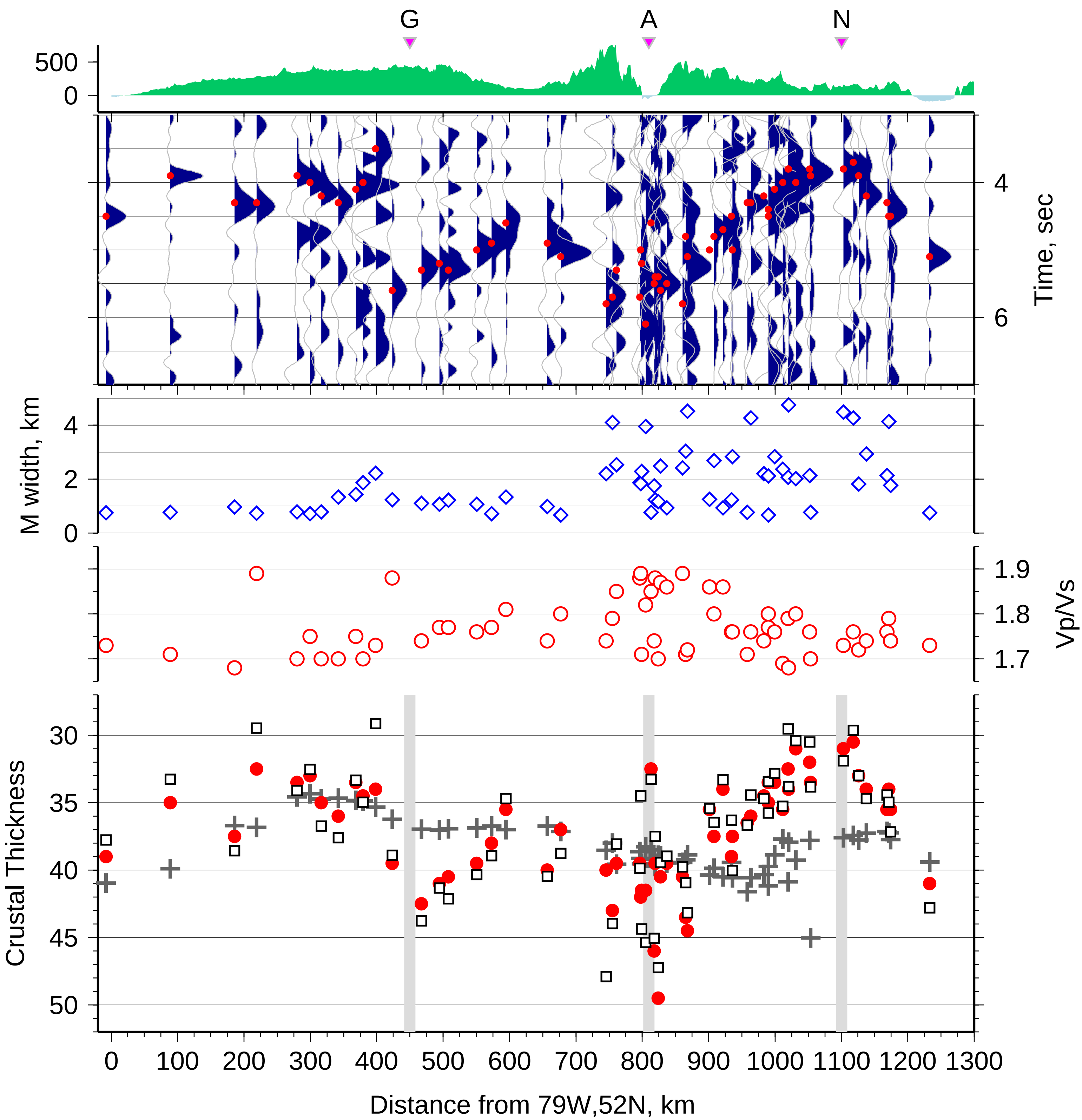

G
A
N
500
0
4
6
Time, sec
M width, km
4
2
0
1.9
1.8
1.7
Vp/Vs
Crustal Thickness
30
35
40
45
50
0
100
200
300
400
500
600
700
800
900
1000
1100
1200
1300
Distance from 79W,52N, km

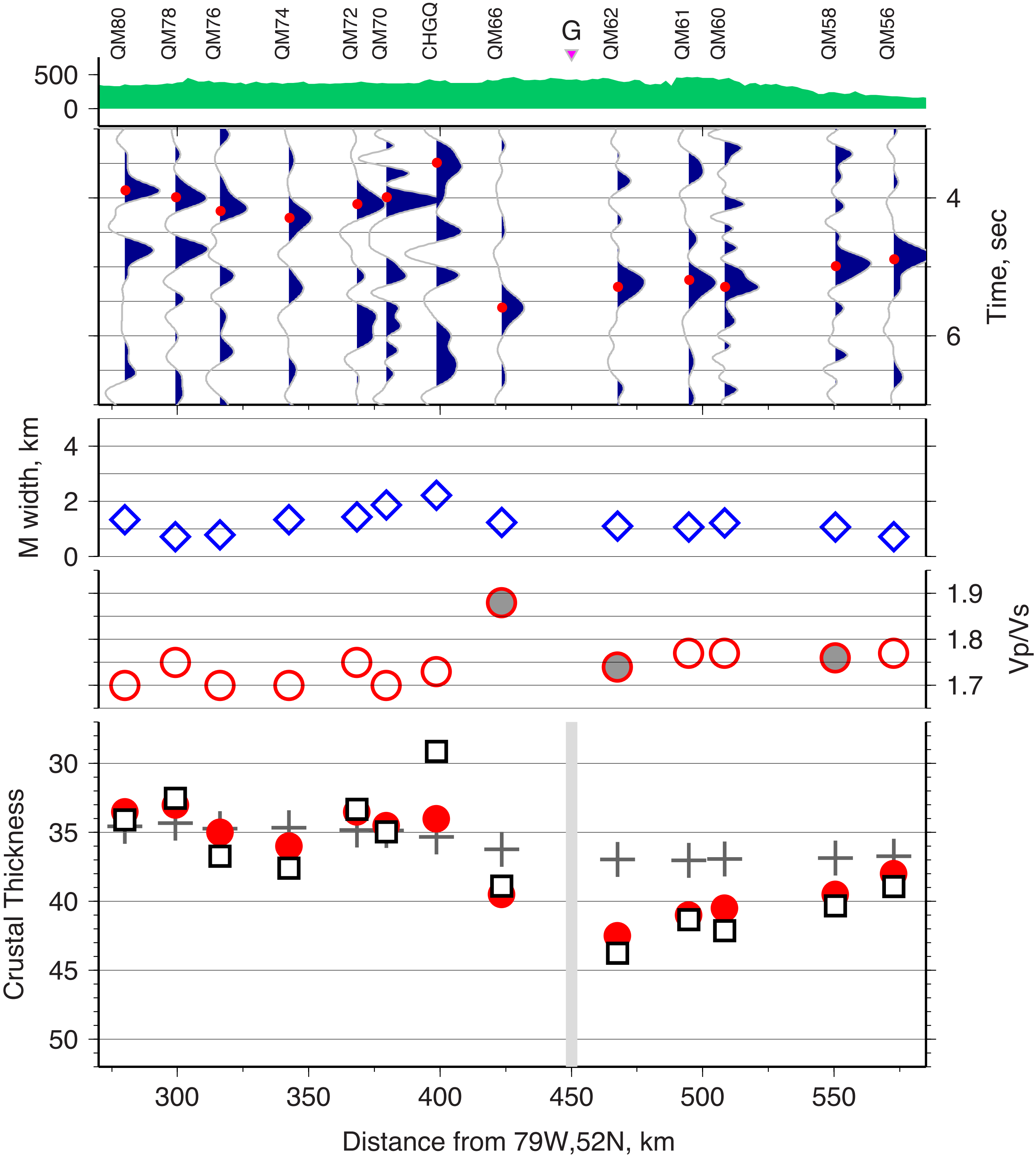
QM80
QM78
QM76
QM74
QM72
QM70
CHGQ
QM66
G
QM62
QM61
QM60
QM58
QM56
500
0
4
6
Time, sec
M width, km
4
2
0
1.9
1.8
1.7
Vp/Vs
Crustal Thickness
30
35
40
45
50
300
350
400
450
500
550
Distance from 79W,52N, km

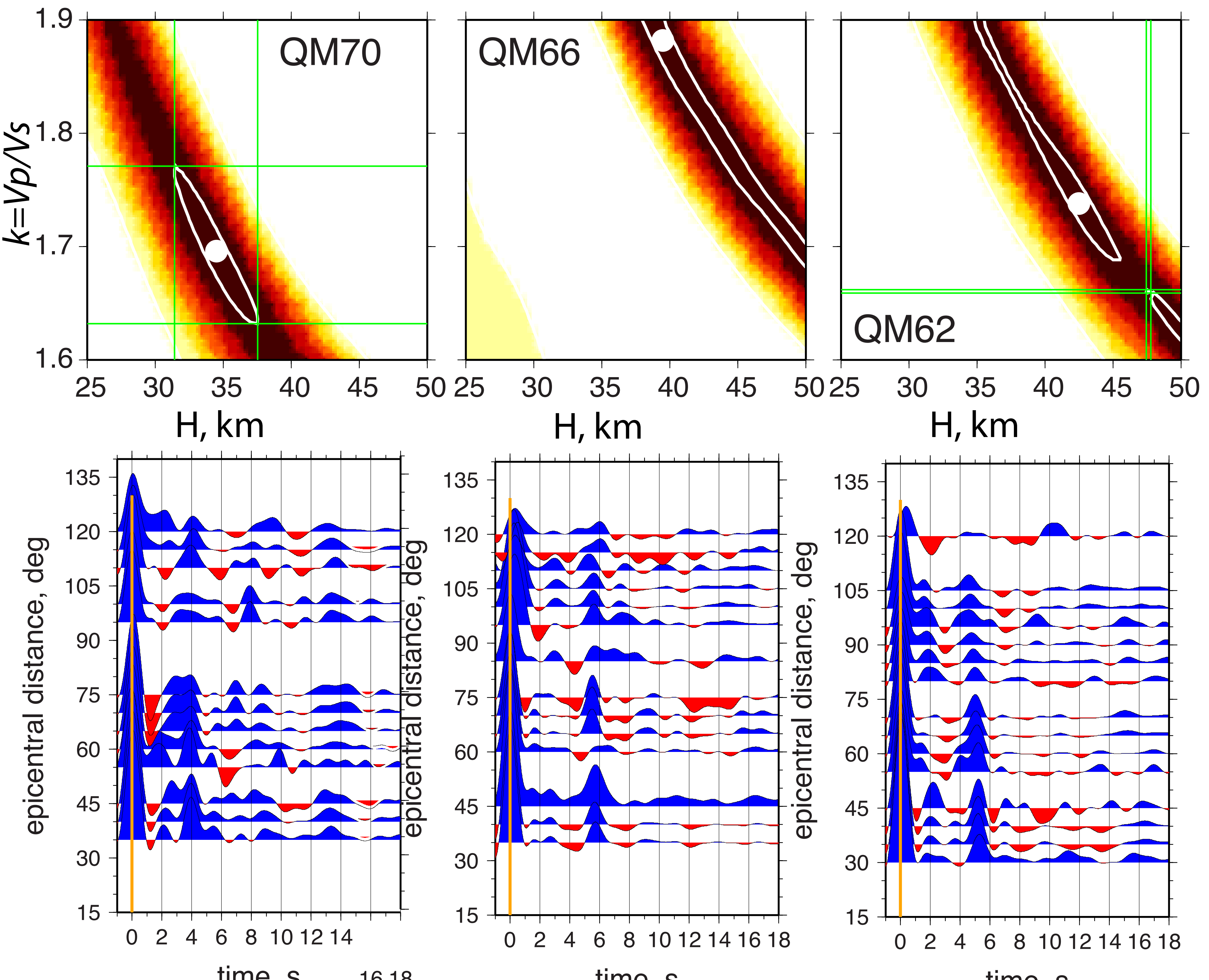

QM70
QM66
QM62
k=Vp/Vs
H, km
epicentral distance, deg
time, s

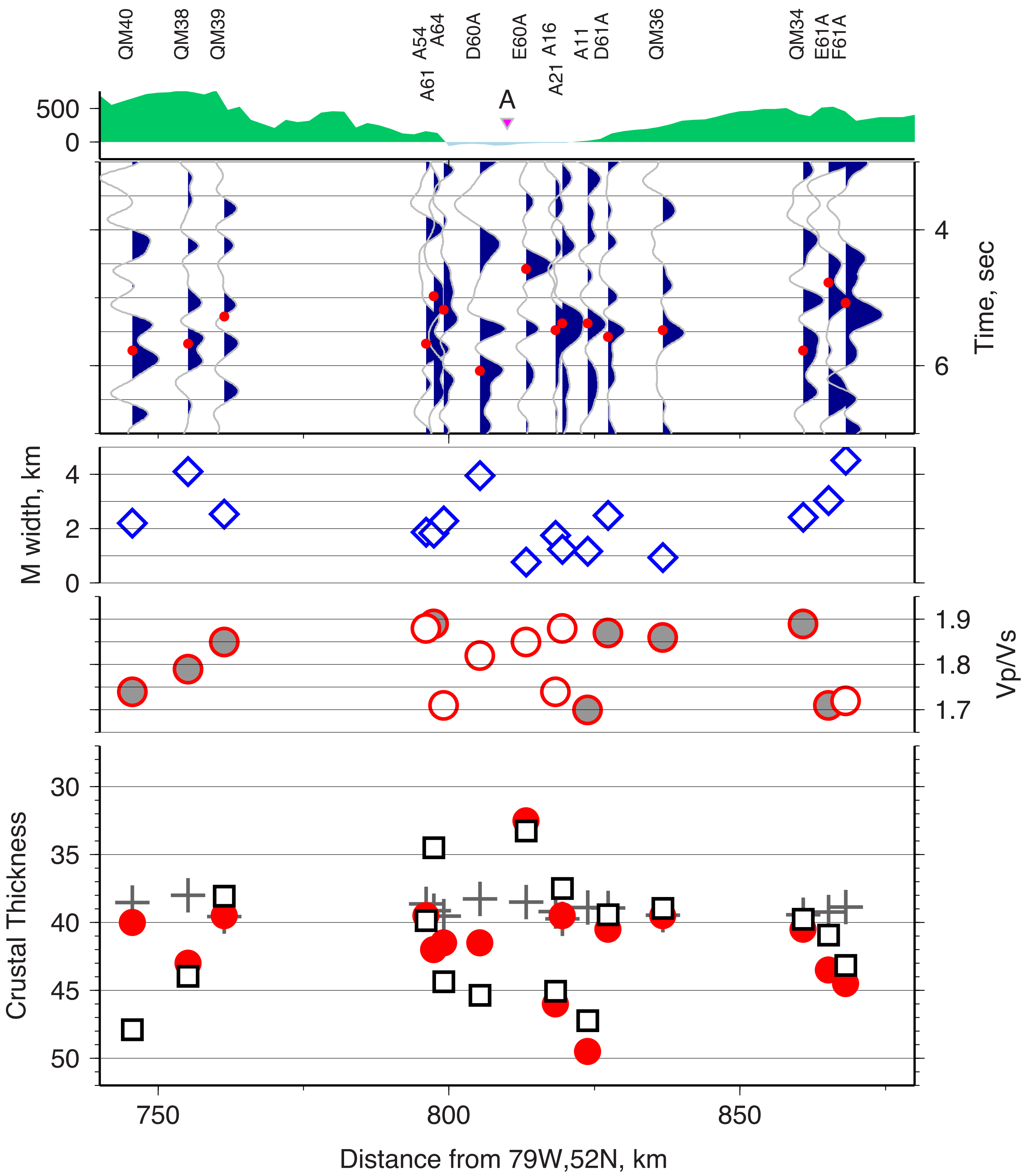

QM40
QM38
QM39
A54
A64
A61
D60A
E60A
A16
A21
A11
D61A
QM36
QM34
E61A
F61A
A
500
0
4
6
Time, sec
M width, km
0
2
4
1.9
1.8
1.7
Vp/Vs
Crustal Thickness
30
35
40
45
50
750
800
850
Distance from 79W,52N, km

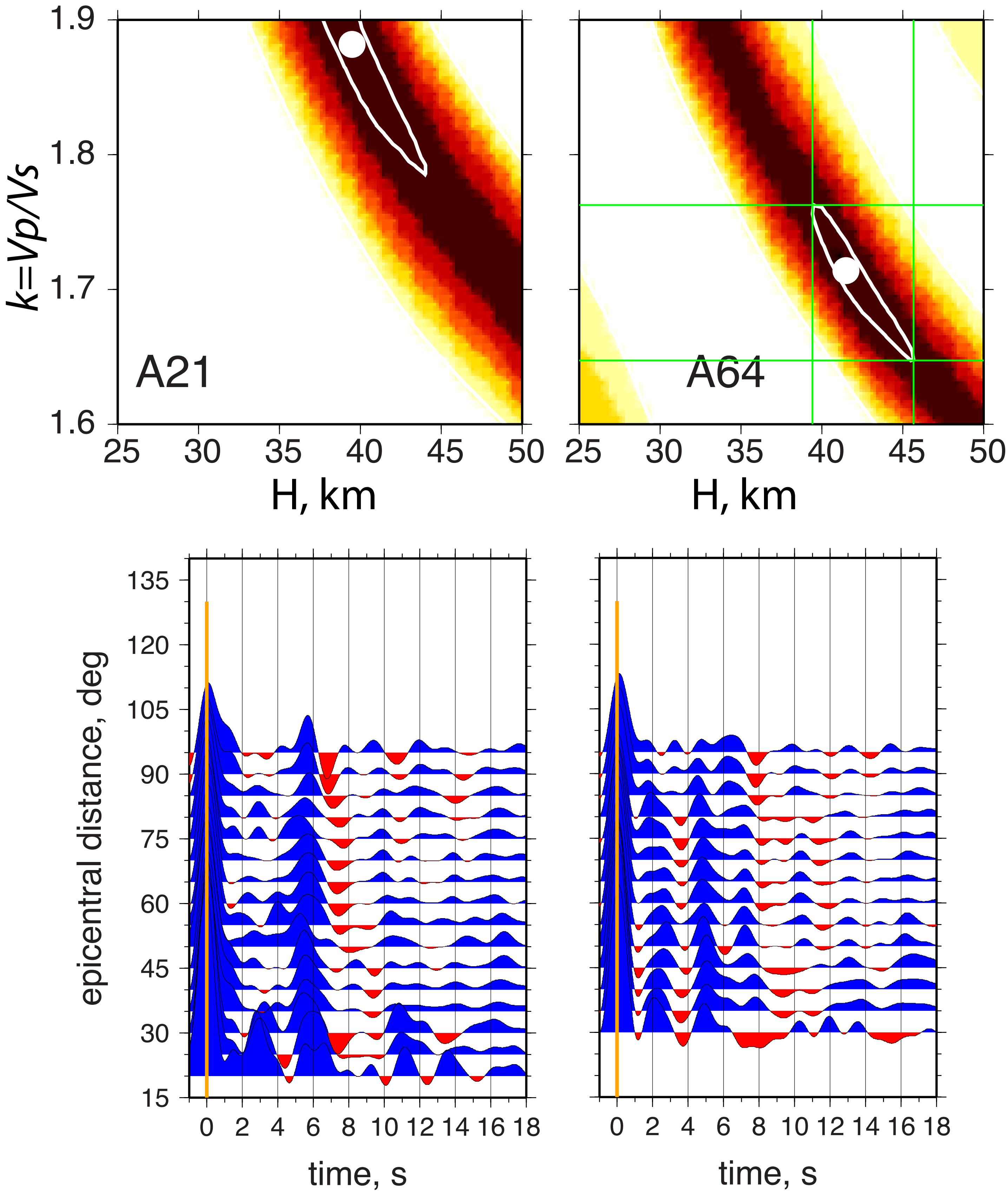

1.9
1.8
1.7
1.6
k=Vp/Vs
A21
A64
25 30 35 40 45 50
H, km
135
120
105
90
75
60
45
30
15
epicentral distance, deg
0 2 4 6 8 10 12 14 16 18
time, s

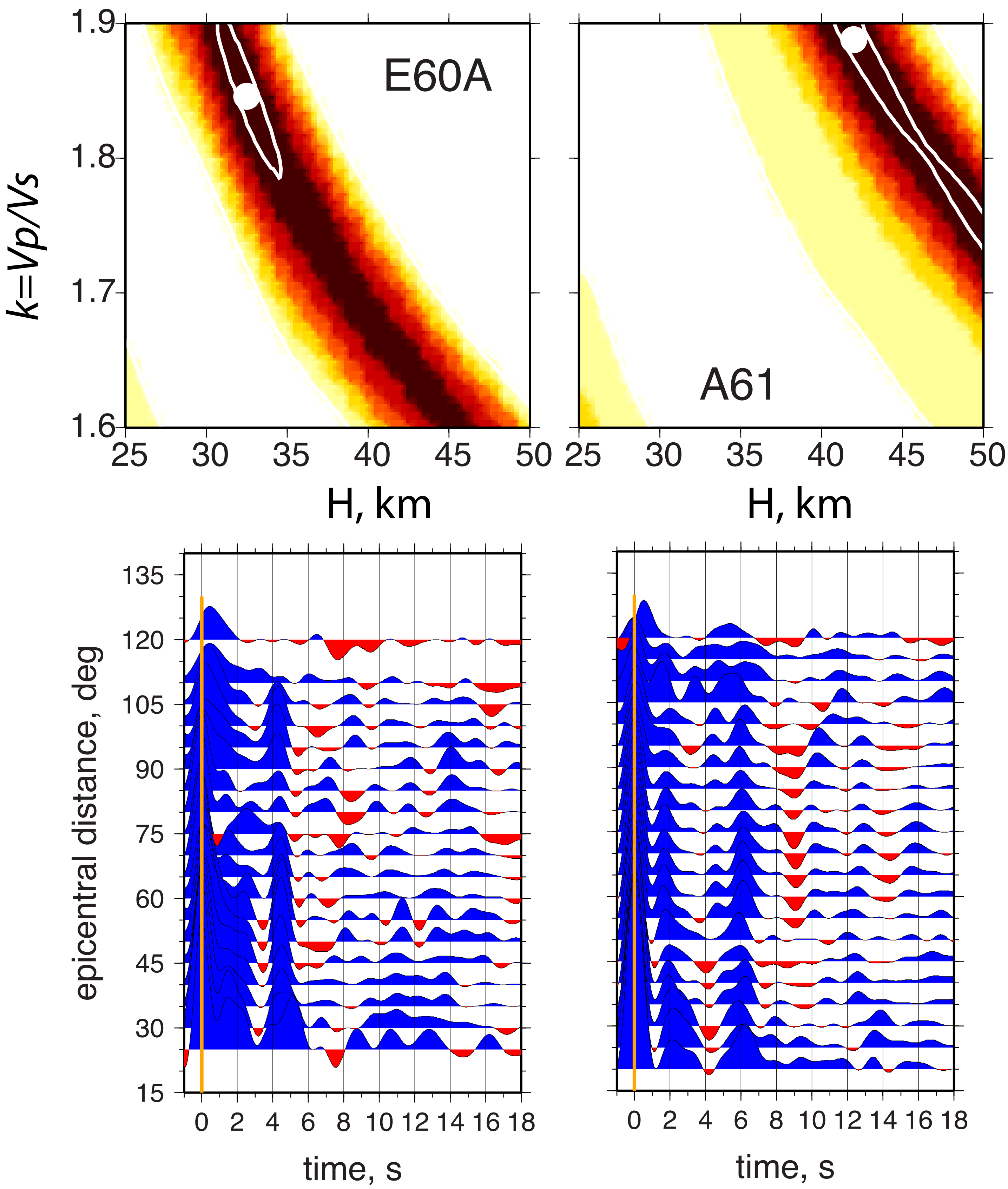

E60A
A61
k=Vp/Vs
1.9
1.8
1.7
1.6
25
30
35
40
45
50
H, km
epicentral distance, deg
135
120
105
90
75
60
45
30
15
0
2
4
6
8
10
12
14
16
18
time, s

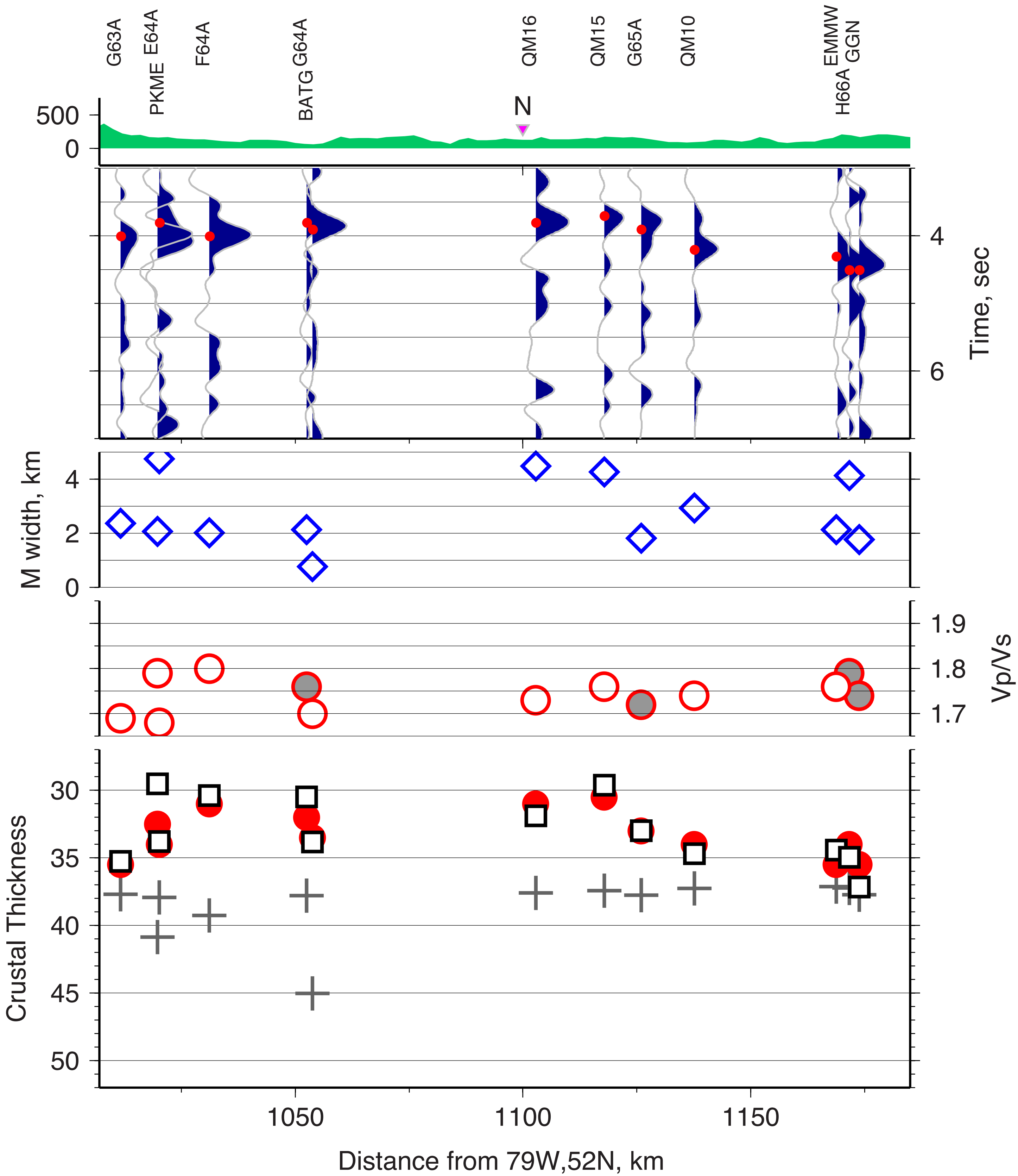

G63A
E64A
PKME
F64A
G64A
BATG
QM16
QM15
G65A
QM10
EMMW
GGN
H66A
N
500
0
4
6
Time, sec
M width, km
4
2
0
1.9
1.8
1.7
Vp/Vs
Crustal Thickness
30
35
40
45
50
1050
1100
1150
Distance from 79W,52N, km

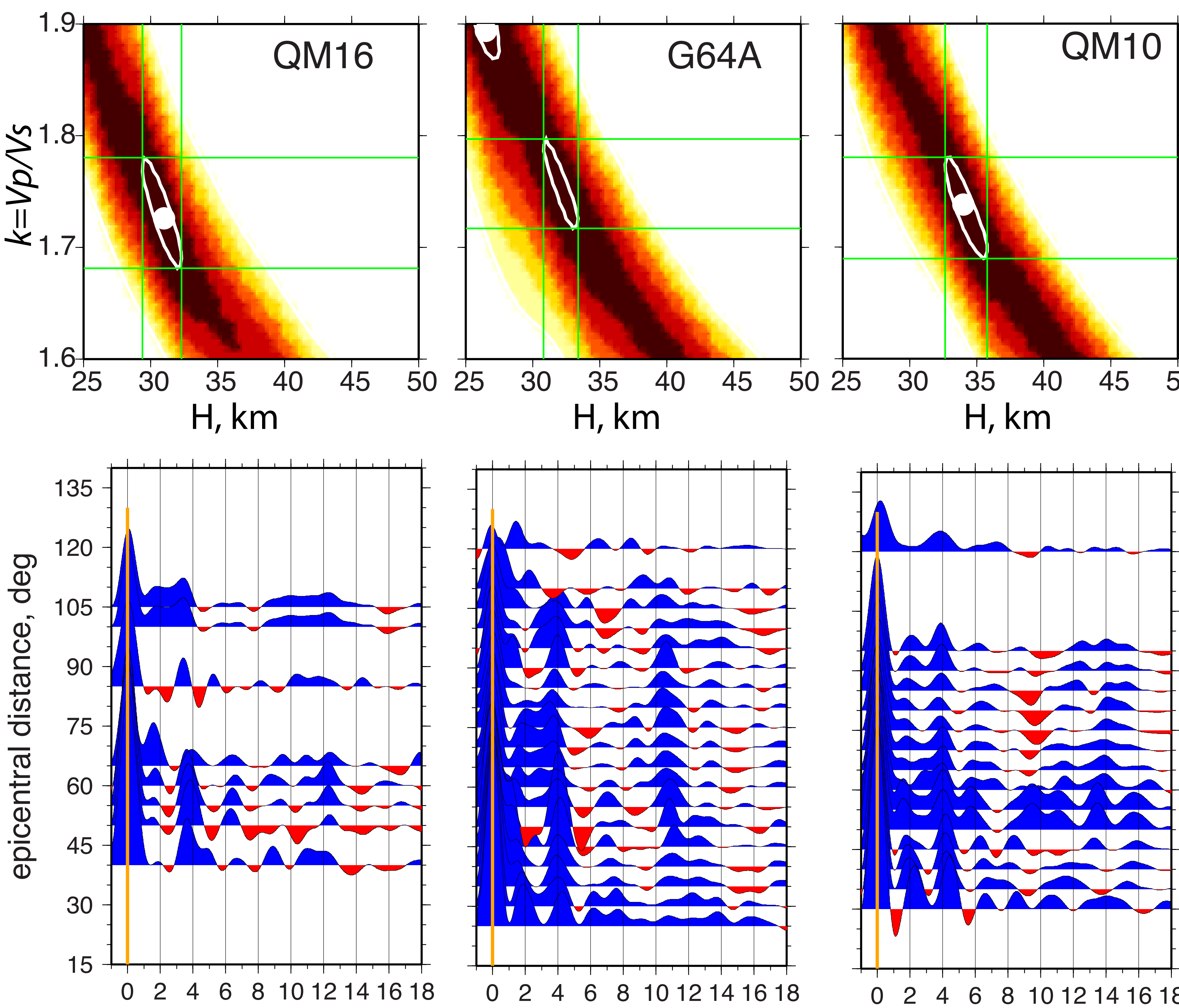

QM16
G64A
QM10
k=Vp/Vs
1.9
1.8
1.7
1.6
25
30
35
40
45
50
H, km
135
120
105
90
75
60
45
30
15
epicentral distance, deg
0
2
4
6
8
10
12
14
16
18
time, s

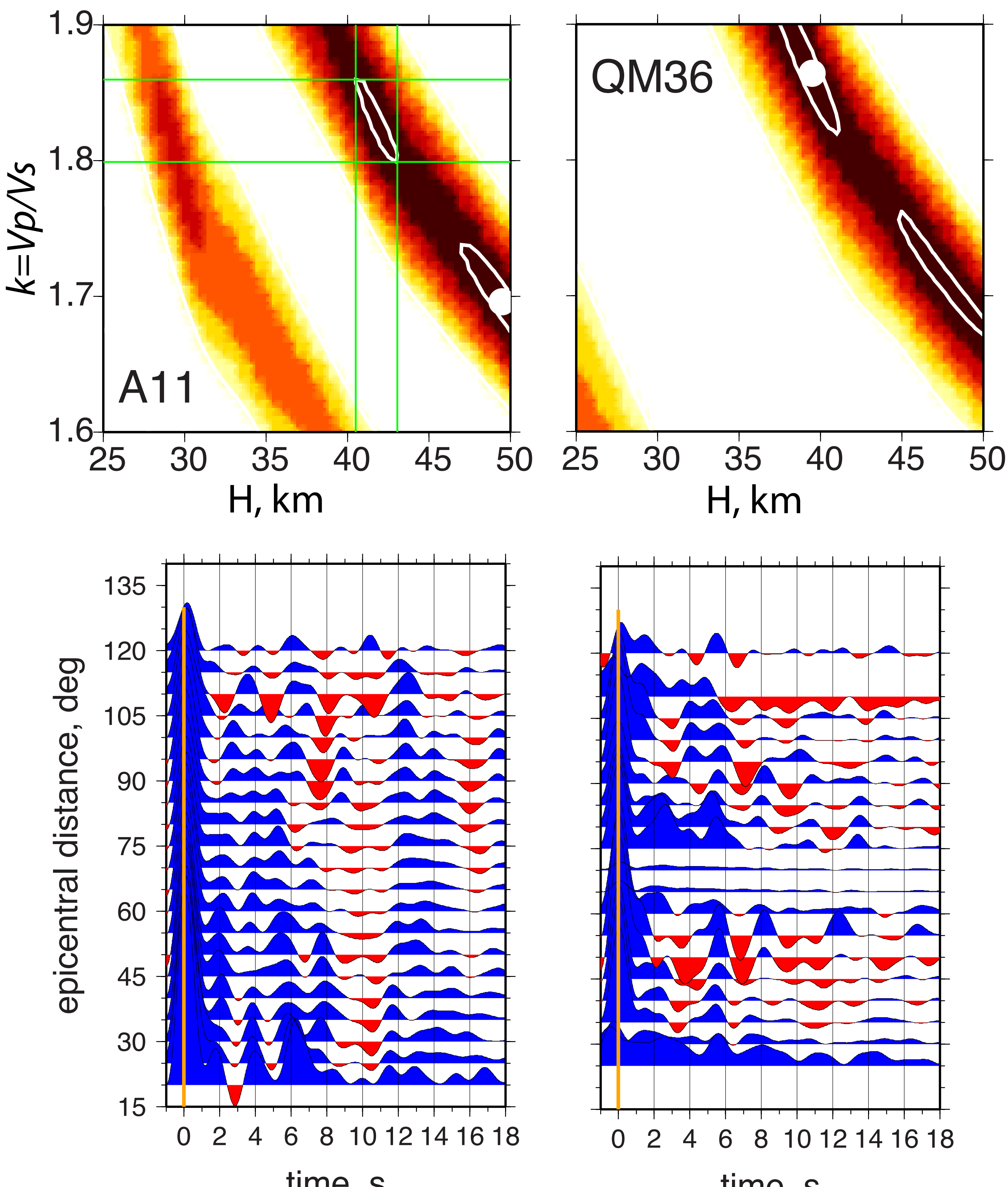

A11
QM36
k=Vp/Vs
H, km
epicentral distance, deg
time, s

Crustal thickness and Moho Width

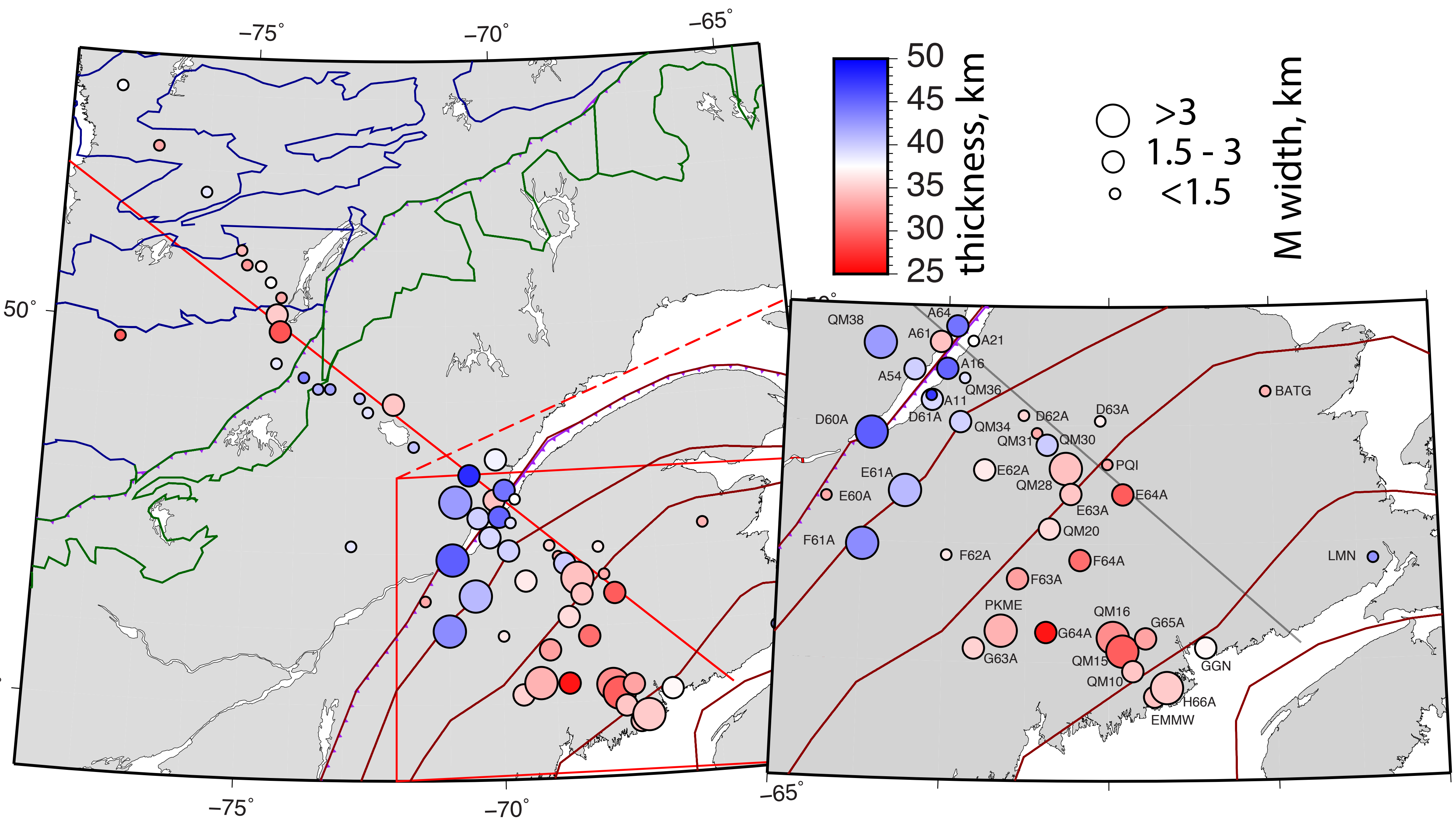

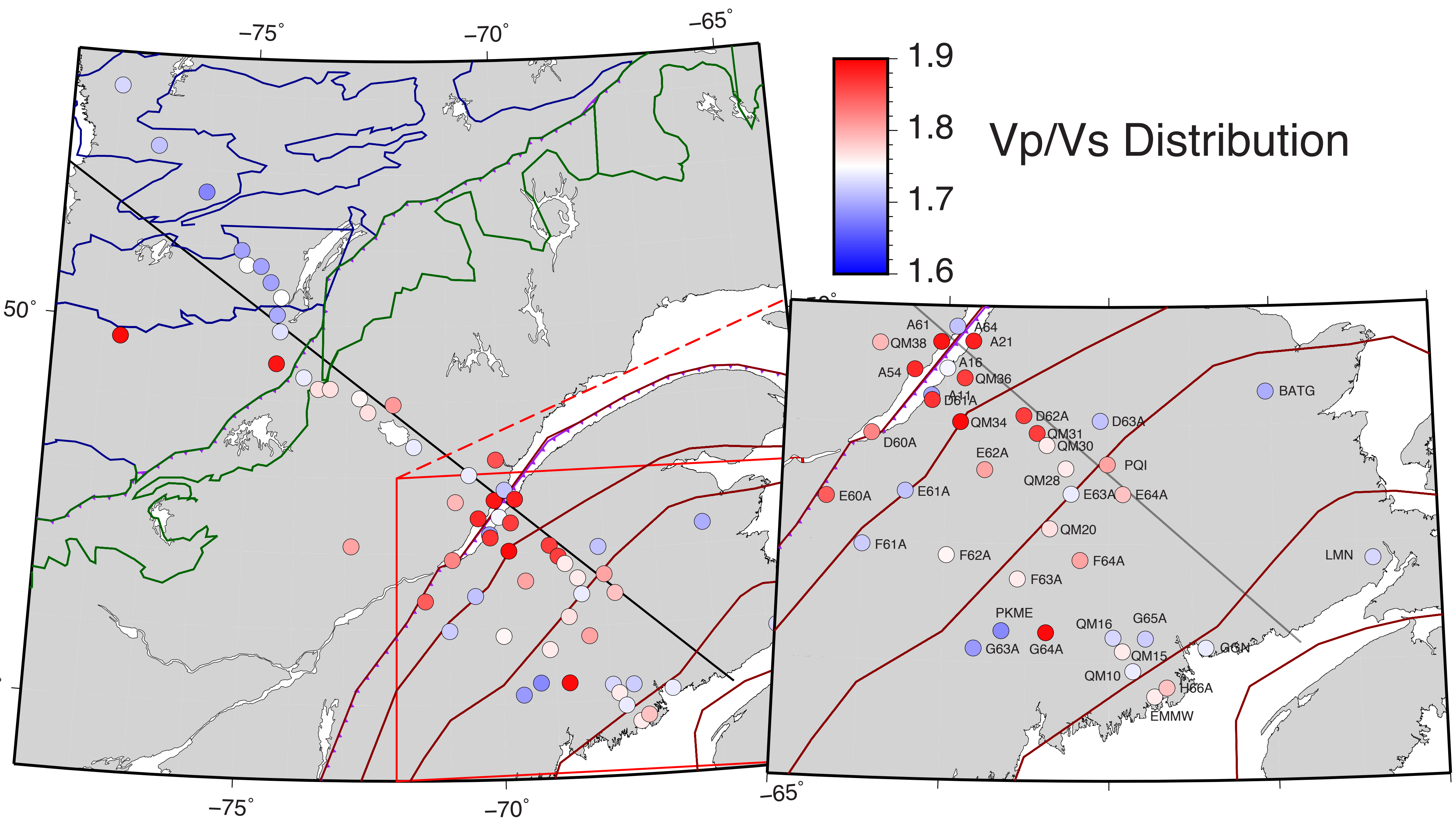
Vp/Vs Distribution
1.9
1.8
1.7
1.6
−75°
−70°
−65°
50°
45°
A61
A64
A21
QM38
A16
A54
QM36
A11
D61A
D62A
D63A
QM34
QM31
QM30
BATG
D60A
E62A
PQI
QM28
E60A
E61A
E63A
E64A
QM20
F61A
F62A
F64A
LMN
F63A
PKME
G63A
G64A
QM16
G65A
QM15
QM10
H66A
EMMW

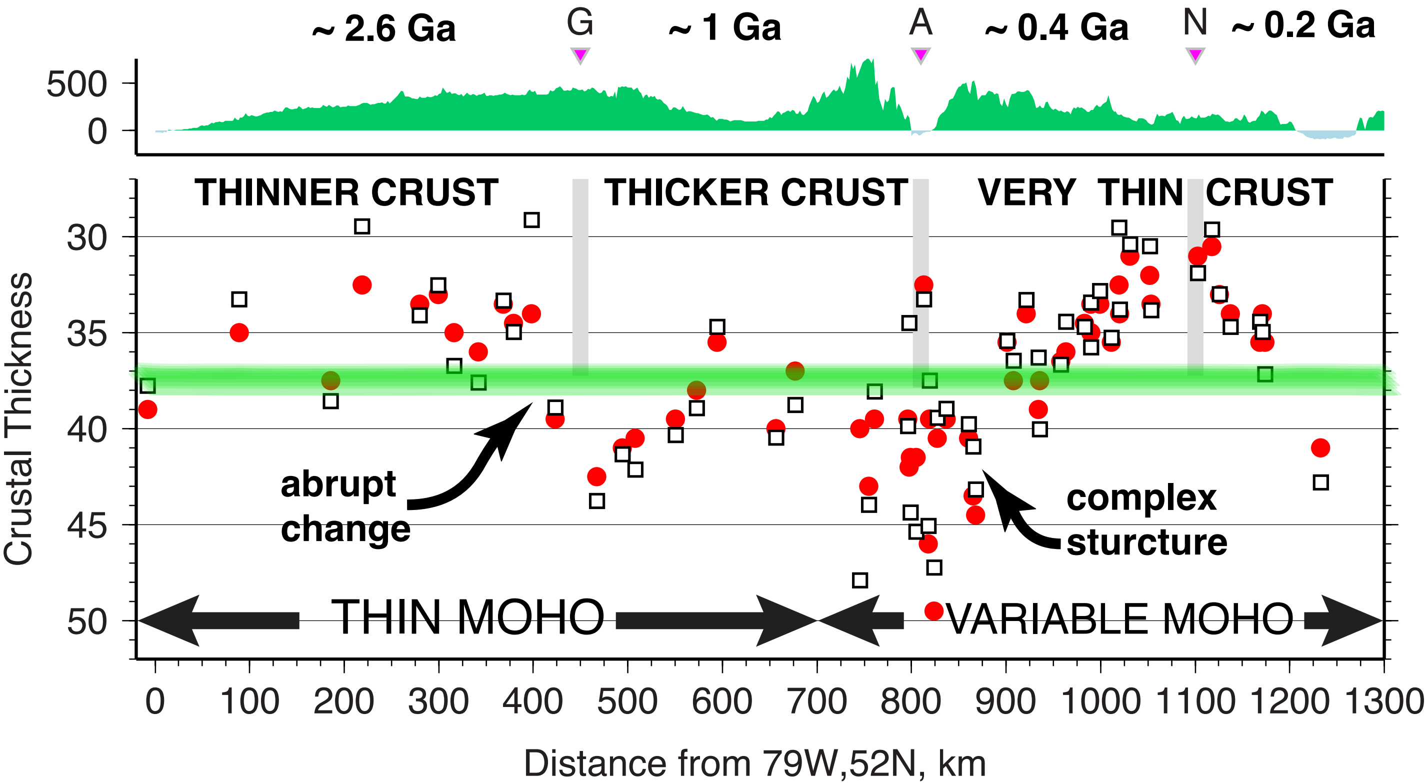
~ 2.6 Ga
G
~ 1 Ga
A
~ 0.4 Ga
N
~ 0.2 Ga
500
0
THINNER CRUST
THICKER CRUST
VERY THIN CRUST
30
35
40
45
50
Crustal Thickness
abrupt change
complex sturcture
THIN MOHO
VARIABLE MOHO
0
100
200
300
400
500
600
700
800
900
1000
1100
1200
1300
Distance from 79W,52N, km

Supplement to

Crust-mantle boundary in eastern North America, from the (oldest) craton to the (youngest) rift.

Vadim Levin1, Andrea Servali1, Jill VanTongeren1, William Menke2, Fiona Darbyshire3

1. Department of Earth and Planetary Sciences, Rutgers University
2. Department of Earth and Environmental Sciences, Columbia University
3. University of Quebec, Montreal

Supplementary Figure 1.
Contours of average compressional wave speed (Vp) in the crust adapted from Tesauro et al. (2014).

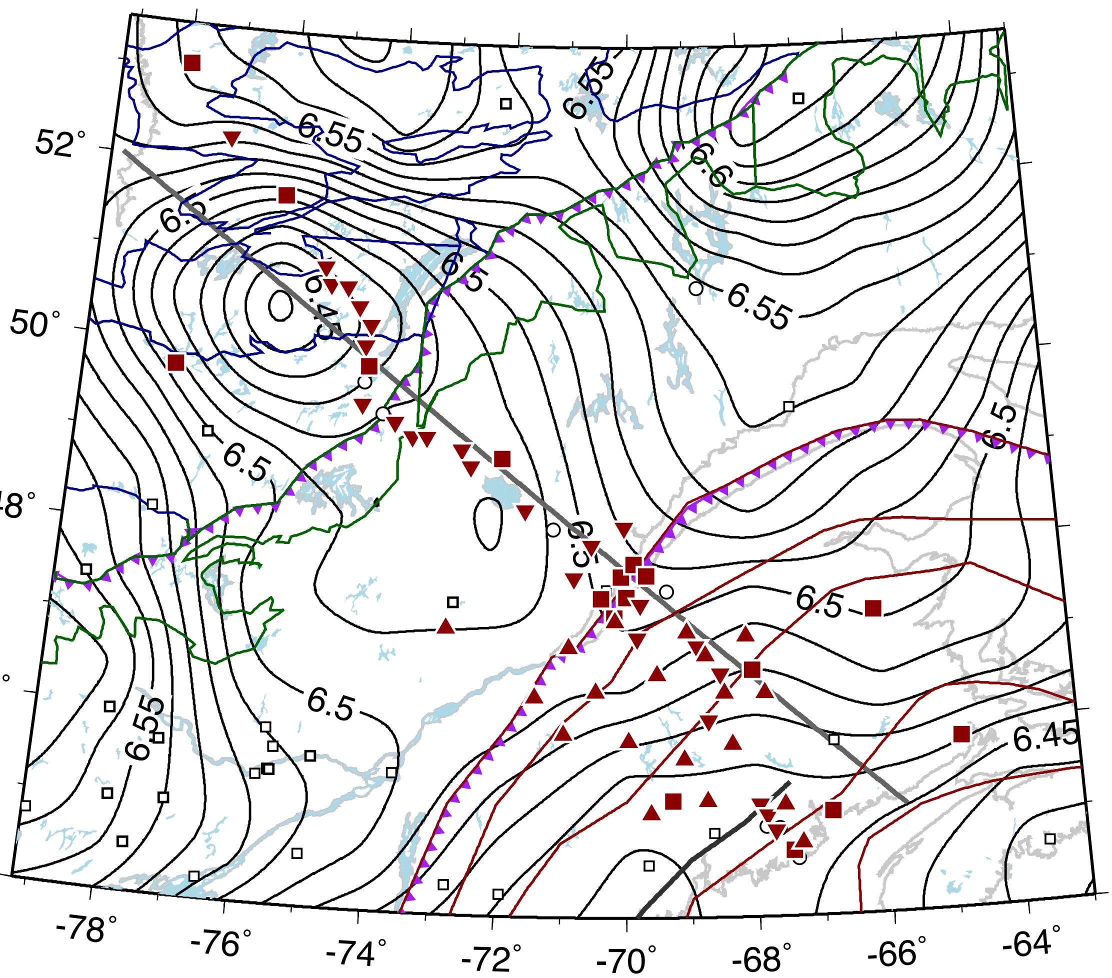

Supplementary Figure 2.

Data plots for all seismic stations included in our analysis.
For every location we show an epicentral gather of receiver functions (left plot), a set of frequency-dependent receiver function beams (right plot), and an H-k stacking result in the form of a shaded surface (center plot).

White dots mark maximum of the stack, the white contours show values at 95% of the maximum. Green lines show min/max values of that contour if they fall within the search box. Exact values of H and k corresponding to the white dot are given in Table 1 of the main text.

Plots are arranged in the order of their appearance on the transect, from NW to SE (see Table 1 of the main text for site names and locations).
Frequency-dependent receiver function beams are constructed for earthquake sources in Central America.

Purple stars mark the timeseries we chose as those with the highest frequency of unmodified PmS phase.

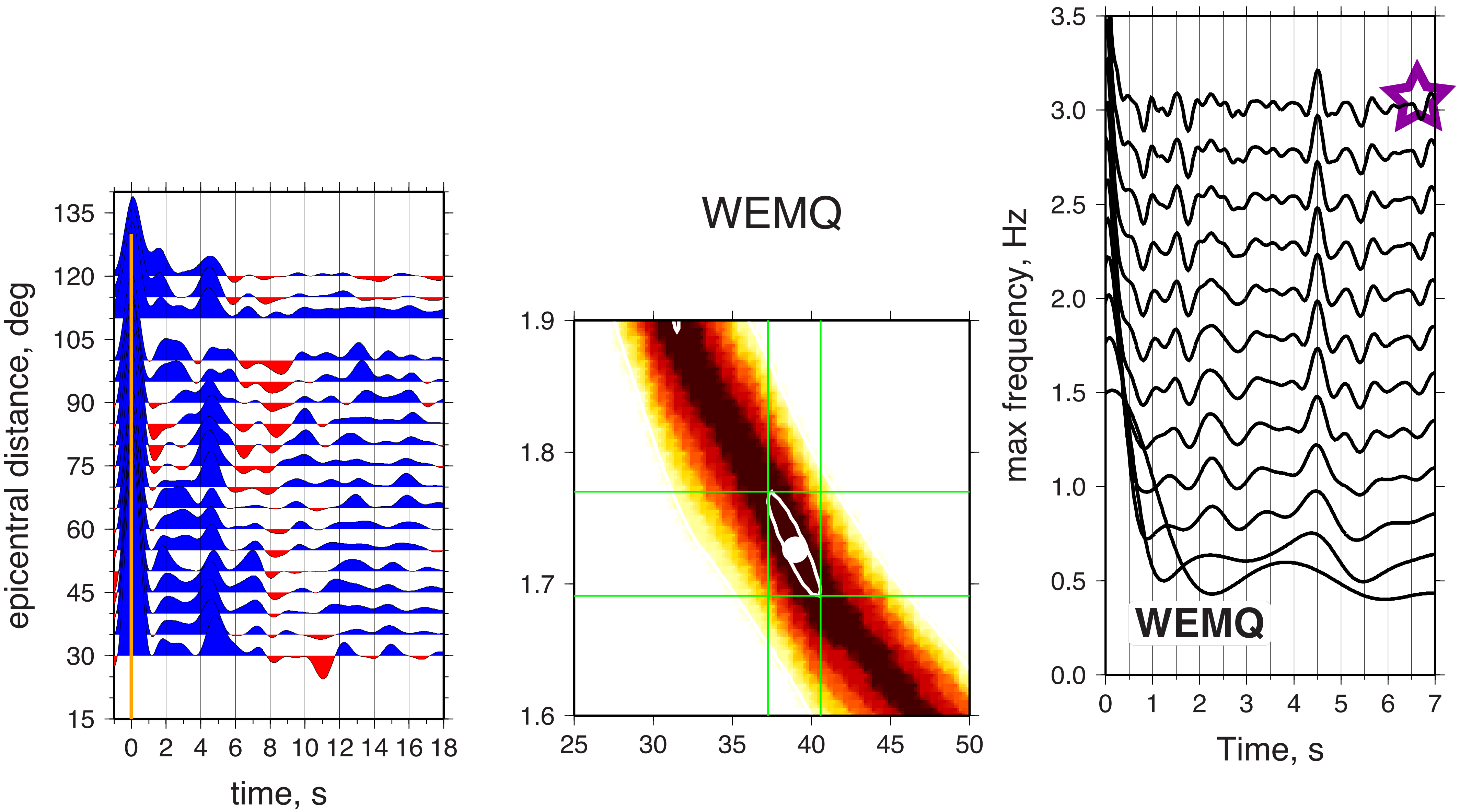

WEMQ
epicentral distance, deg
135
120
105
90
75
60
45
30
15
0
2
4
6
8
10
12
14
16
18
time, s
1.9
1.8
1.7
1.6
25
30
35
40
45
50
max frequency, Hz
3.5
3.0
2.5
2.0
1.5
1.0
0.5
0.0
0
1
2
3
4
5
6
7
Time, s
WEMQ

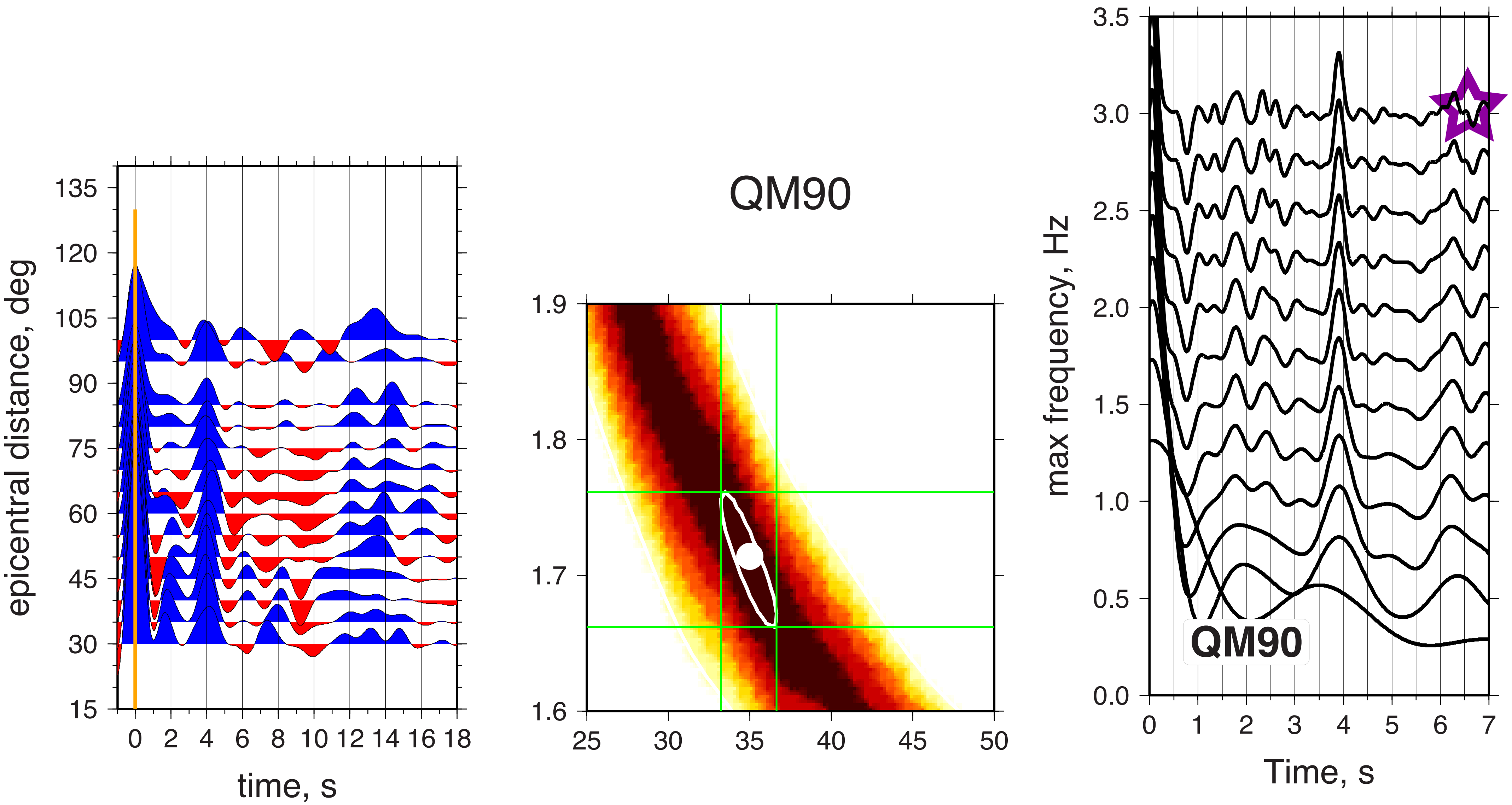

epicentral distance, deg
135
120
105
90
75
60
45
30
15
0 2 4 6 8 10 12 14 16 18
time, s
QM90
1.9
1.8
1.7
1.6
25 30 35 40 45 50
max frequency, Hz
3.5
3.0
2.5
2.0
1.5
1.0
0.5
0.0
0 1 2 3 4 5 6 7
Time, s
QM90

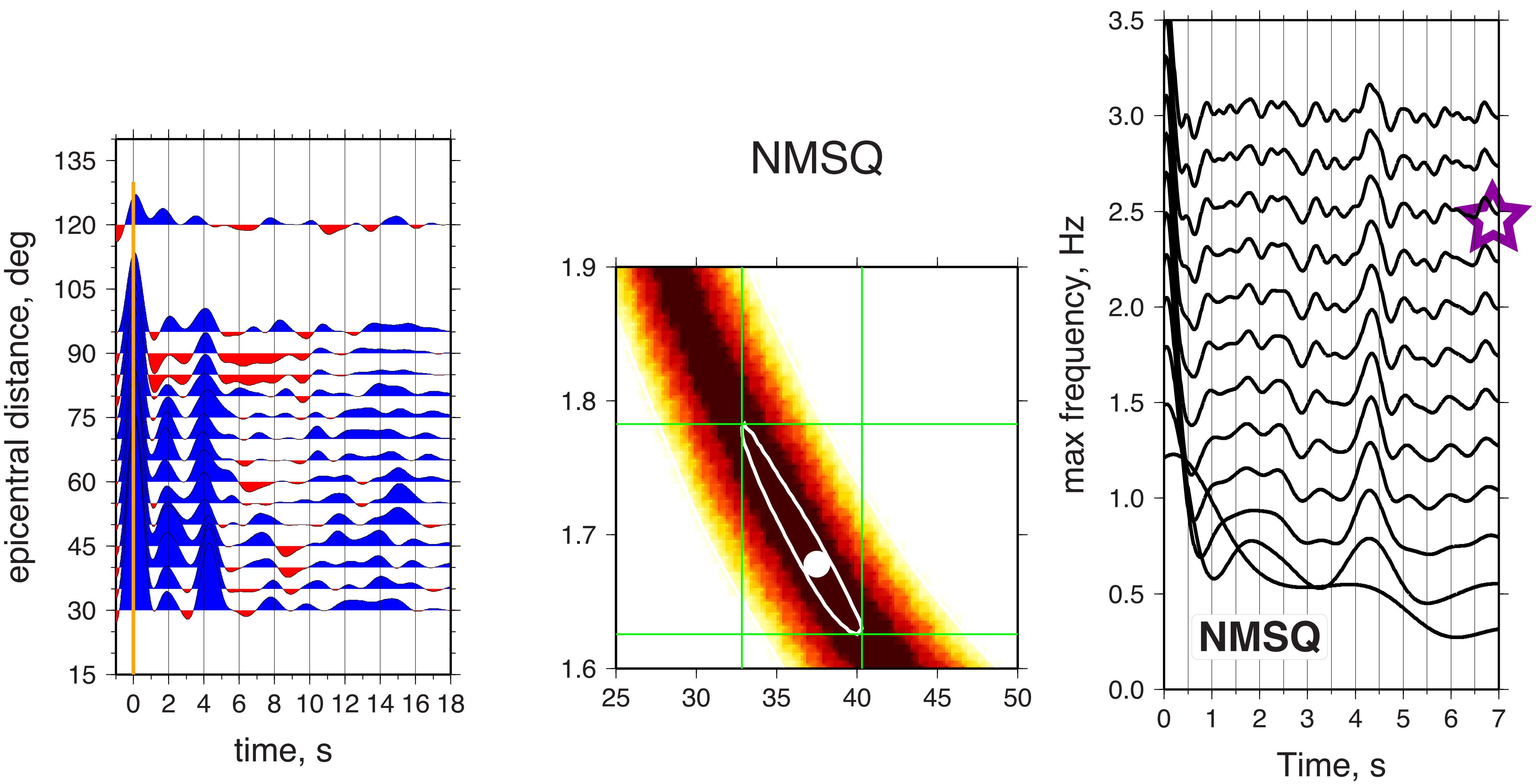

epicentral distance, deg
time, s
NMSQ
max frequency, Hz
Time, s
NMSQ

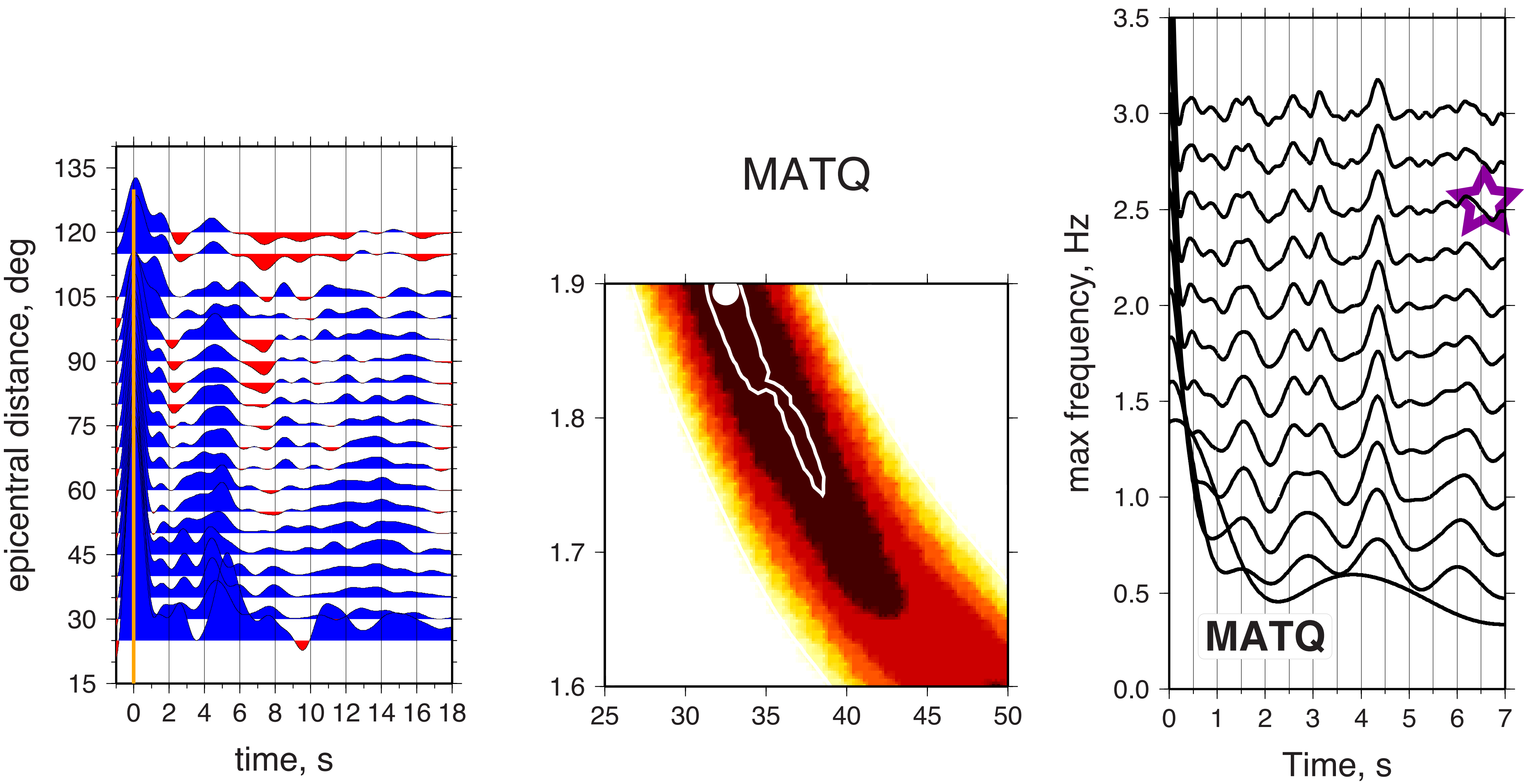
MATQ
epicentral distance, deg
time, s
max frequency, Hz
Time, s
MATQ

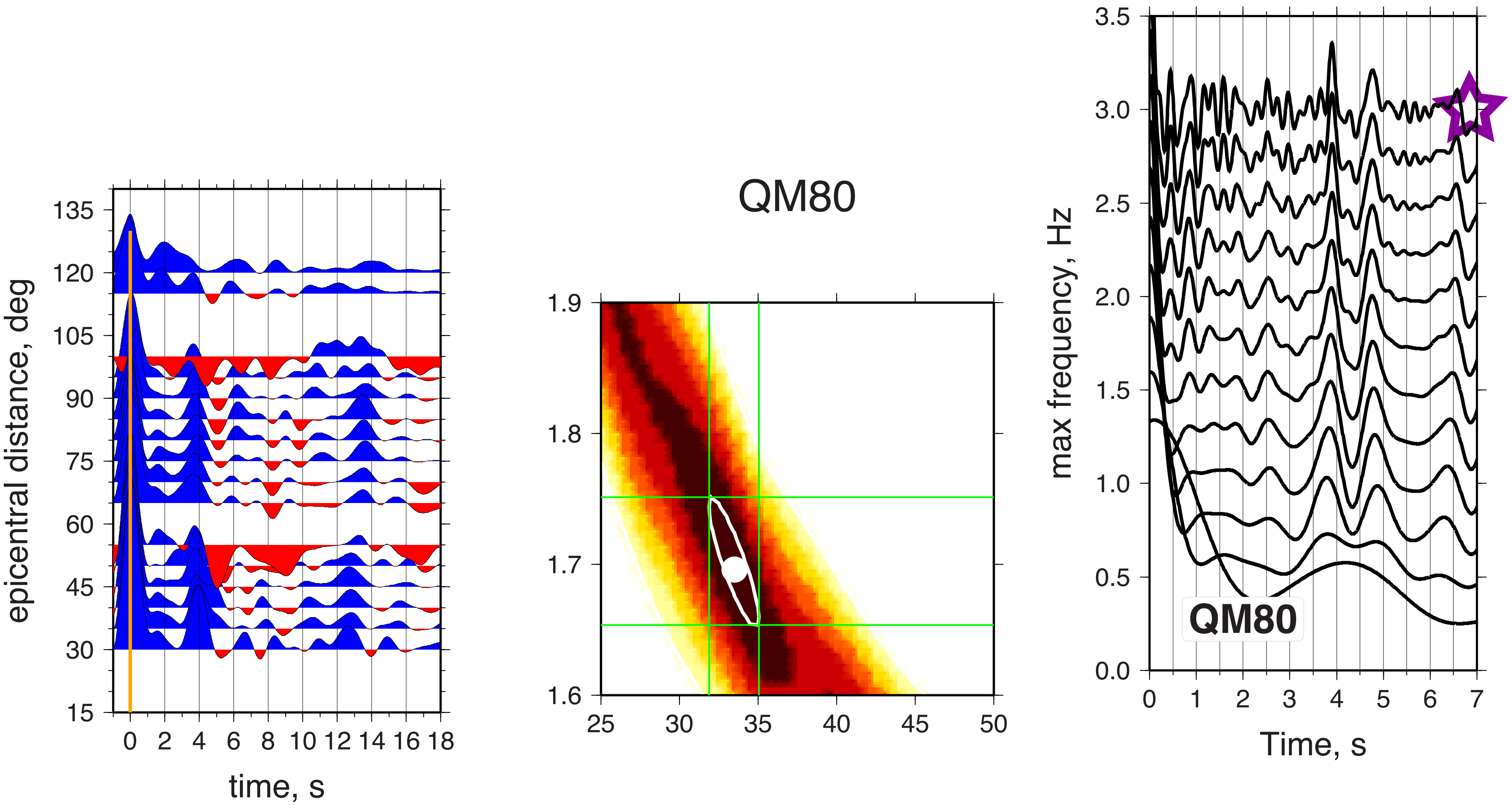

QM80
epicentral distance, deg
135
120
105
90
75
60
45
30
15
0 2 4 6 8 10 12 14 16 18
time, s
1.9
1.8
1.7
1.6
25 30 35 40 45 50
3.5
3.0
2.5
2.0
1.5
1.0
0.5
0.0
max frequency, Hz
QM80
0 1 2 3 4 5 6 7
Time, s

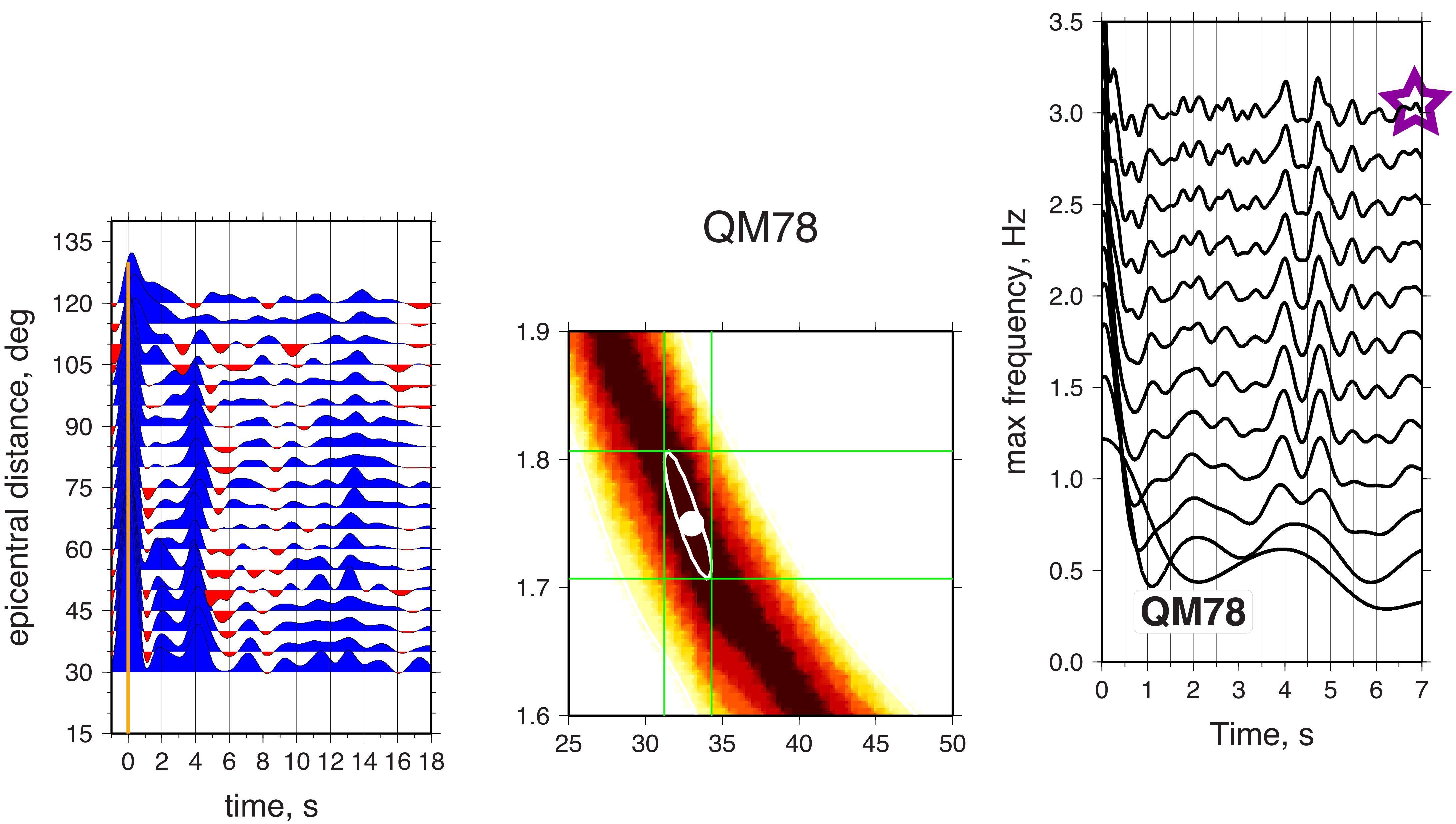
epicentral distance, deg
135
120
105
90
75
60
45
30
15
0 2 4 6 8 10 12 14 16 18
time, s
QM78
1.9
1.8
1.7
1.6
25 30 35 40 45 50
max frequency, Hz
3.5
3.0
2.5
2.0
1.5
1.0
0.5
0.0
QM78
0 1 2 3 4 5 6 7
Time, s

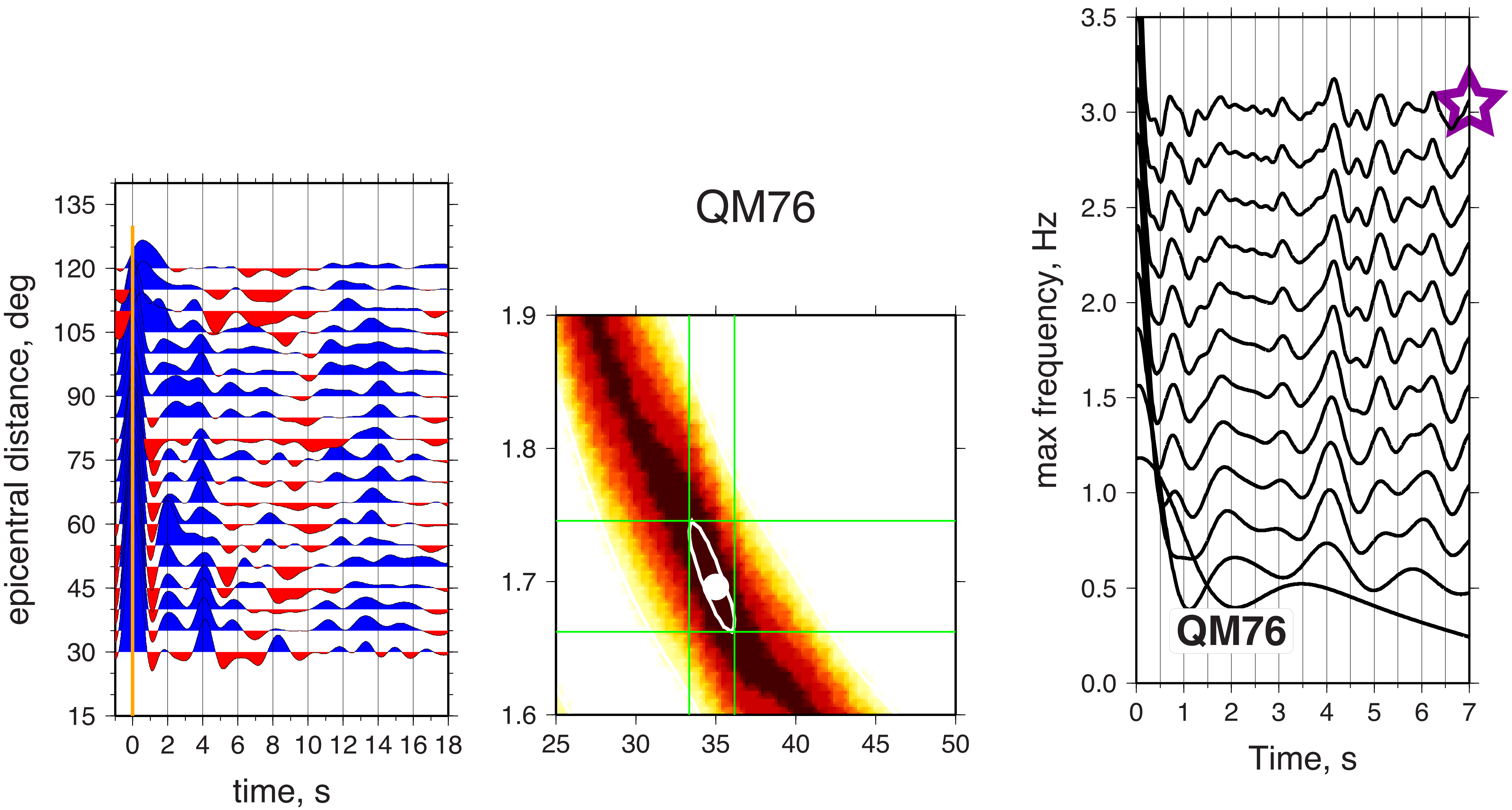

QM76
epicentral distance, deg
time, s
QM76
max frequency, Hz
Time, s

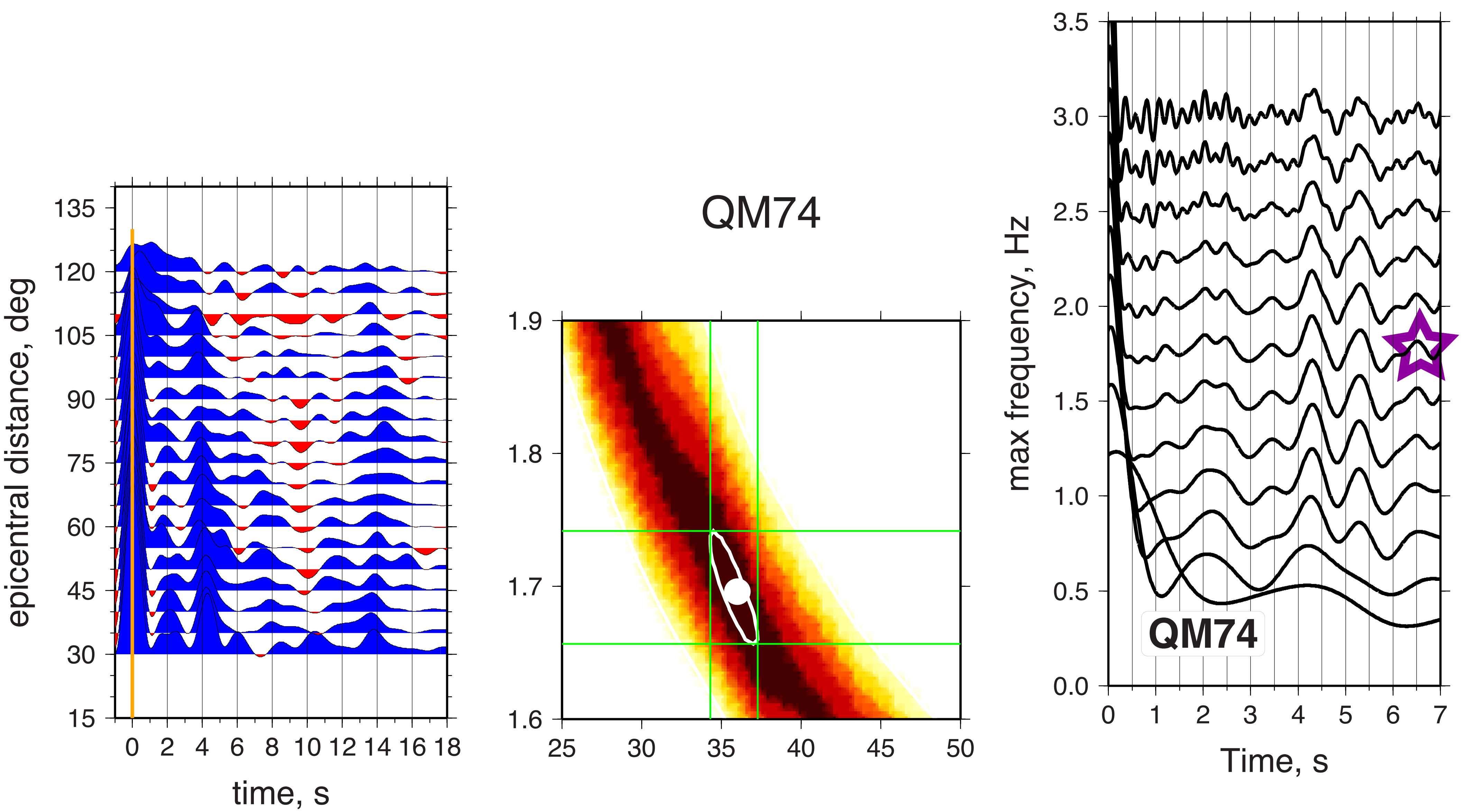

QM74
epicentral distance, deg
135
120
105
90
75
60
45
30
15
time, s
0
2
4
6
8
10
12
14
16
18
1.9
1.8
1.7
1.6
25
30
35
40
45
50
max frequency, Hz
3.5
3.0
2.5
2.0
1.5
1.0
0.5
0.0
Time, s
0
1
2
3
4
5
6
7
QM74

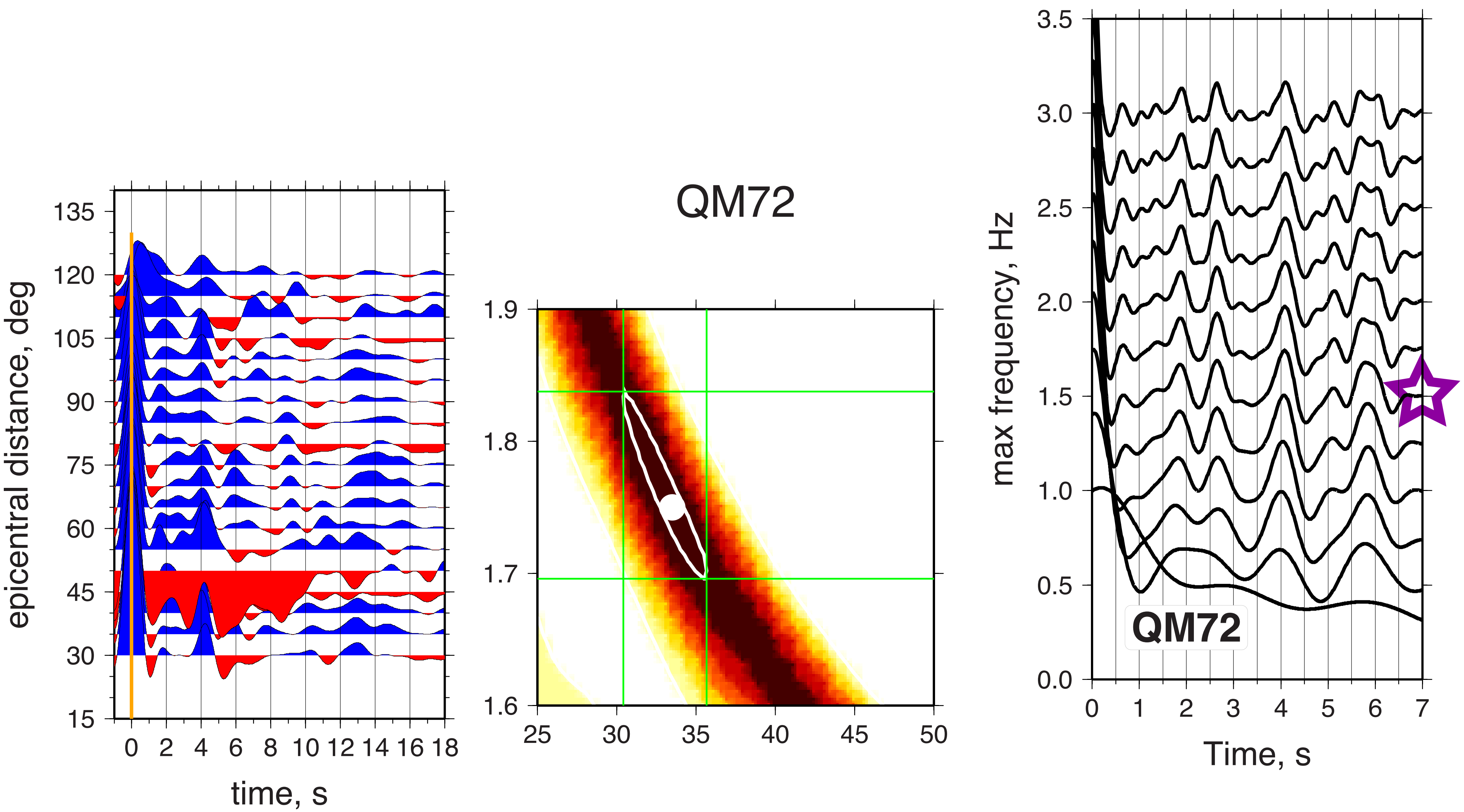
QM72
epicentral distance, deg
time, s
135
120
105
90
75
60
45
30
15
0 2 4 6 8 10 12 14 16 18
1.9
1.8
1.7
1.6
25 30 35 40 45 50
max frequency, Hz
3.5
3.0
2.5
2.0
1.5
1.0
0.5
0.0
0 1 2 3 4 5 6 7
Time, s
QM72

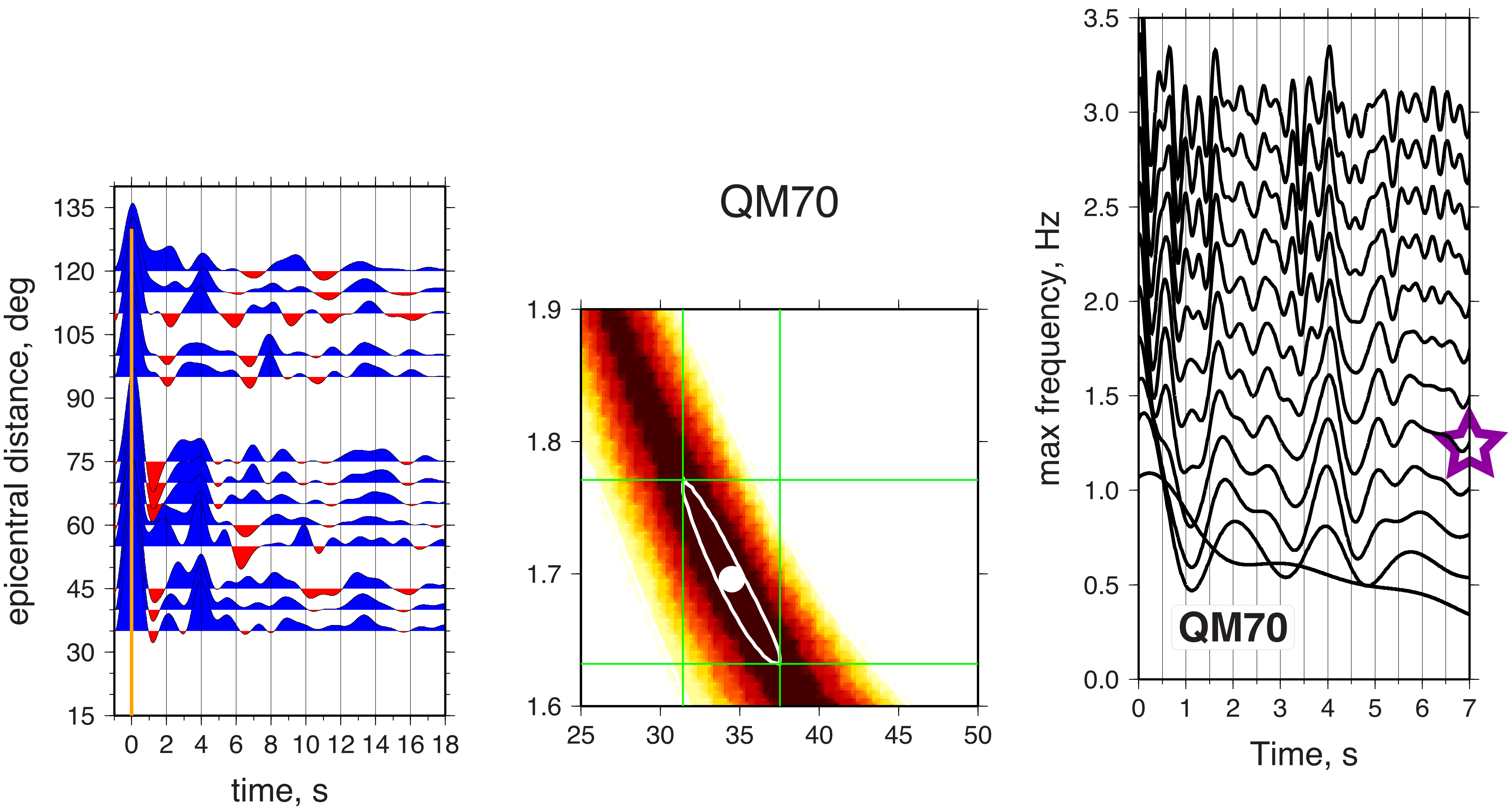

QM70
epicentral distance, deg
135
120
105
90
75
60
45
30
15
time, s
0
2
4
6
8
10
12
14
16
18
1.9
1.8
1.7
1.6
25
30
35
40
45
50
max frequency, Hz
3.5
3.0
2.5
2.0
1.5
1.0
0.5
0.0
Time, s
0
1
2
3
4
5
6
7
QM70

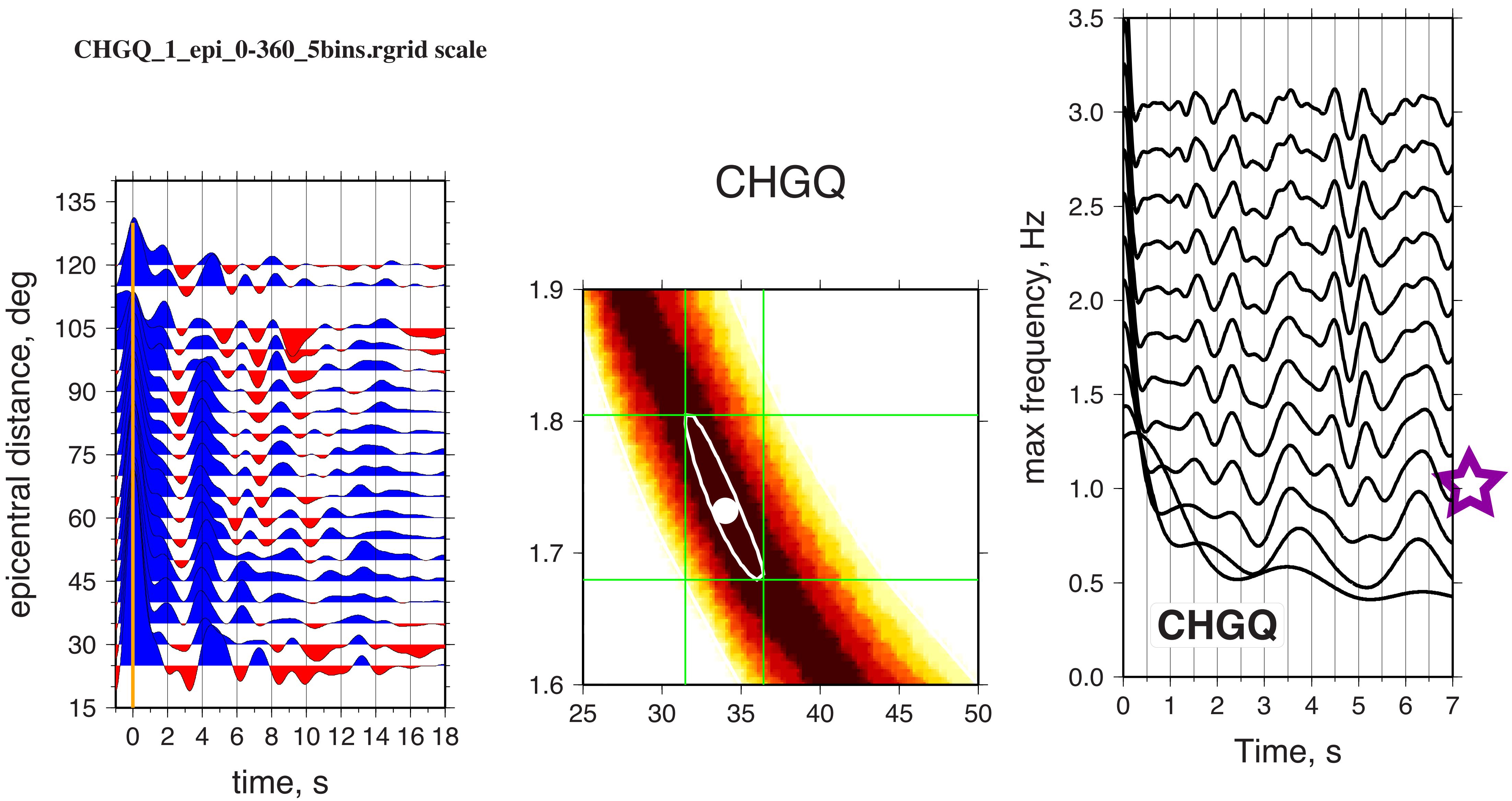

CHGQ_1_epi_0-360_5bins.rgrid scale
epicentral distance, deg
135
120
105
90
75
60
45
30
15
0
2
4
6
8
10
12
14
16
18
time, s
CHGQ
1.9
1.8
1.7
1.6
25
30
35
40
45
50
max frequency, Hz
3.5
3.0
2.5
2.0
1.5
1.0
0.5
0.0
0
1
2
3
4
5
6
7
Time, s
CHGQ

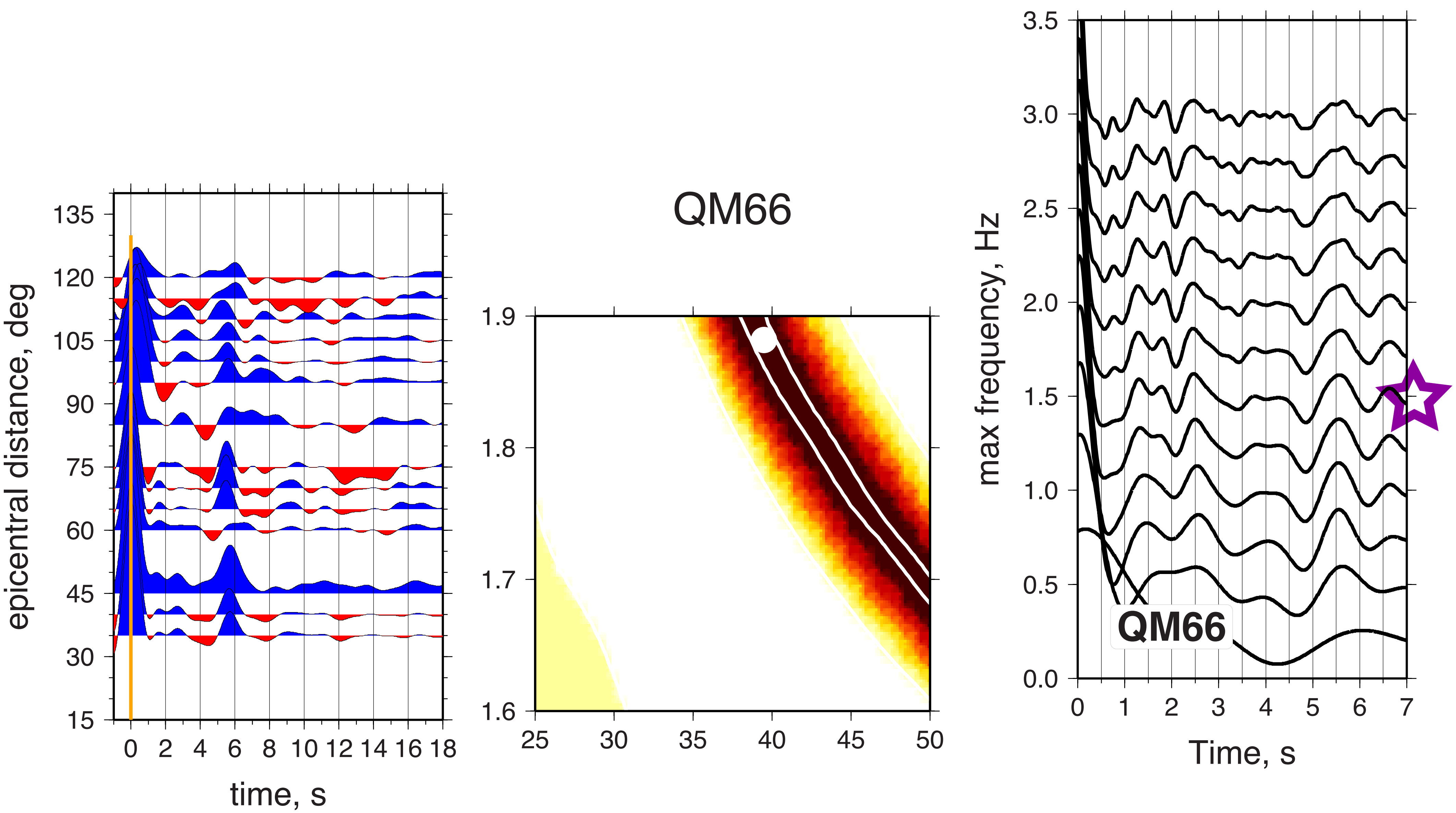
QM66
epicentral distance, deg
135
120
105
90
75
60
45
30
15
0
2
4
6
8
10
12
14
16
18
time, s
1.9
1.8
1.7
1.6
25
30
35
40
45
50
max frequency, Hz
3.5
3.0
2.5
2.0
1.5
1.0
0.5
0.0
1
3
5
7
Time, s
QM66

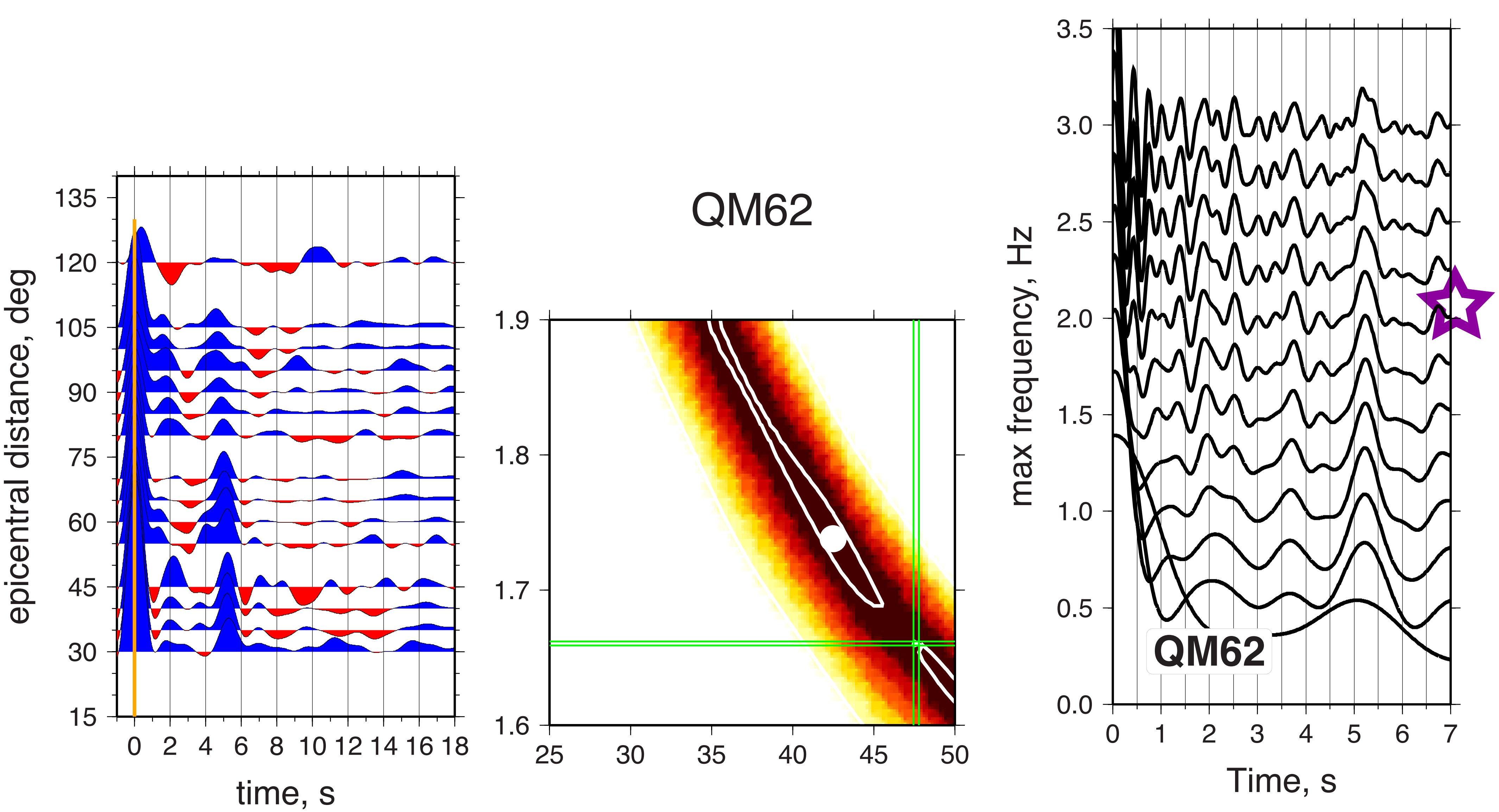
epicentral distance, deg
135
120
105
90
75
60
45
30
15
0
2
4
6
8
10
12
14
16
18
time, s
QM62
1.9
1.8
1.7
1.6
25
30
35
40
45
50
max frequency, Hz
3.5
3.0
2.5
2.0
1.5
1.0
0.5
0.0
0
1
2
3
4
5
6
7
Time, s
QM62

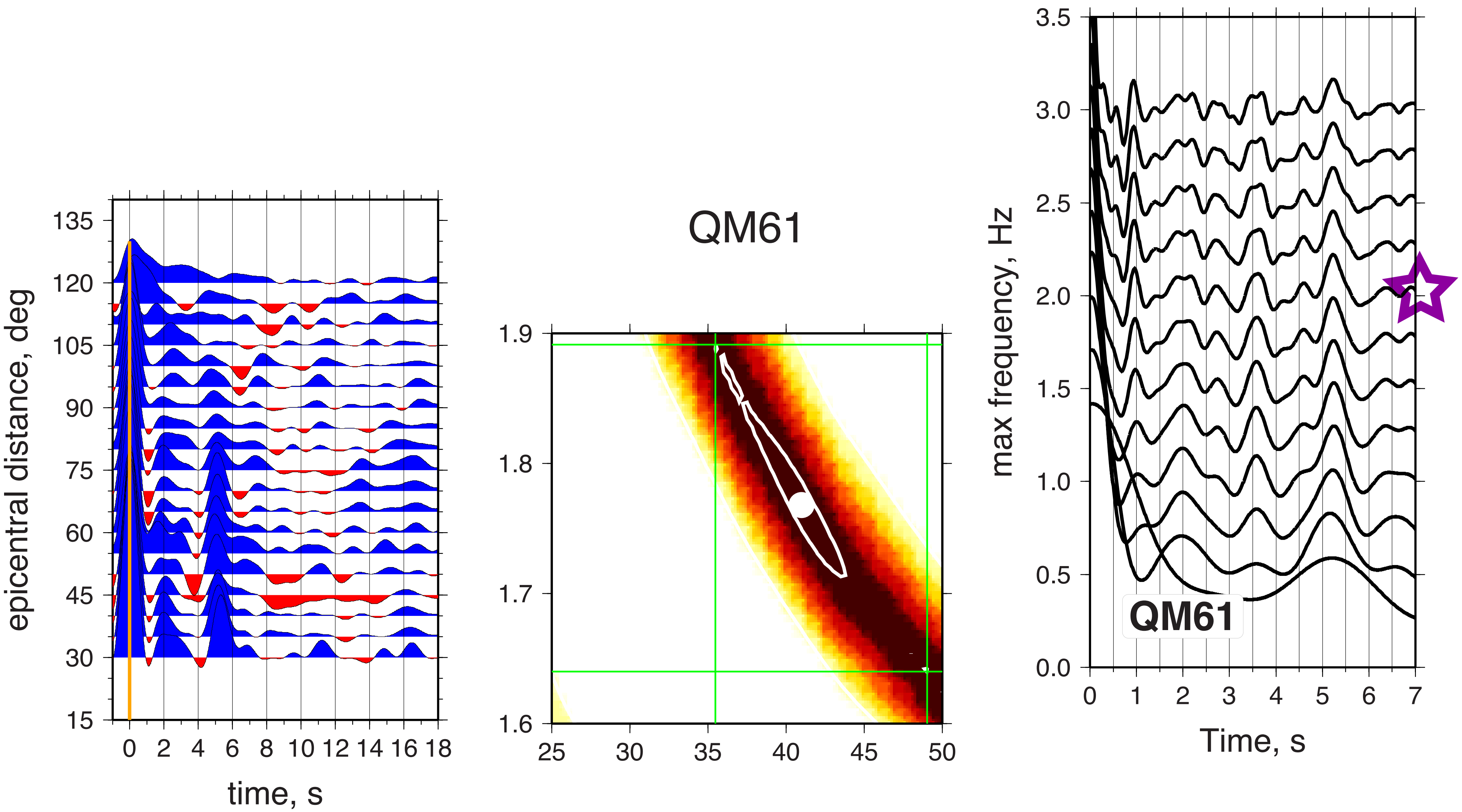

epicentral distance, deg
135
120
105
90
75
60
45
30
15
0 2 4 6 8 10 12 14 16 18
time, s
QM61
1.9
1.8
1.7
1.6
25 30 35 40 45 50
max frequency, Hz
3.5
3.0
2.5
2.0
1.5
1.0
0.5
0.0
0 1 2 3 4 5 6 7
Time, s
QM61

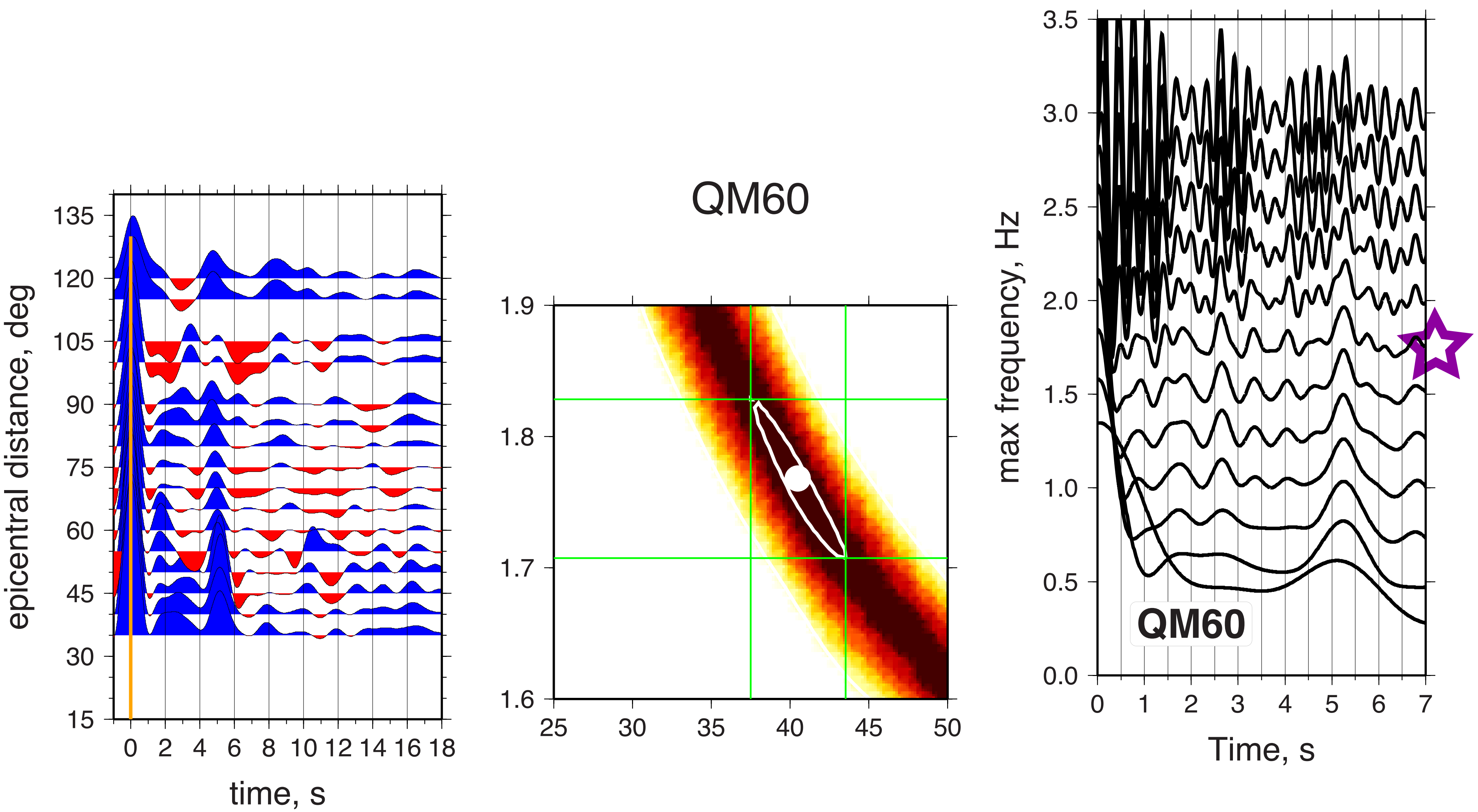

QM60
epicentral distance, deg
time, s
max frequency, Hz
Time, s
QM60

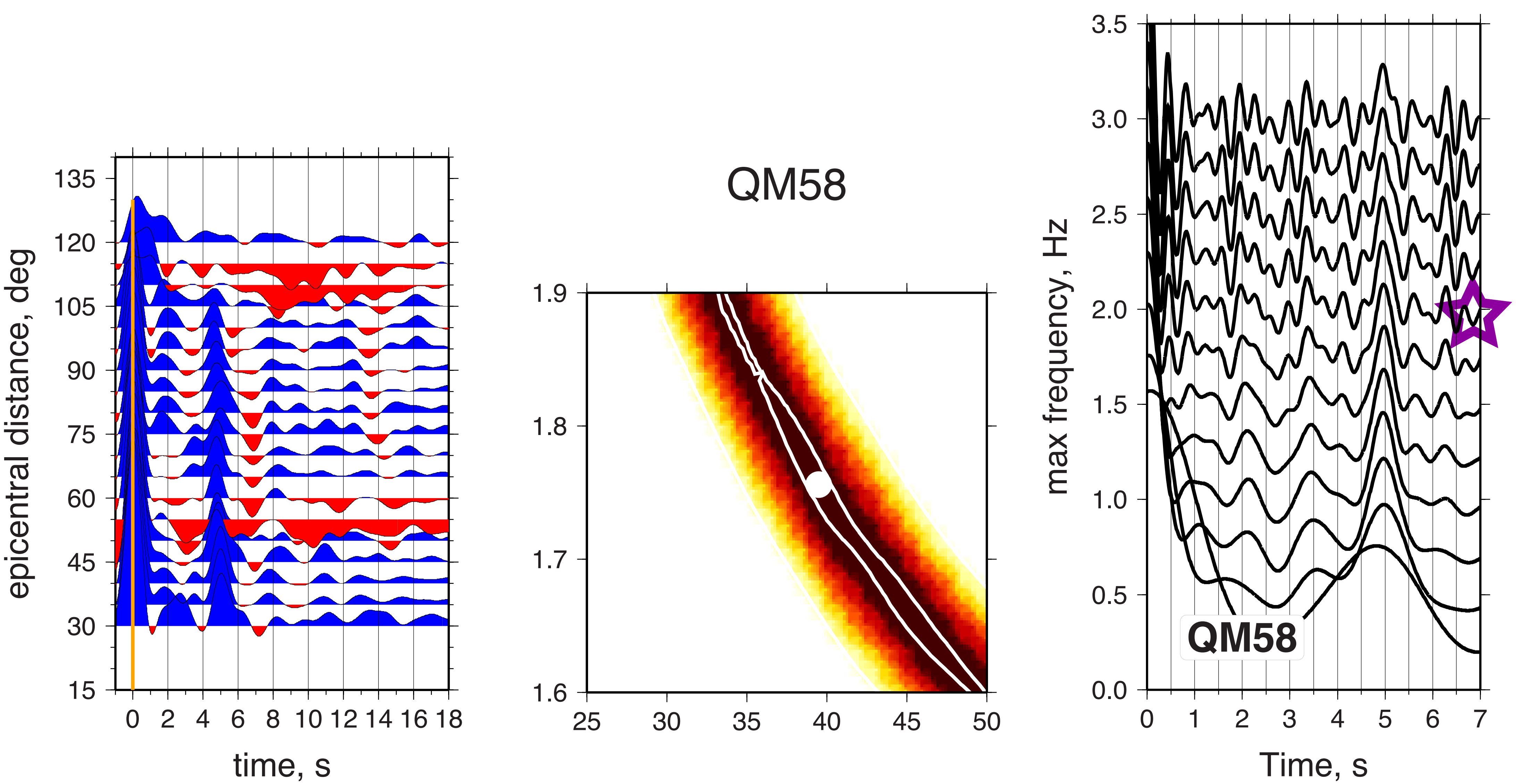
QM58
epicentral distance, deg
time, s
max frequency, Hz
Time, s
QM58
QM58

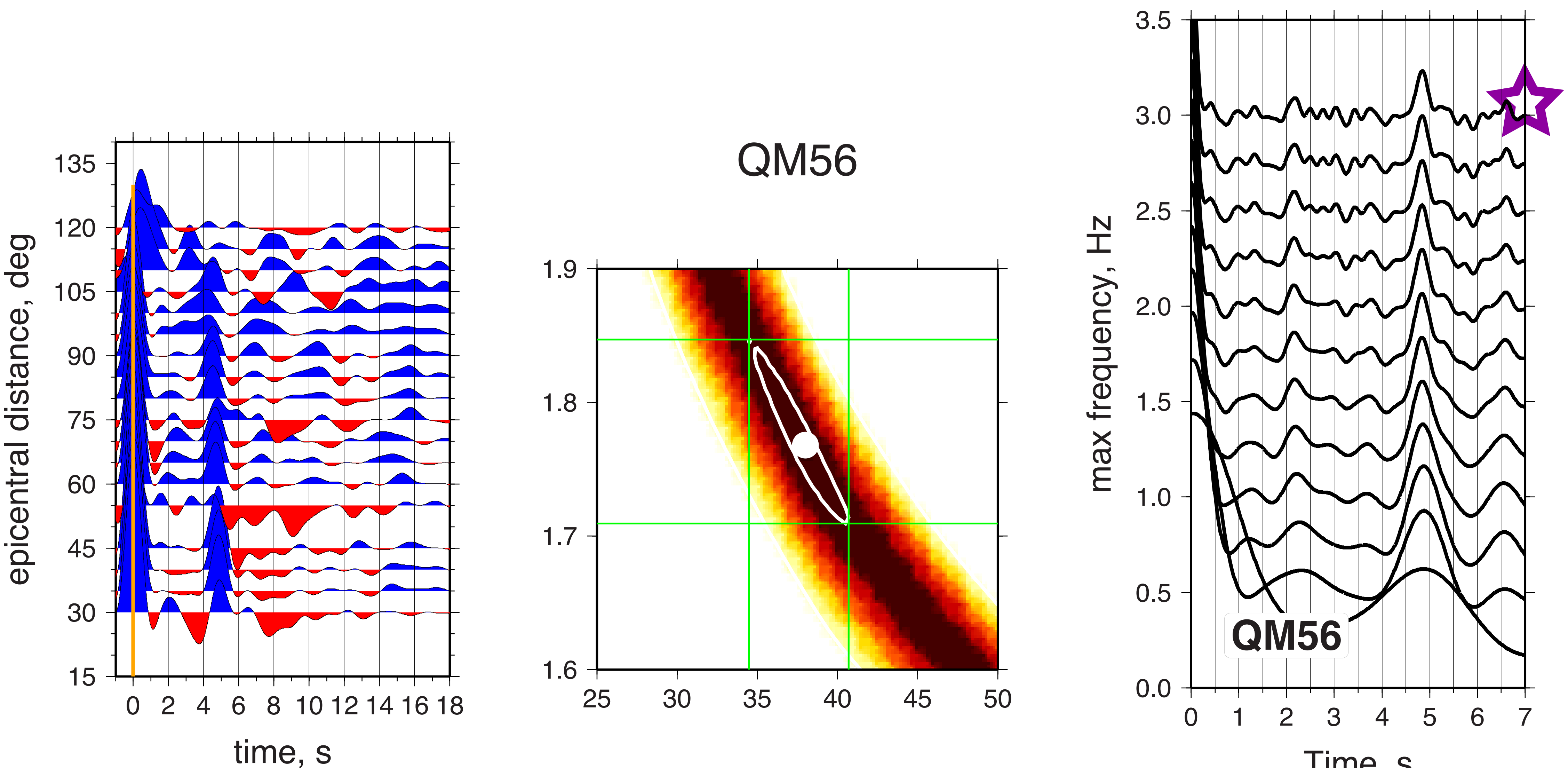

epicentral distance, deg
135
120
105
90
75
60
45
30
15
0 2 4 6 8 10 12 14 16 18
time, s
QM56
1.9
1.8
1.7
1.6
25 30 35 40 45 50
max frequency, Hz
3.5
3.0
2.5
2.0
1.5
1.0
0.5
0.0
0 1 2 3 4 5 6 7
Time, s
QM56

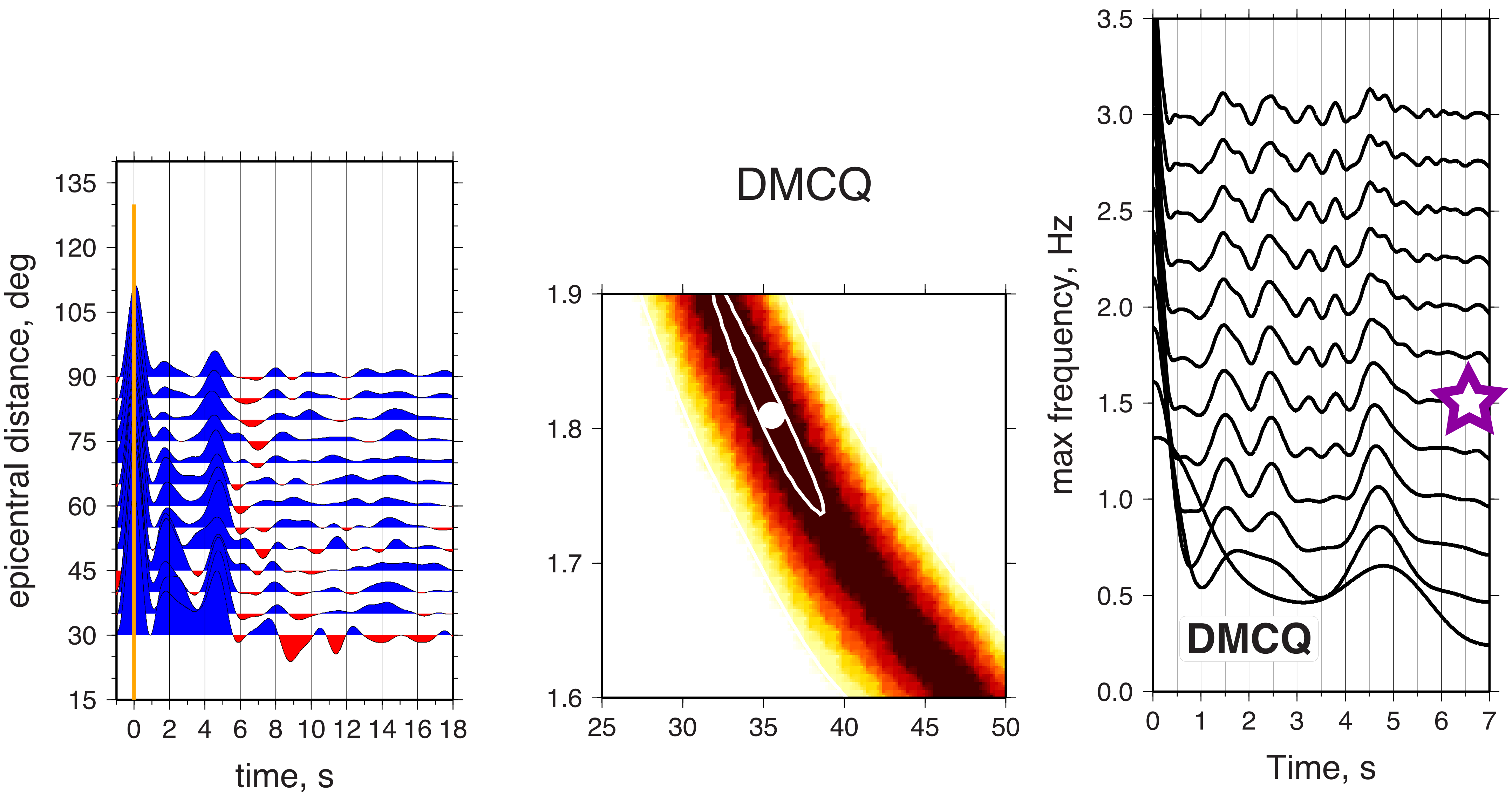

epicentral distance, deg
time, s
DMCQ
max frequency, Hz
Time, s
DMCQ

QM50_1_epi_0-360_5bins.rgrid scale

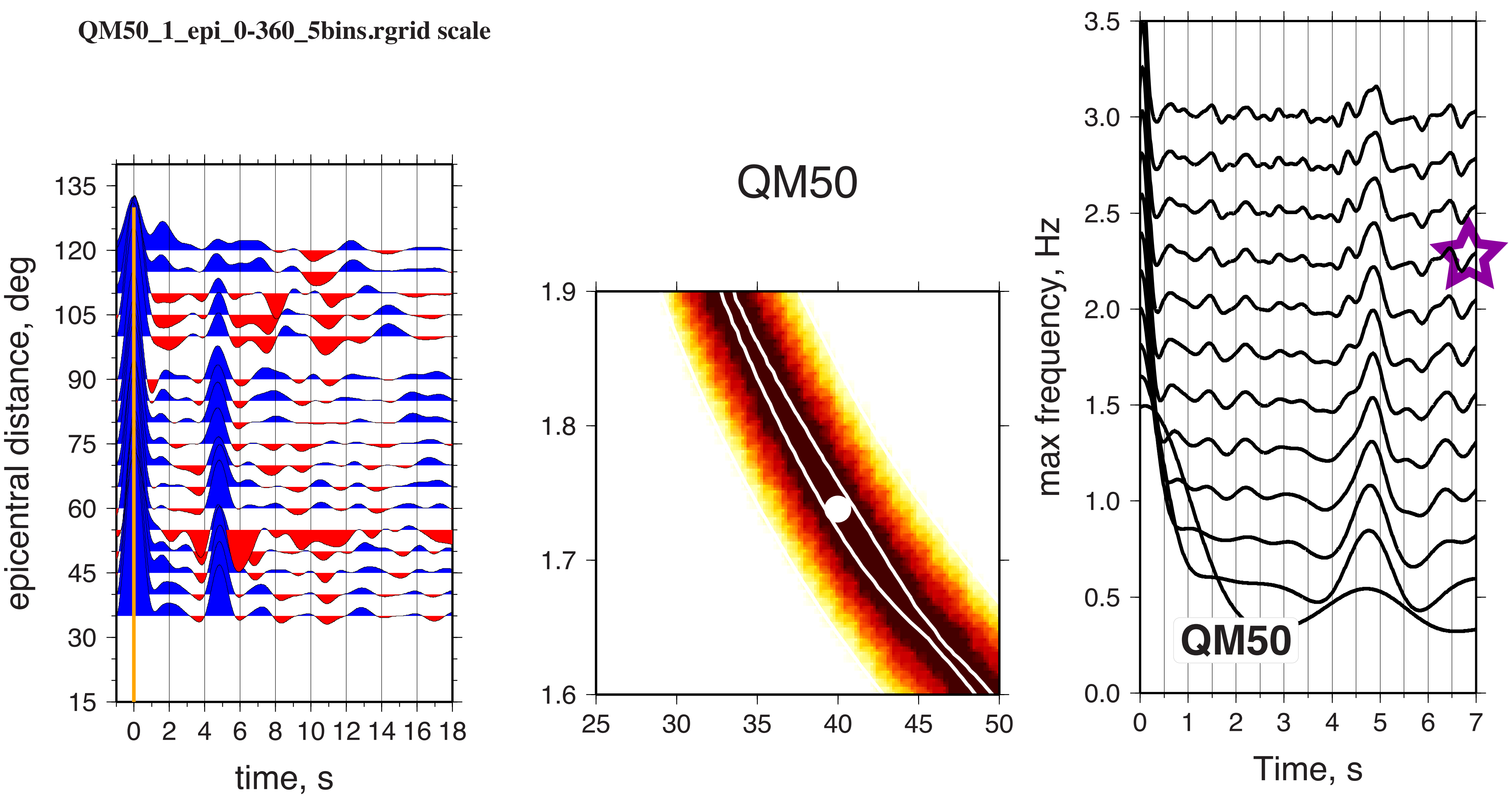

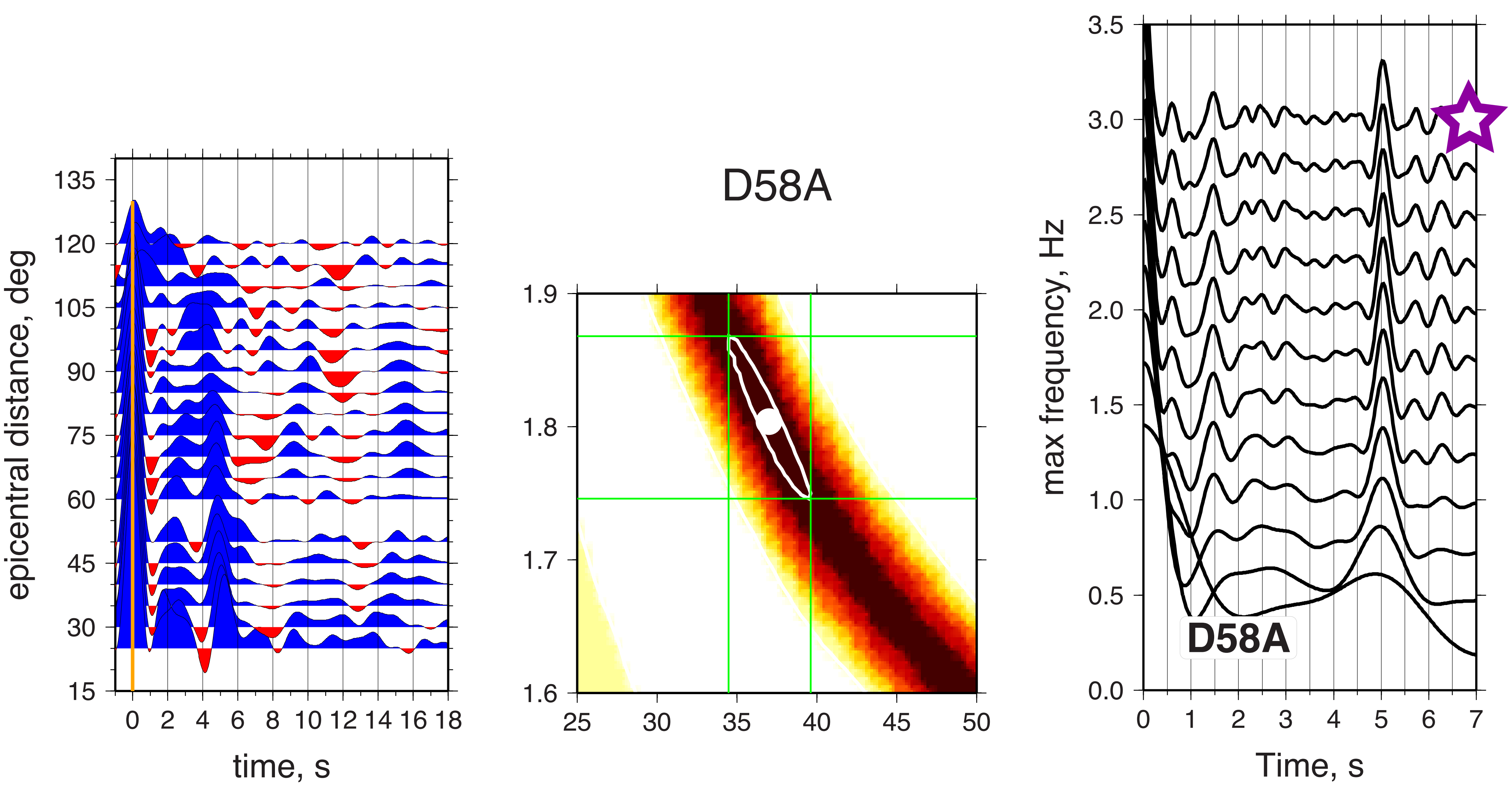

epicentral distance, deg
135
120
105
90
75
60
45
30
15
0
2
4
6
8
10
12
14
16
18
time, s
D58A
1.9
1.8
1.7
1.6
25
30
35
40
45
50
3.5
3.0
2.5
2.0
1.5
1.0
0.5
0.0
max frequency, Hz
D58A
0
1
2
3
4
5
6
7
Time, s

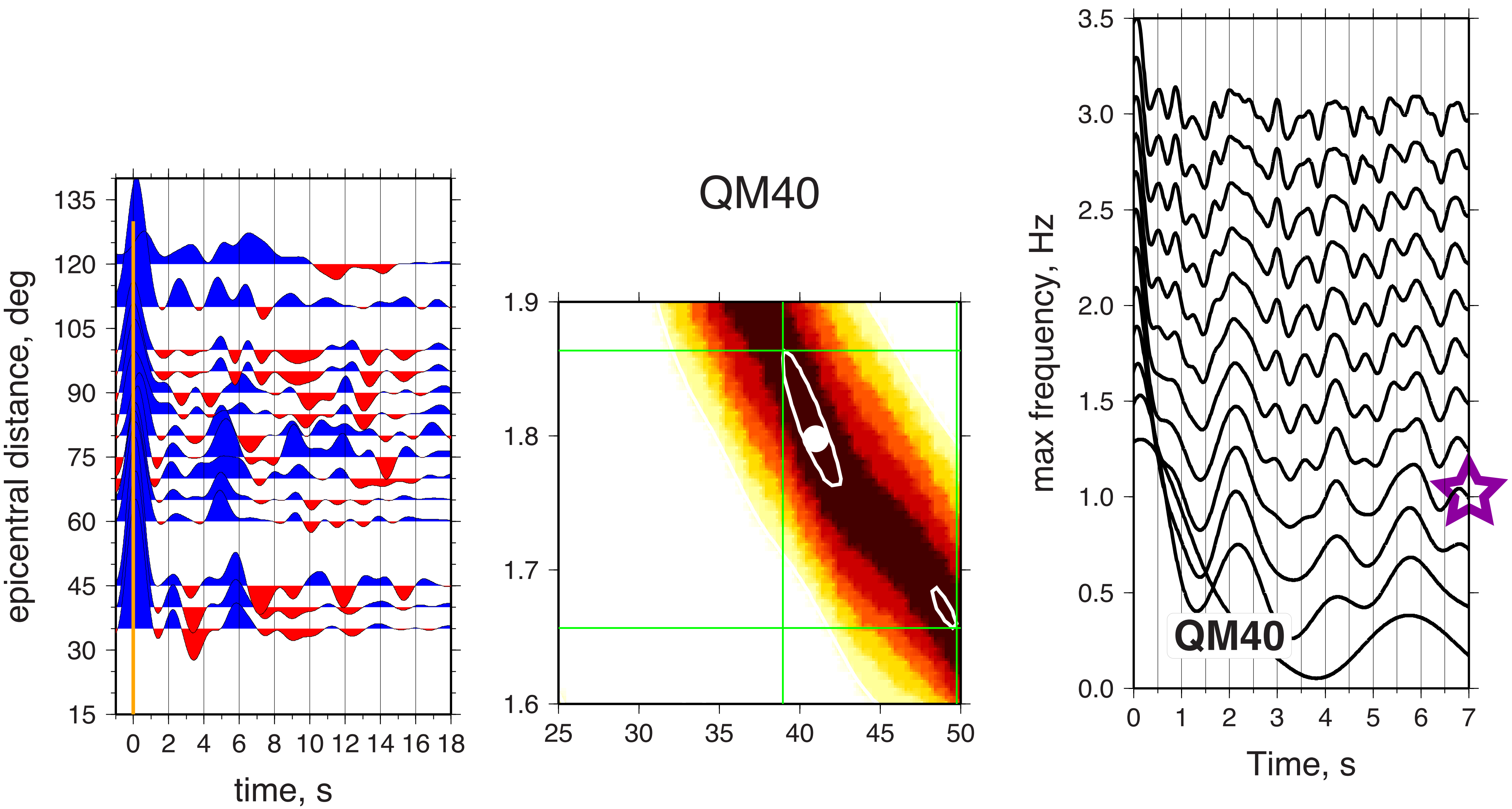
QM40
epicentral distance, deg
135
120
105
90
75
60
45
30
15
0 2 4 6 8 10 12 14 16 18
time, s
1.9
1.8
1.7
1.6
25 30 35 40 45 50
max frequency, Hz
3.5
3.0
2.5
2.0
1.5
1.0
0.5
0.0
0 1 2 3 4 5 6 7
Time, s
QM40

QM38_1_epi_0-360_5bins.rgrid scale

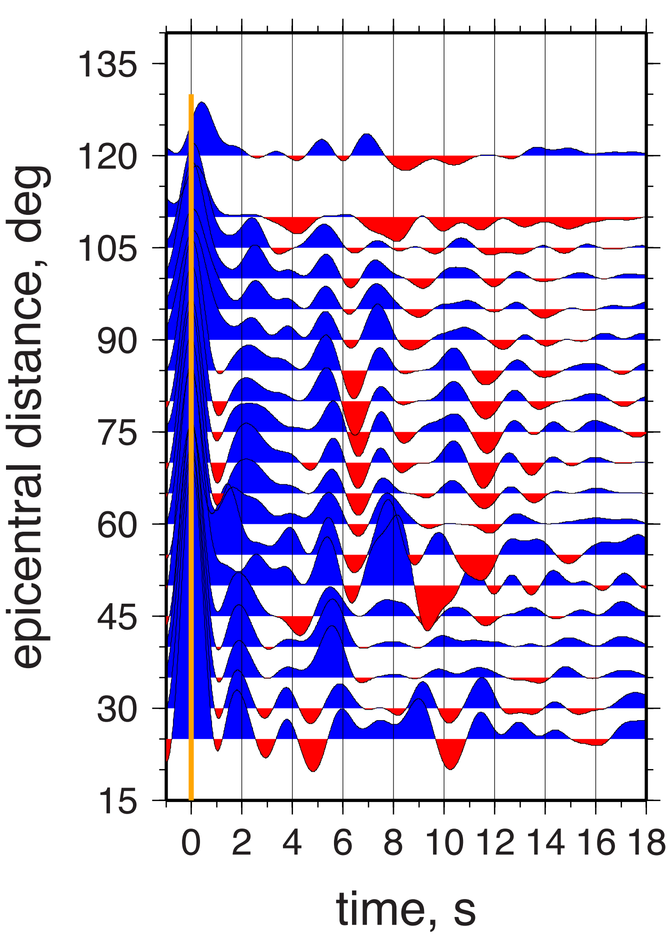

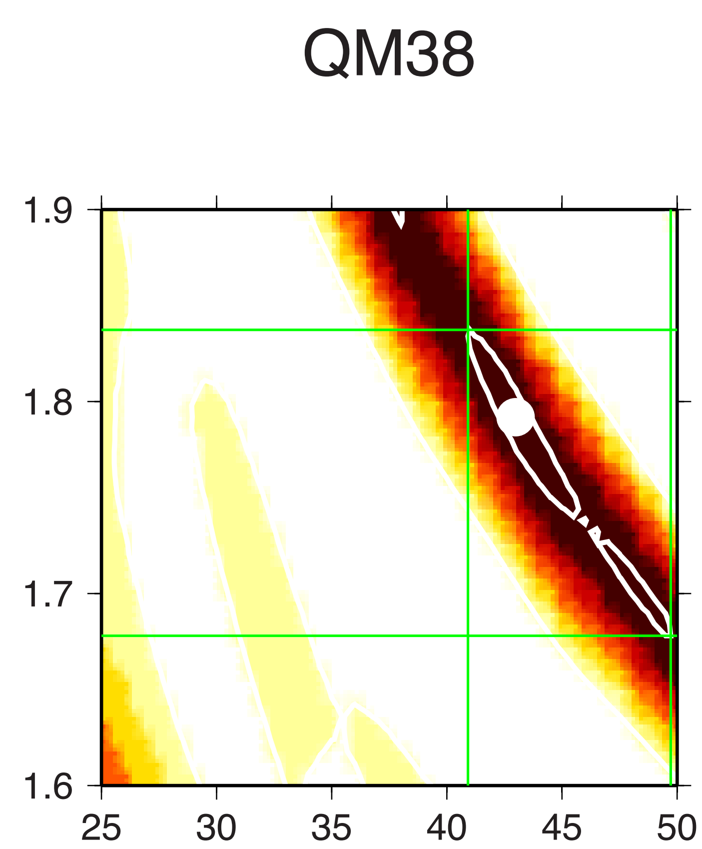

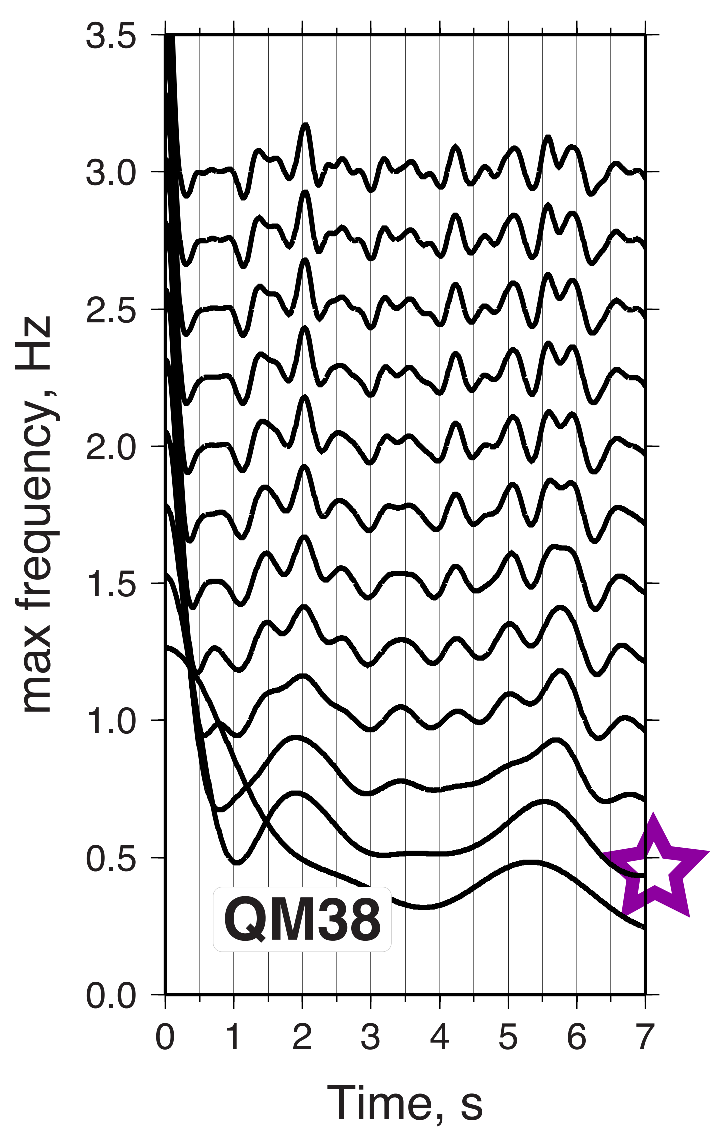

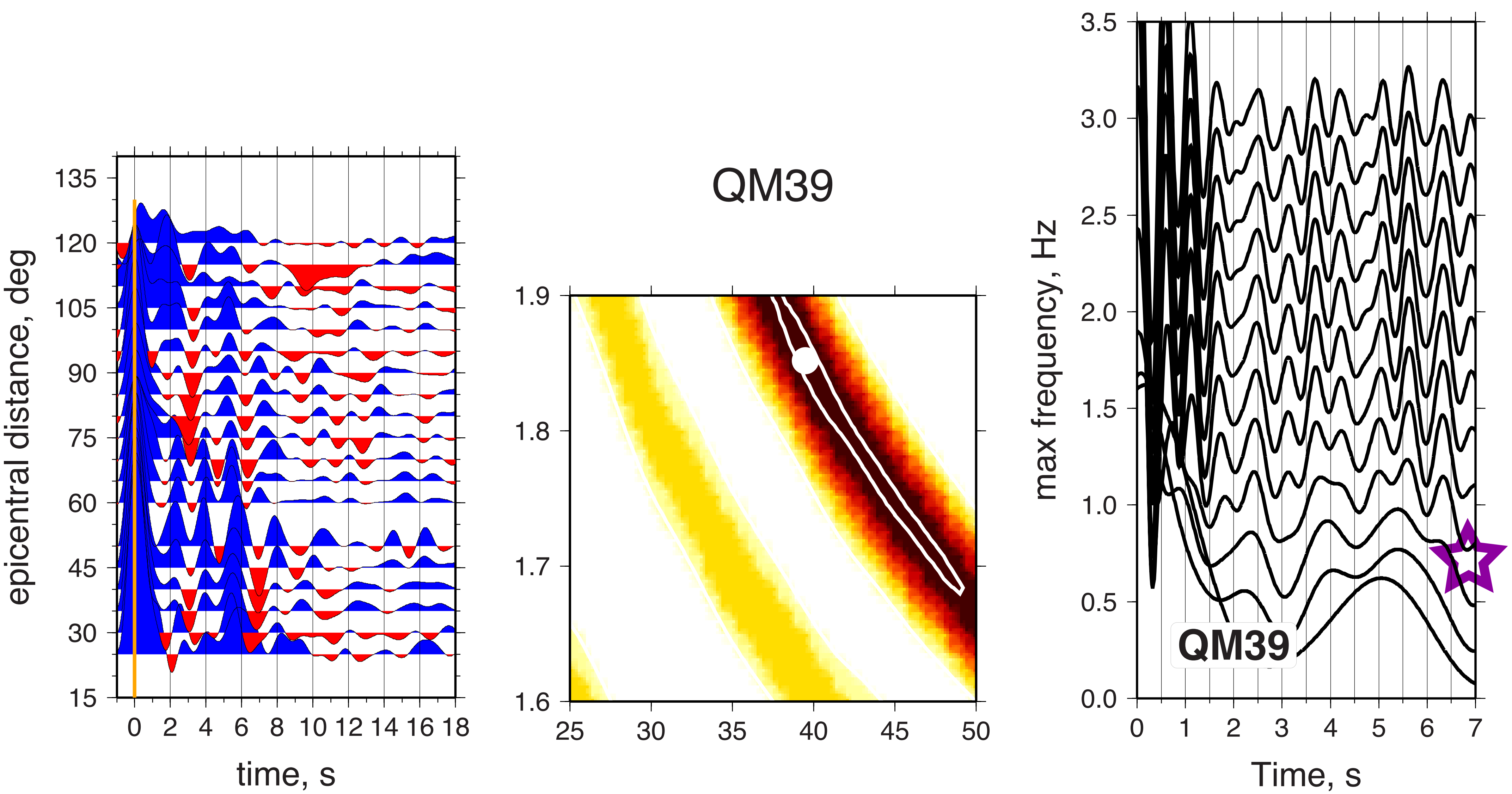
QM39
epicentral distance, deg
time, s
max frequency, Hz
Time, s
QM39

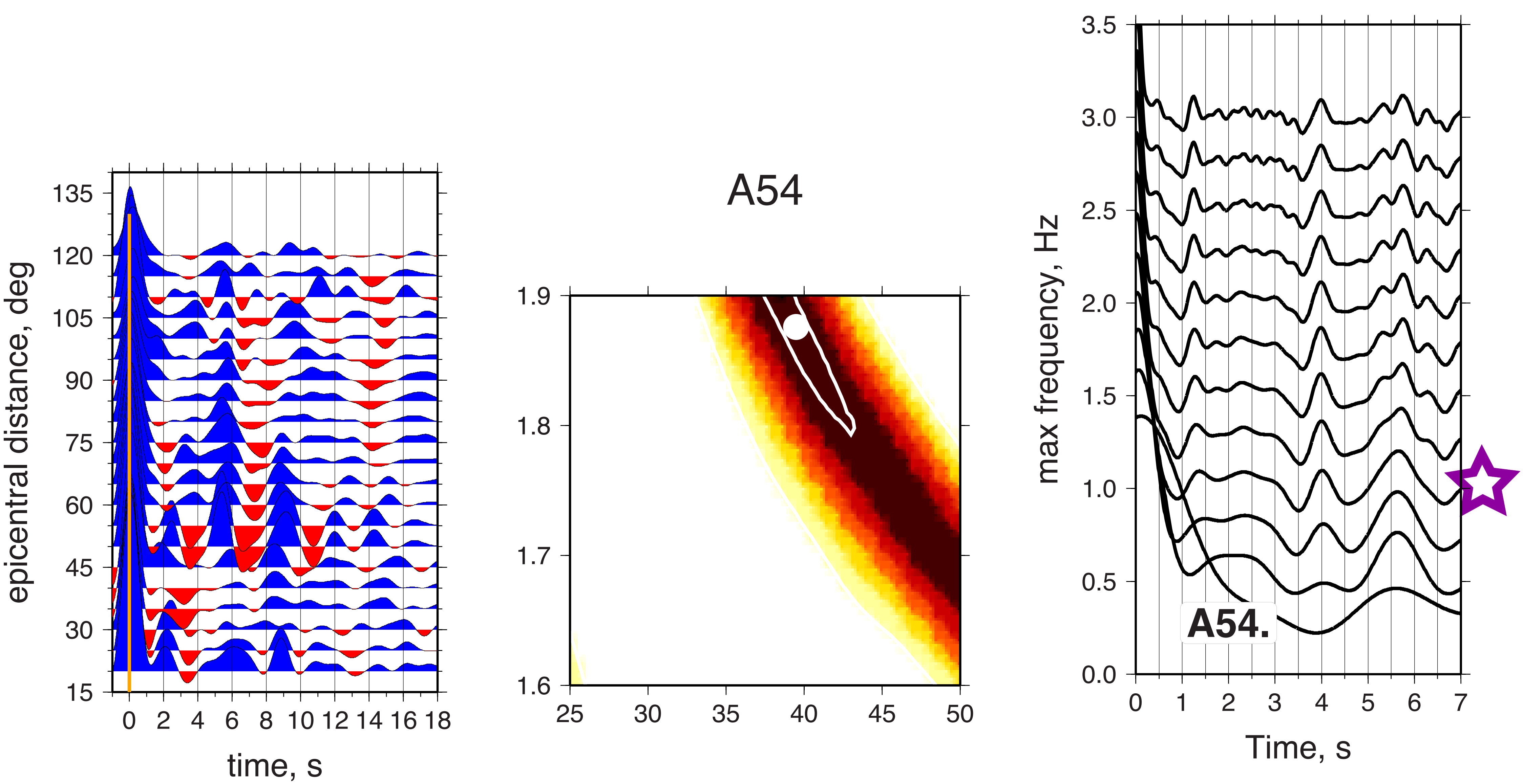
A54
epicentral distance, deg
time, s
max frequency, Hz
Time, s
A54.

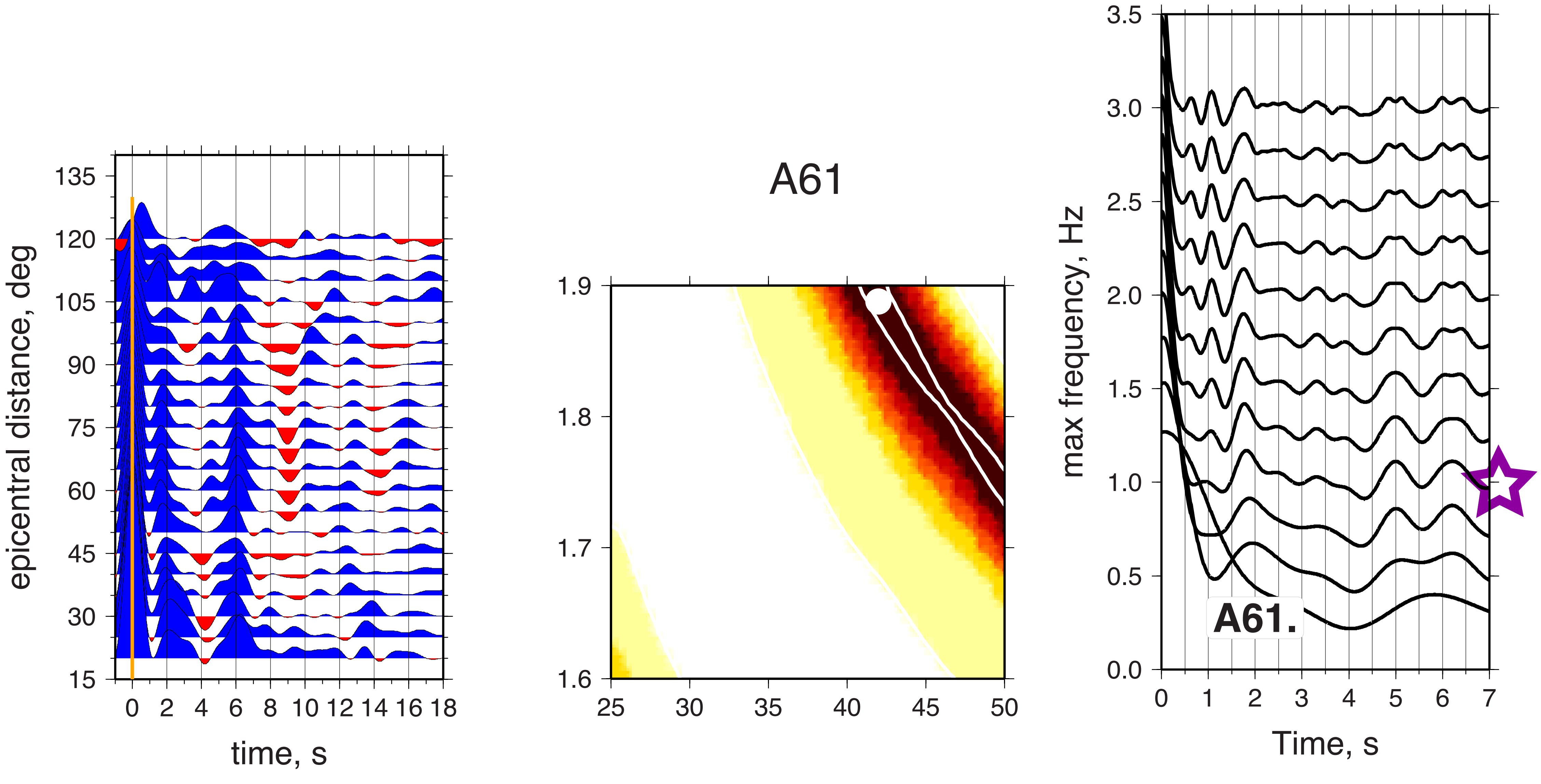

A61
epicentral distance, deg
135
120
105
90
75
60
45
30
15
time, s
0
2
4
6
8
10
12
14
16
18
1.9
1.8
1.7
1.6
25
30
35
40
45
50
max frequency, Hz
3.5
3.0
2.5
2.0
1.5
1.0
0.5
0.0
Time, s
0
1
2
3
4
5
6
7
A61.

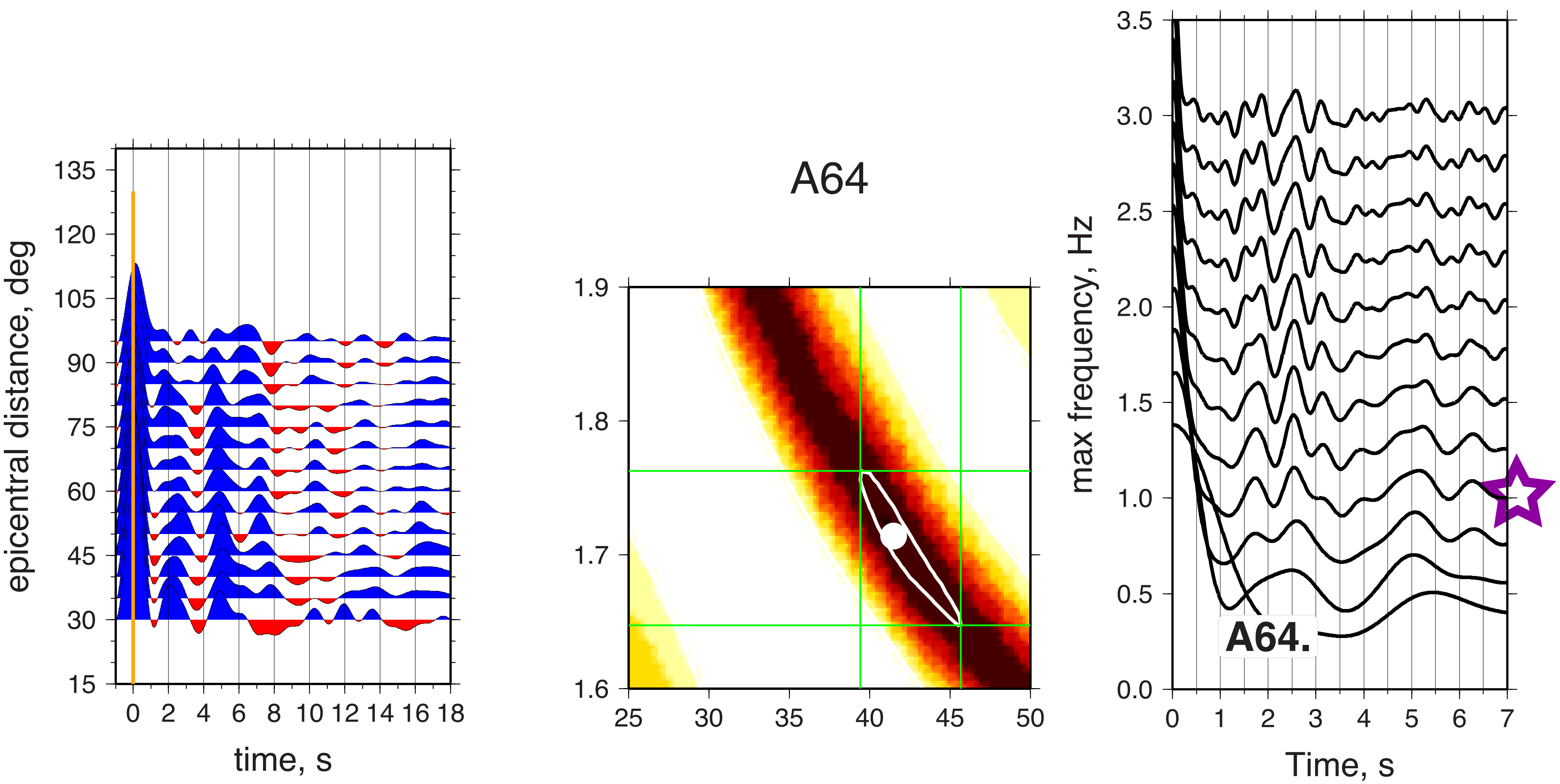
A64
epicentral distance, deg
time, s
max frequency, Hz
Time, s
A64.

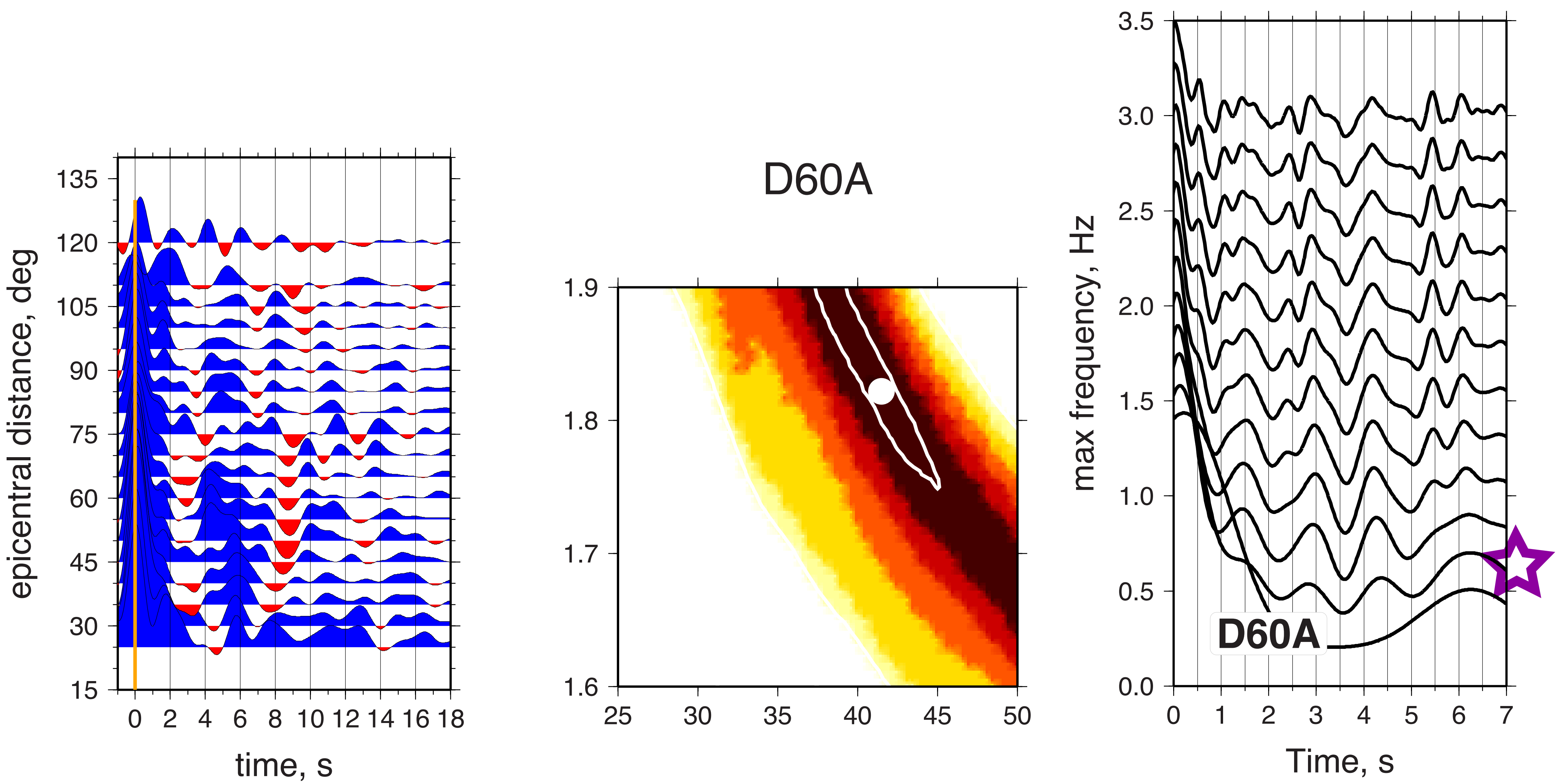

epicentral distance, deg
135
120
105
90
75
60
45
30
15
0
2
4
6
8
10
12
14
16
18
time, s
D60A
1.9
1.8
1.7
1.6
25
30
35
40
45
50
max frequency, Hz
3.5
3.0
2.5
2.0
1.5
1.0
0.5
0.0
0
1
2
3
4
5
6
7
Time, s
D60A

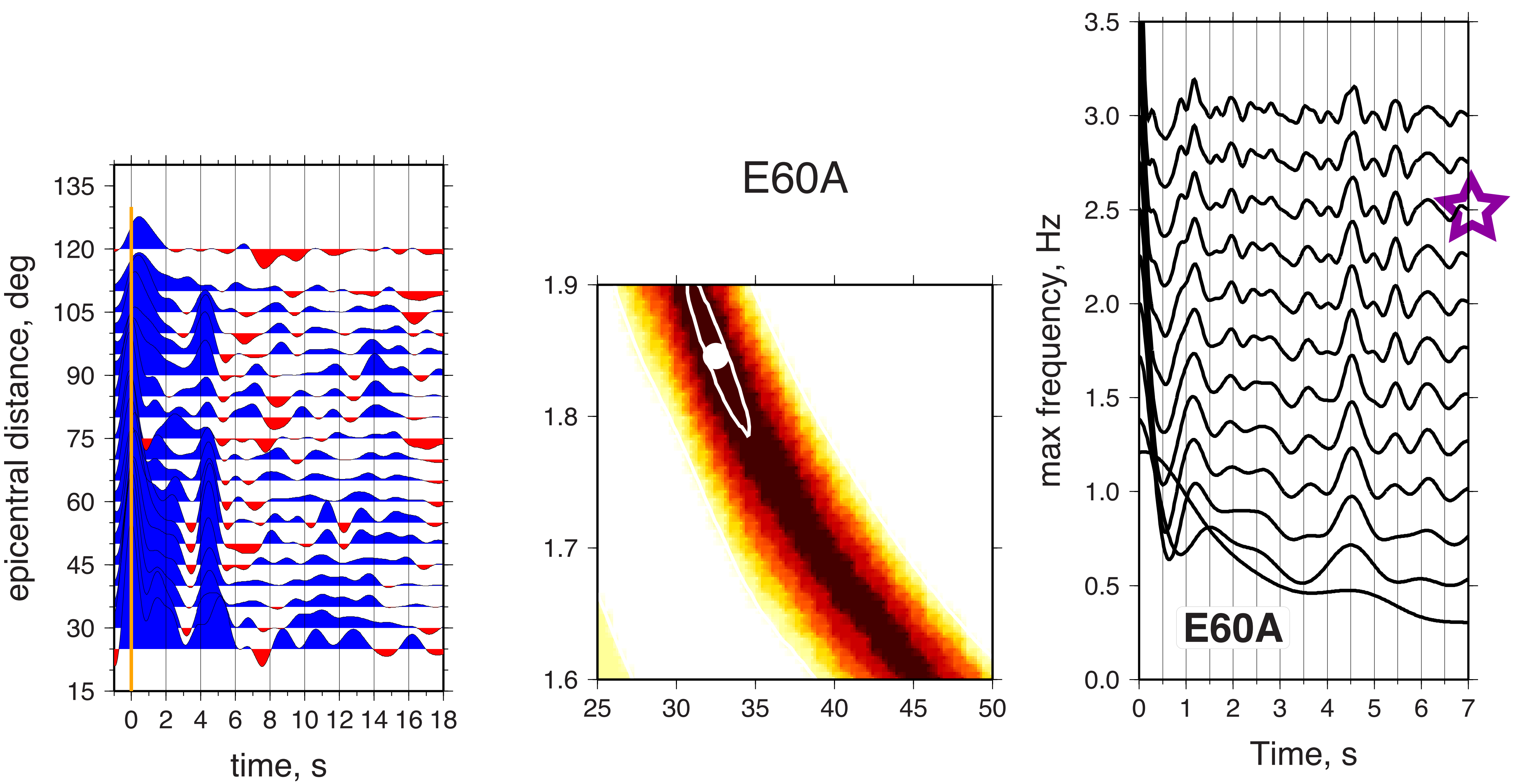

E60A
epicentral distance, deg
135
120
105
90
75
60
45
30
15
time, s
0
2
4
6
8
10
12
14
16
18
1.9
1.8
1.7
1.6
25
30
35
40
45
50
max frequency, Hz
3.5
3.0
2.5
2.0
1.5
1.0
0.5
0.0
Time, s
0
1
2
3
4
5
6
7
E60A

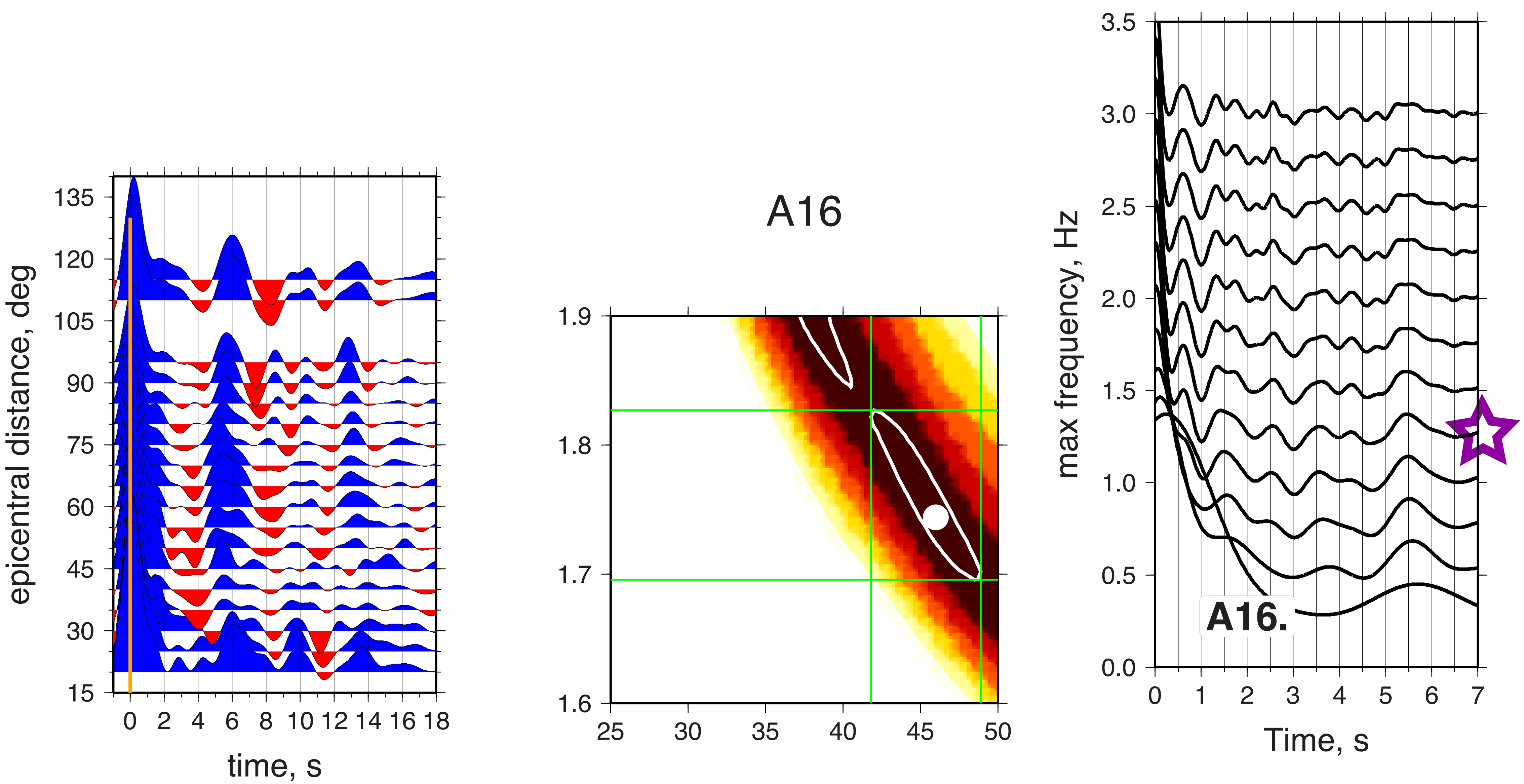

epicentral distance, deg
135
120
105
90
75
60
45
30
15
0 2 4 6 8 10 12 14 16 18
time, s
A16
1.9
1.8
1.7
1.6
25 30 35 40 45 50
max frequency, Hz
3.5
3.0
2.5
2.0
1.5
1.0
0.5
0.0
0 1 2 3 4 5 6 7
Time, s
A16.

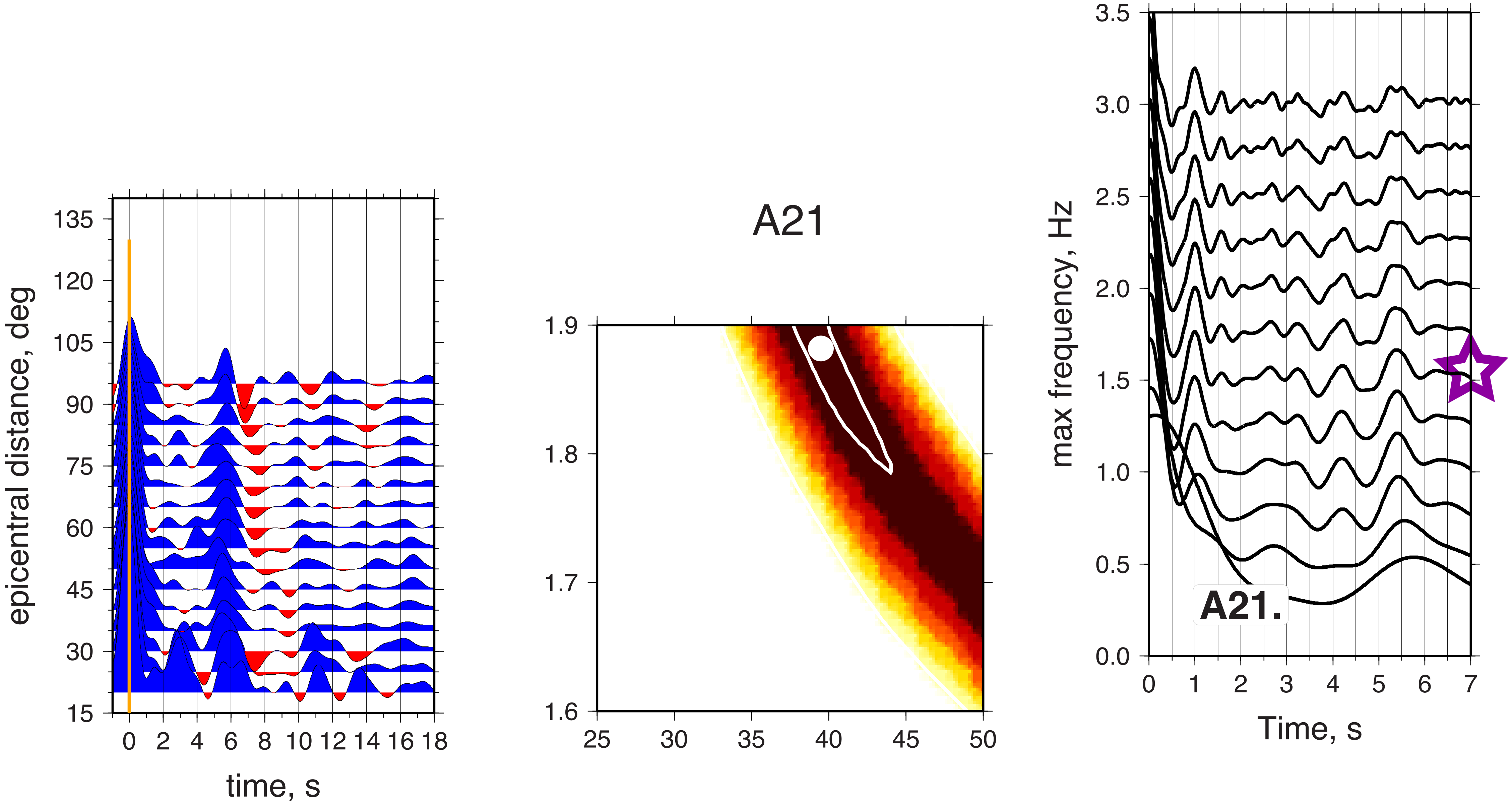

epicentral distance, deg
135
120
105
90
75
60
45
30
15
0
2
4
6
8
10
12
14
16
18
time, s
A21
1.9
1.8
1.7
1.6
25
30
35
40
45
50
max frequency, Hz
3.5
3.0
2.5
2.0
1.5
1.0
0.5
0.0
0
1
2
3
4
5
6
7
Time, s
A21.

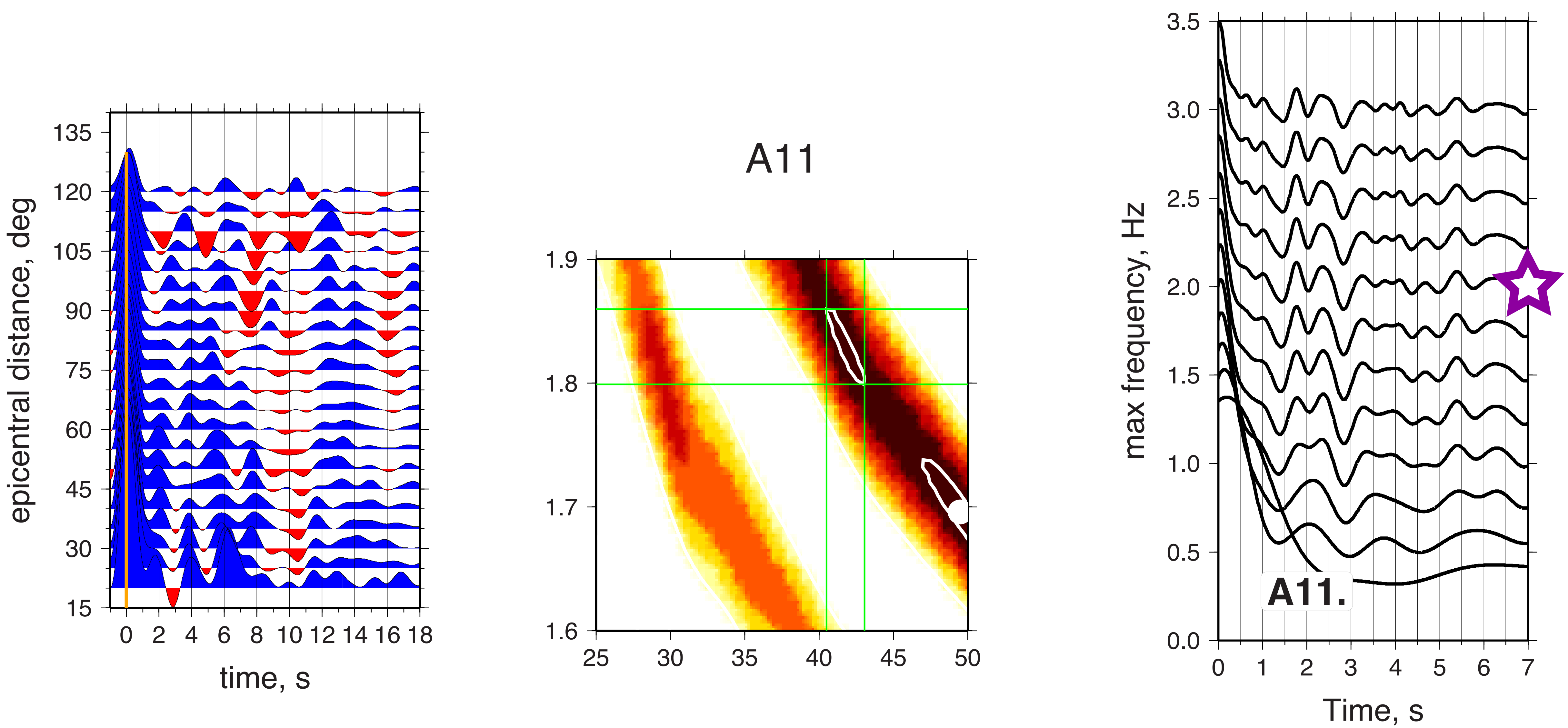

A11
epicentral distance, deg
time, s
max frequency, Hz
Time, s
A11.

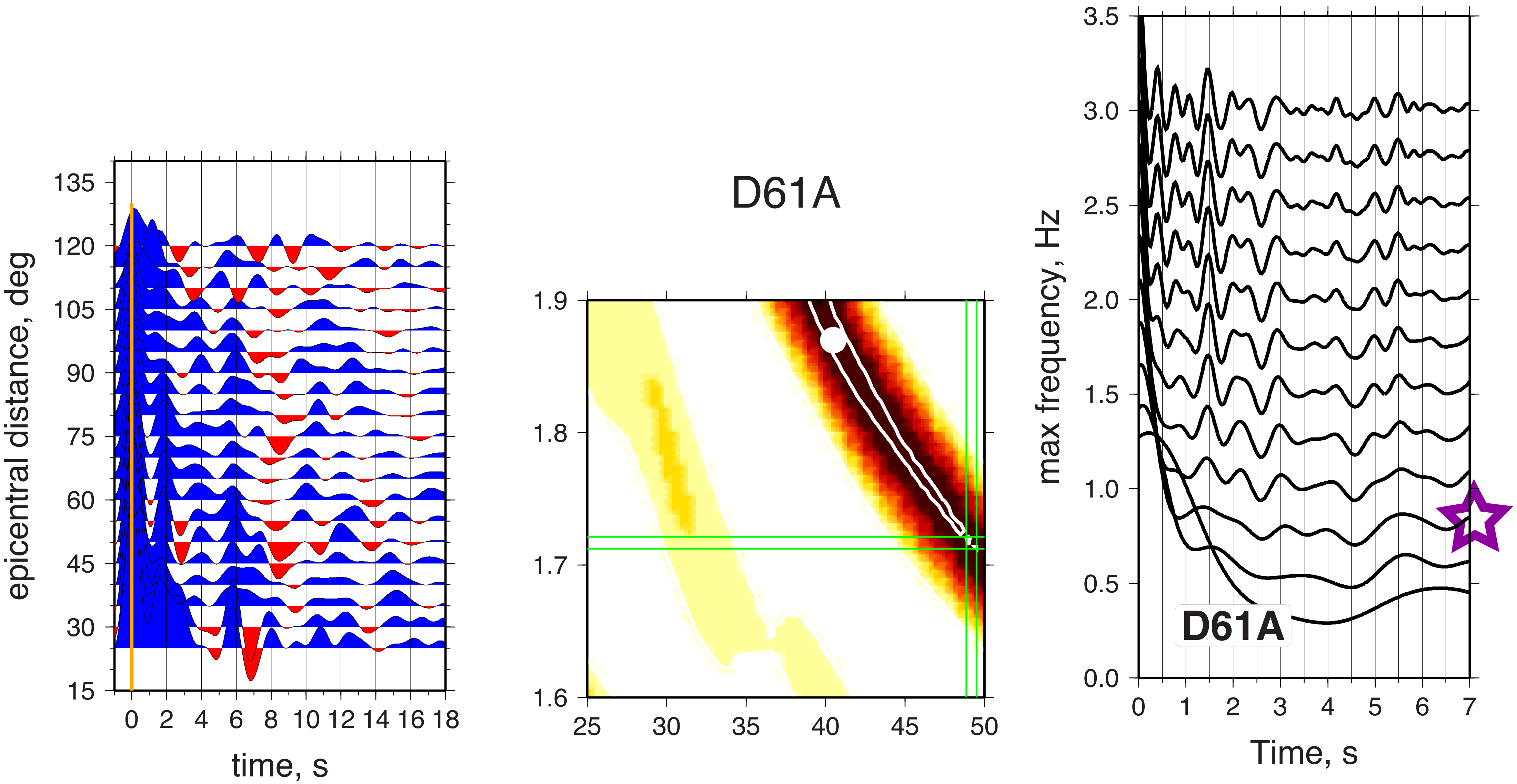

D61A
epicentral distance, deg
time, s
max frequency, Hz
Time, s
D61A

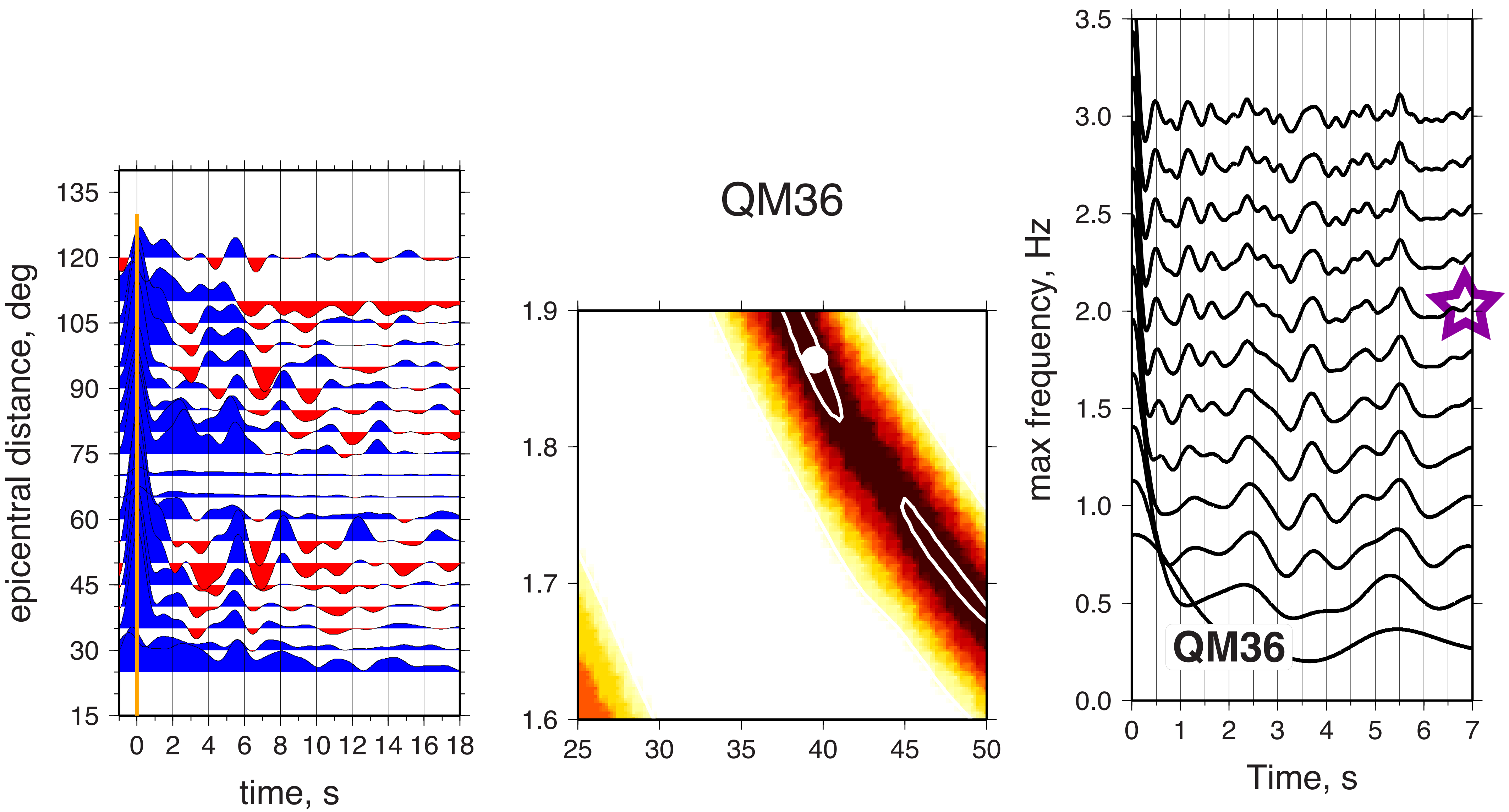

QM36
epicentral distance, deg
time, s
max frequency, Hz
Time, s
QM36

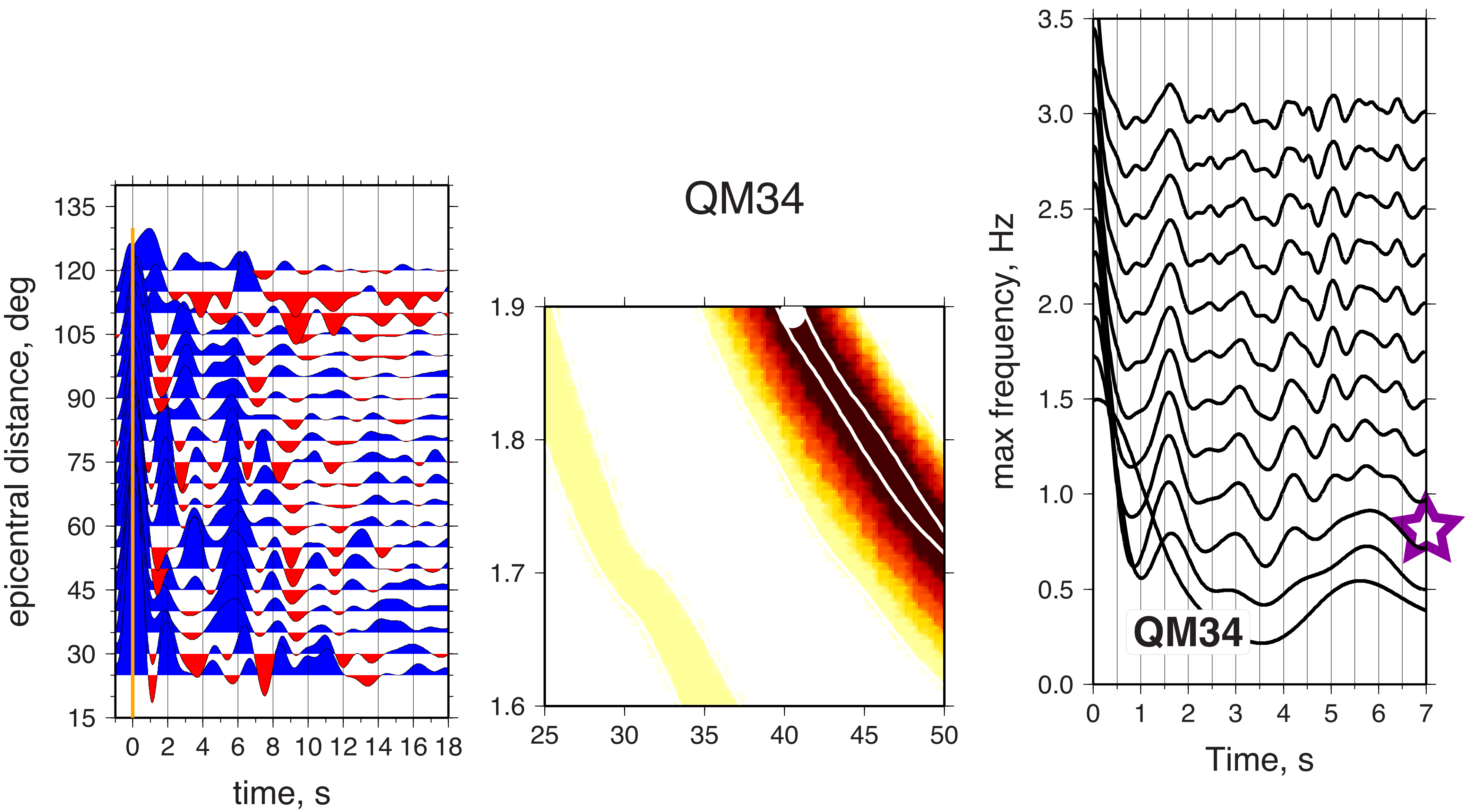

QM34
epicentral distance, deg
time, s
max frequency, Hz
Time, s
QM34

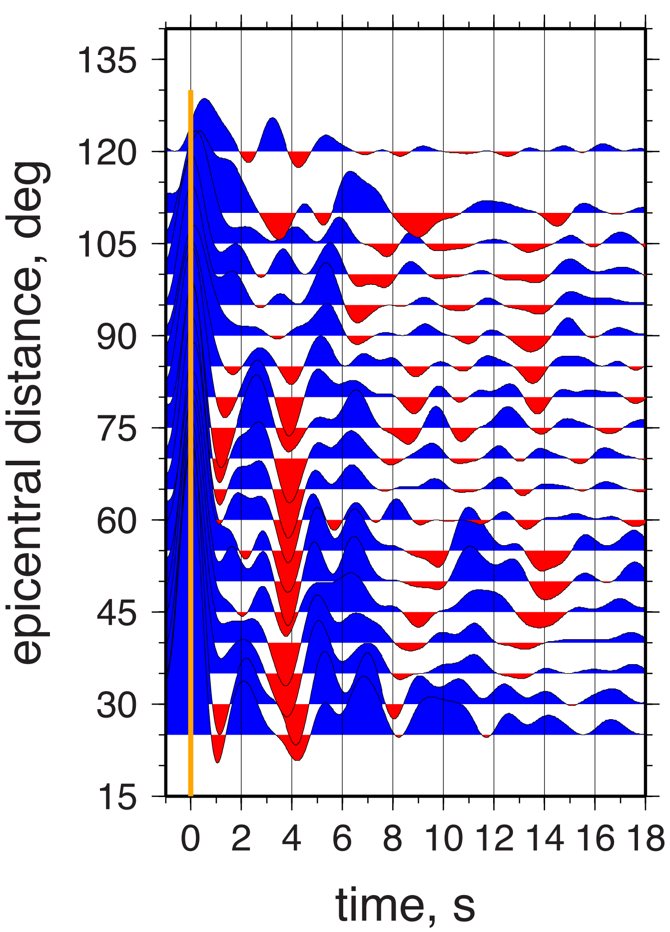

epicentral distance, deg
time, s

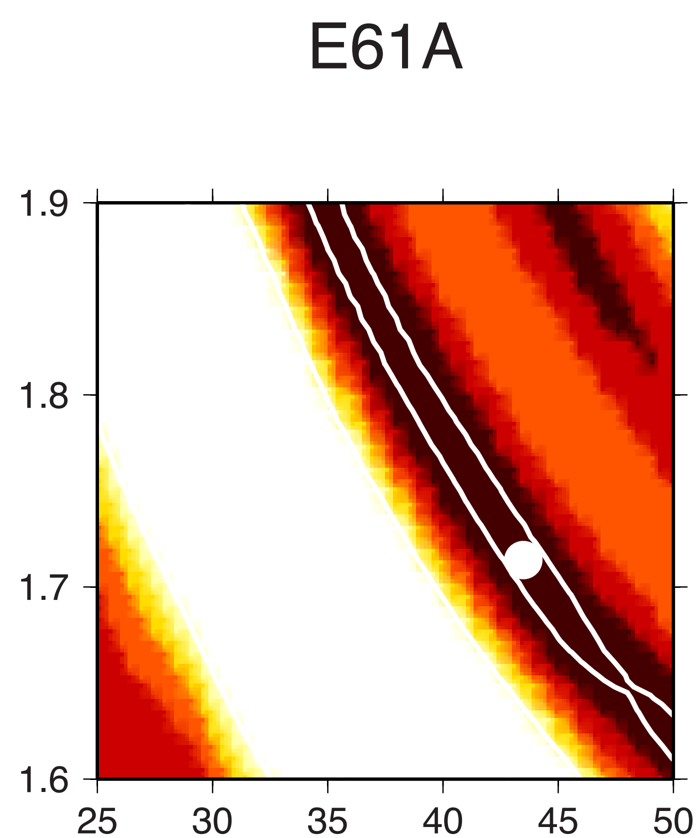

E61A

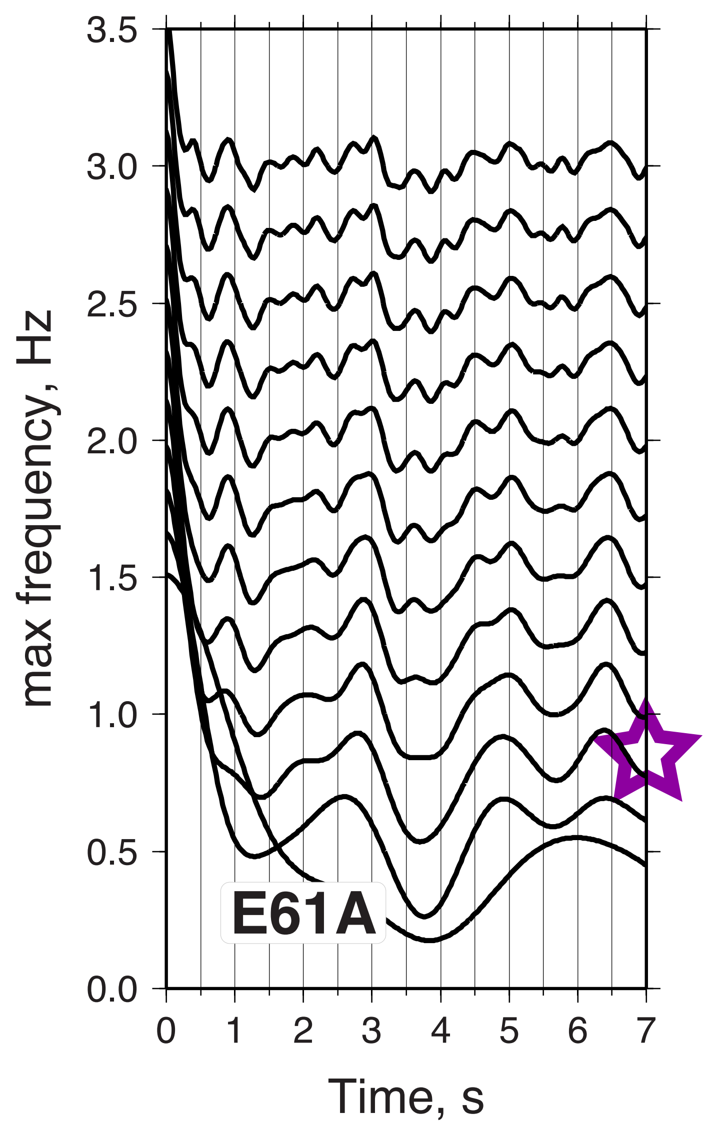

max frequency, Hz
Time, s
E61A

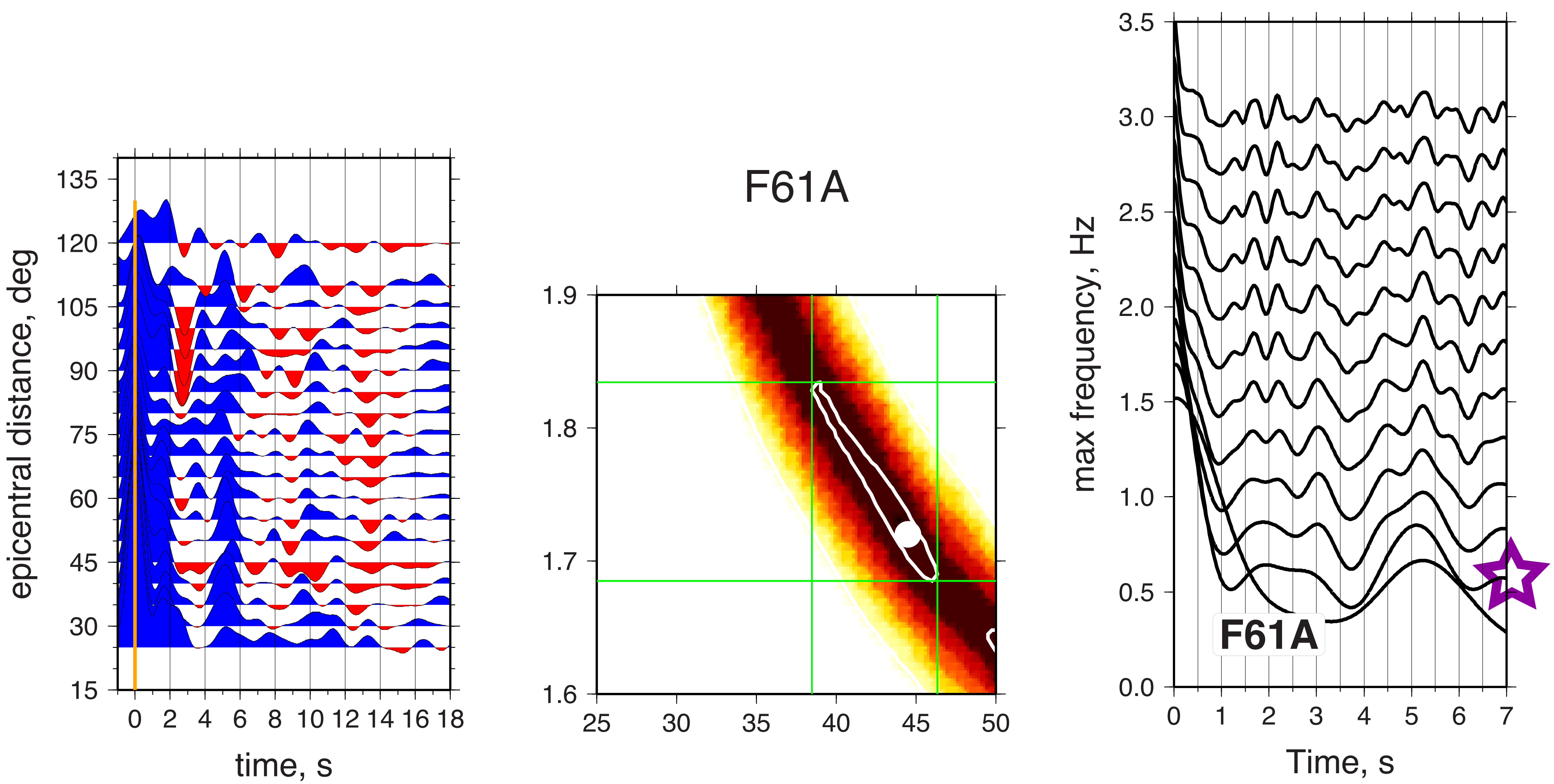

epicentral distance, deg
135
120
105
90
75
60
45
30
15
0
2
4
6
8
10
12
14
16
18
time, s
F61A
1.9
1.8
1.7
1.6
25
30
35
40
45
50
max frequency, Hz
3.5
3.0
2.5
2.0
1.5
1.0
0.5
0.0
0
1
2
3
4
5
6
7
Time, s
F61A

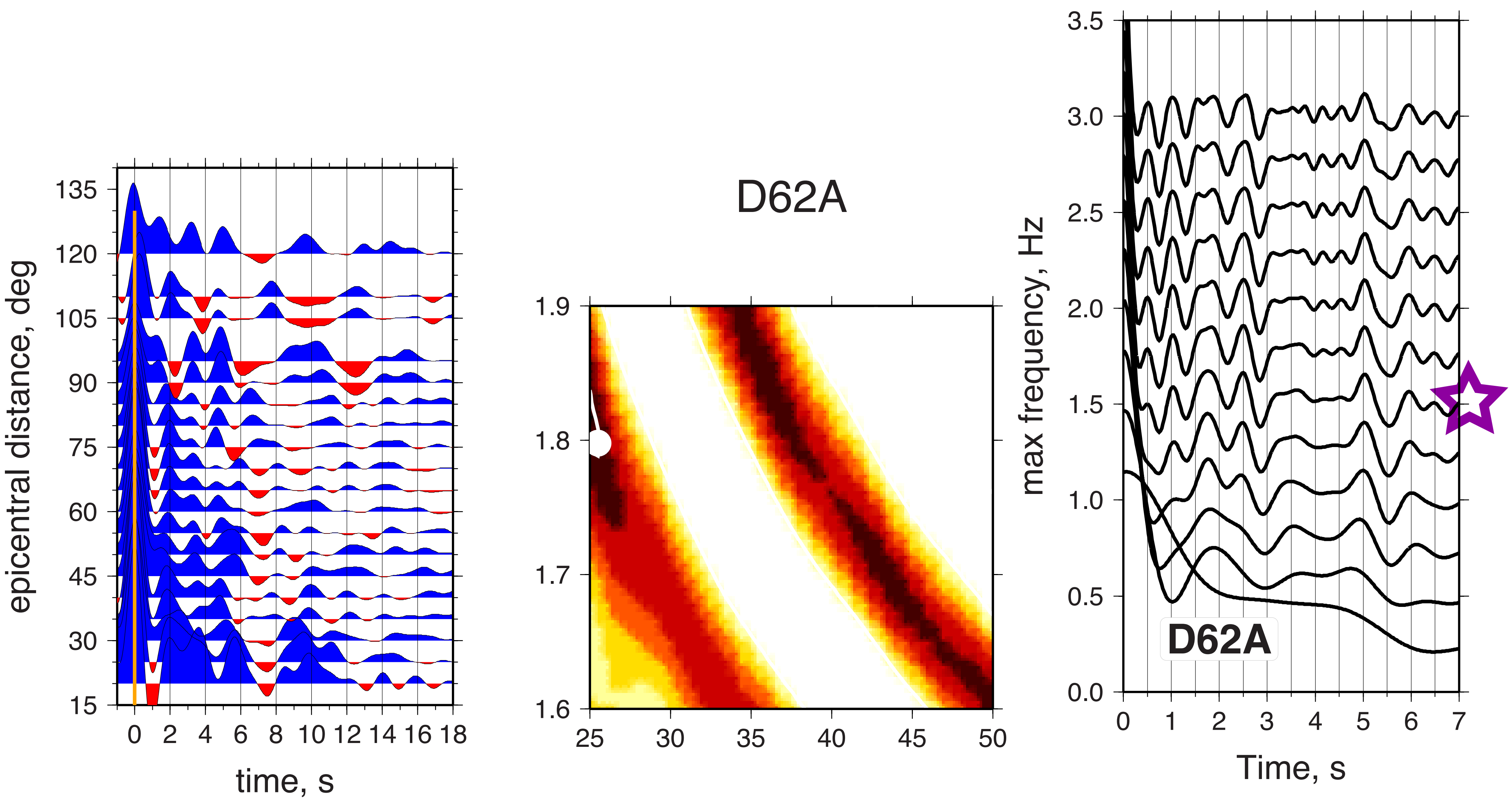

D62A
epicentral distance, deg
135
120
105
90
75
60
45
30
15
0
2
4
6
8
10
12
14
16
18
time, s
1.9
1.8
1.7
1.6
25
30
35
40
45
50
max frequency, Hz
3.5
3.0
2.5
2.0
1.5
1.0
0.5
0.0
0
1
2
3
4
5
6
7
Time, s
D62A

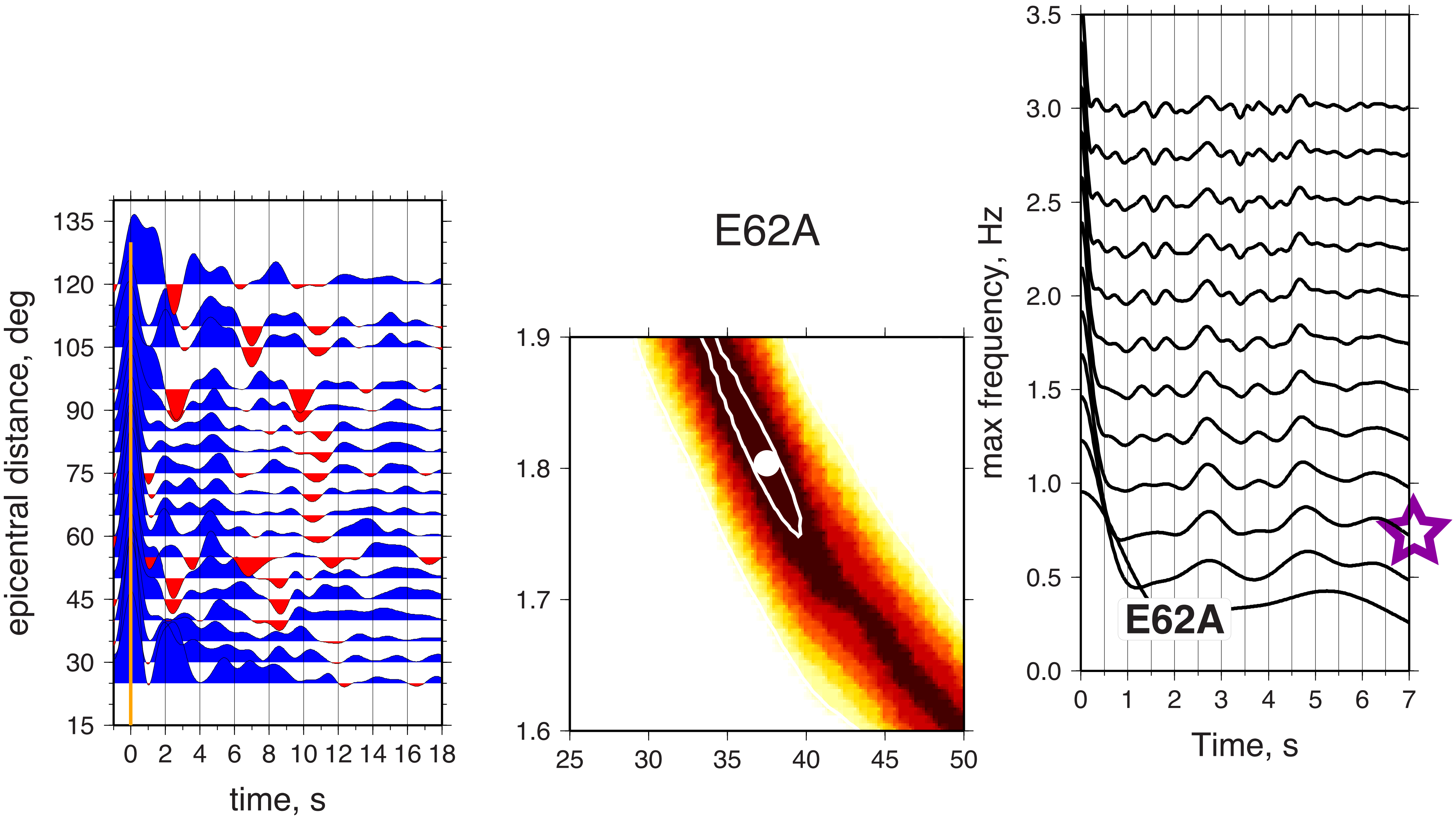

E62A
epicentral distance, deg
time, s
max frequency, Hz
Time, s
E62A

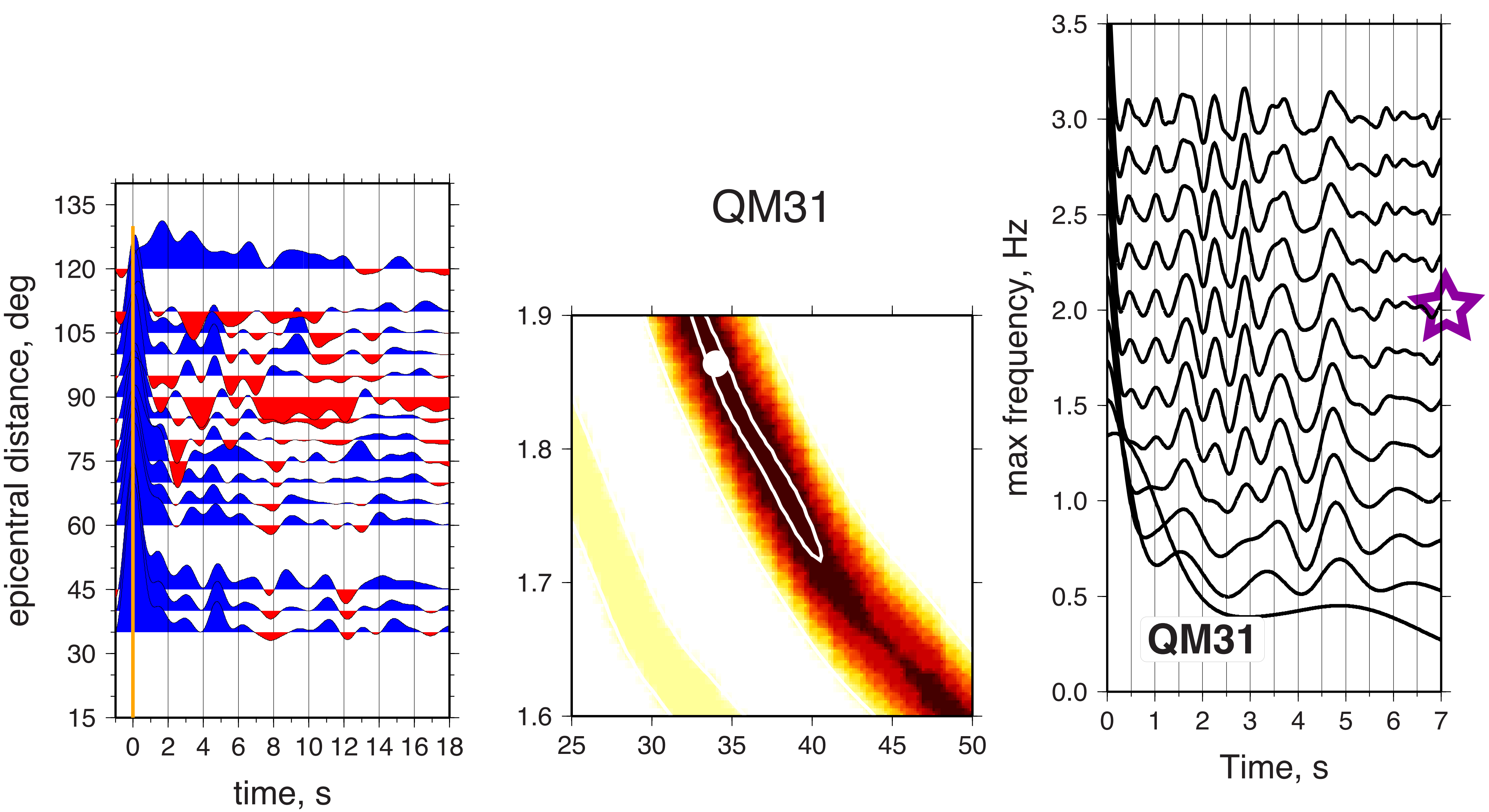

135
120
105
90
75
60
45
30
15
epicentral distance, deg
0 2 4 6 8 10 12 14 16 18
time, s
QM31
1.9
1.8
1.7
1.6
25 30 35 40 45 50
3.5
3.0
2.5
2.0
1.5
1.0
0.5
0.0
max frequency, Hz
QM31
0 1 2 3 4 5 6 7
Time, s

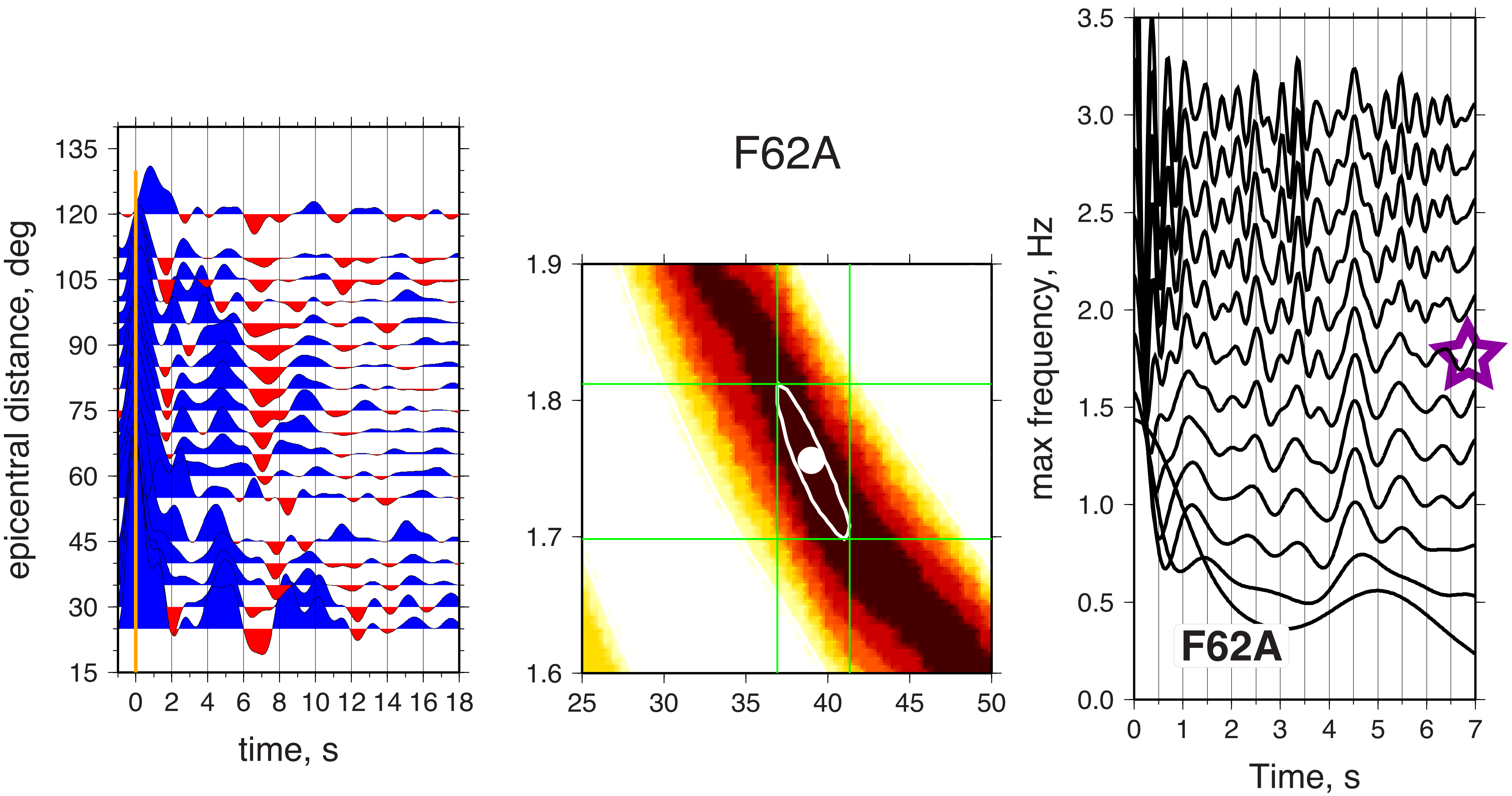

F62A
epicentral distance, deg
time, s
max frequency, Hz
Time, s
F62A

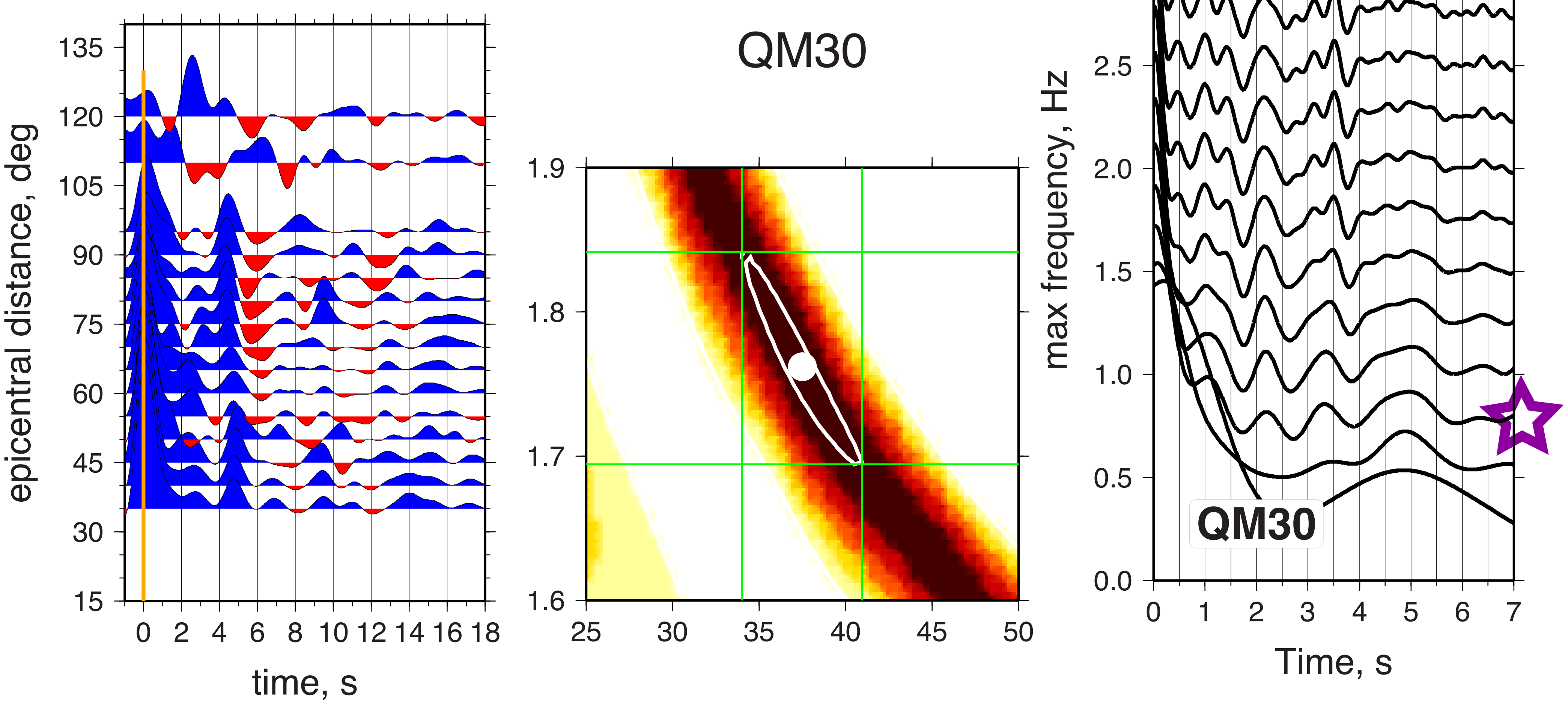

135
120
105
90
75
60
45
30
15
epicentral distance, deg
0
2
4
6
8
10
12
14
16
18
time, s
QM30
1.9
1.8
1.7
1.6
25
30
35
40
45
50
3.5
3.0
2.5
2.0
1.5
1.0
0.5
0.0
max frequency, Hz
QM30
0
1
2
3
4
5
6
7
Time, s

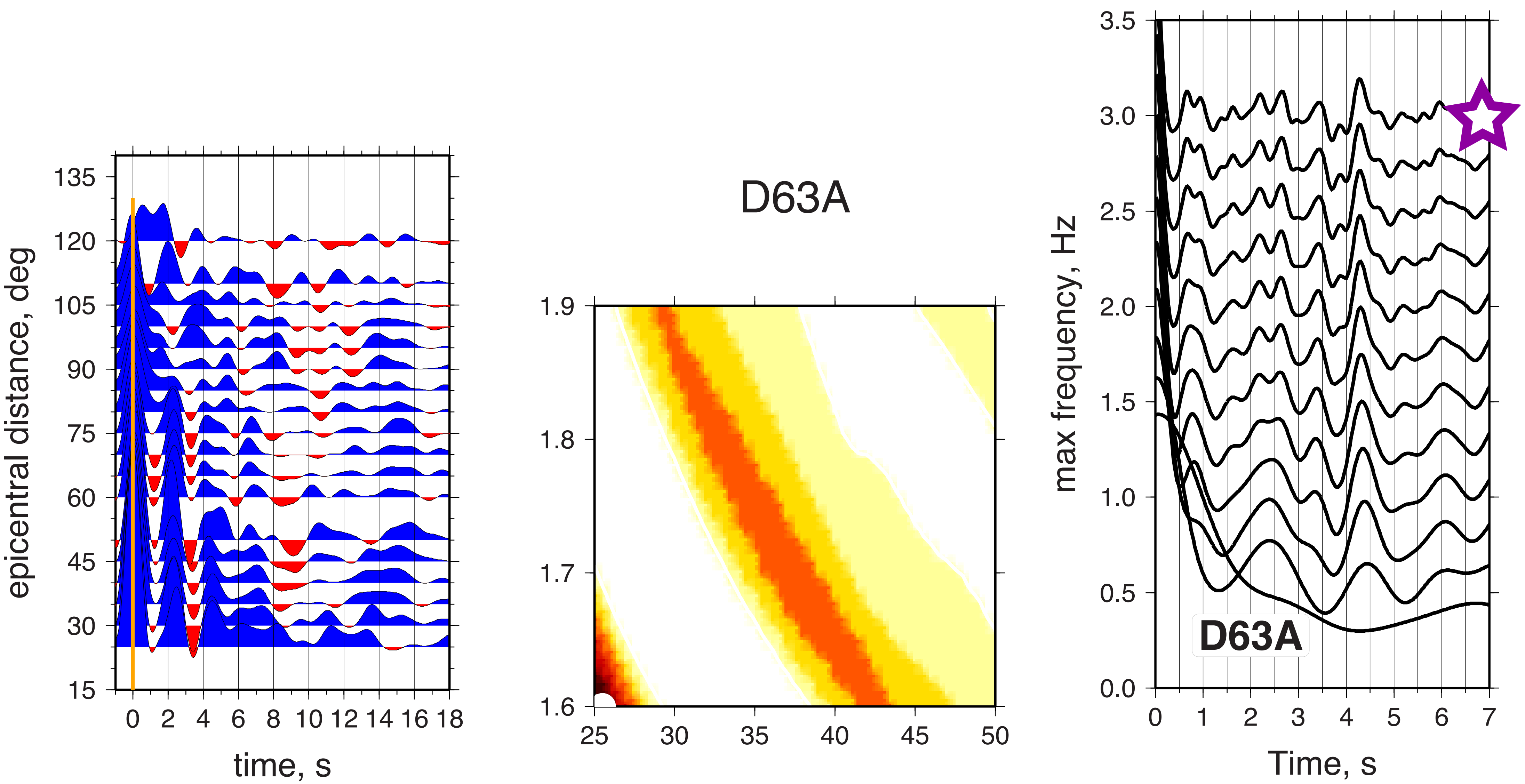
D63A
epicentral distance, deg
135
120
105
90
75
60
45
30
15
0 2 4 6 8 10 12 14 16 18
time, s
1.9
1.8
1.7
1.6
25 30 35 40 45 50
max frequency, Hz
3.5
3.0
2.5
2.0
1.5
1.0
0.5
0.0
0 1 2 3 4 5 6 7
Time, s
D63A

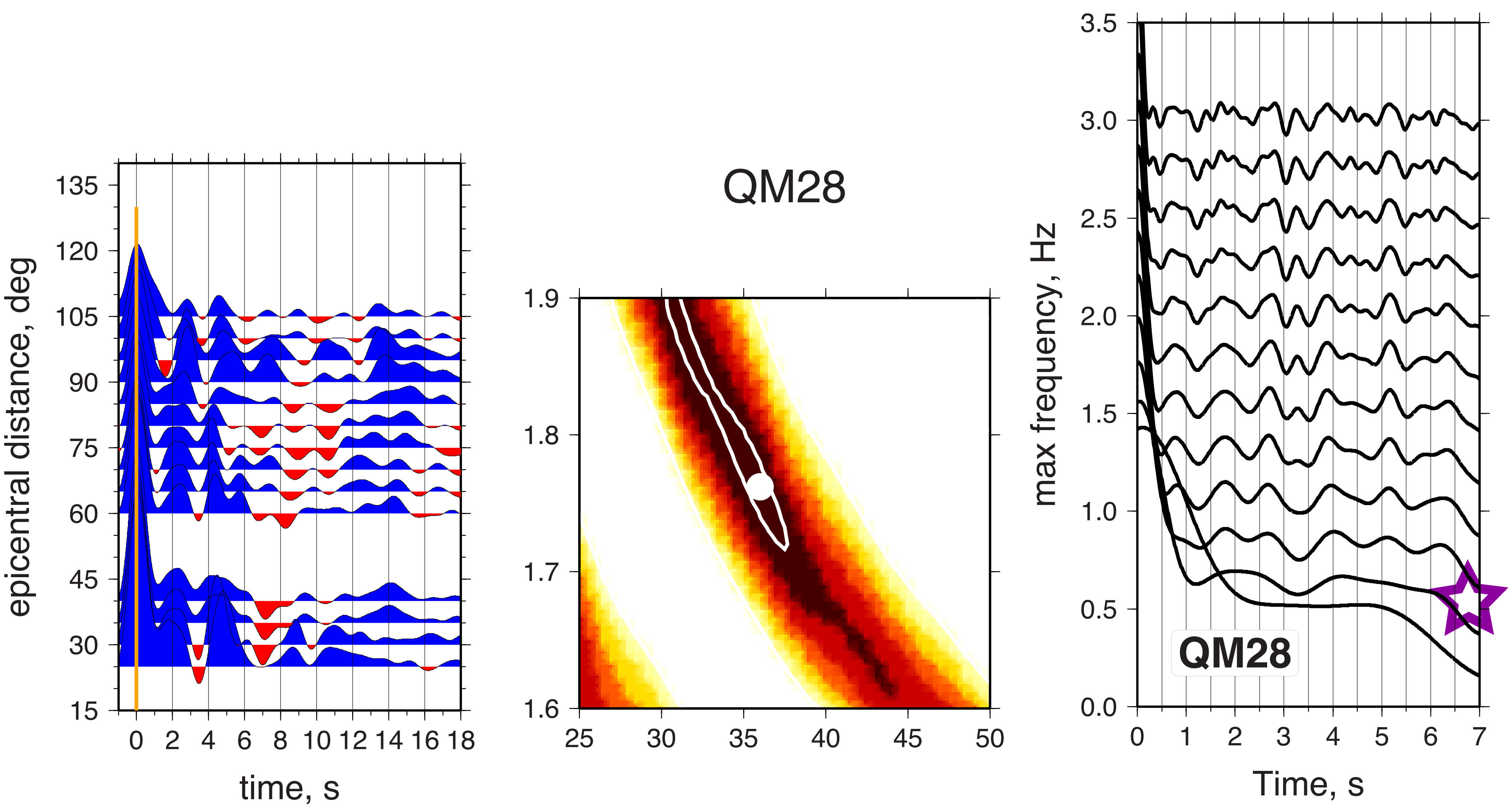

QM28
epicentral distance, deg
time, s
max frequency, Hz
Time, s
QM28

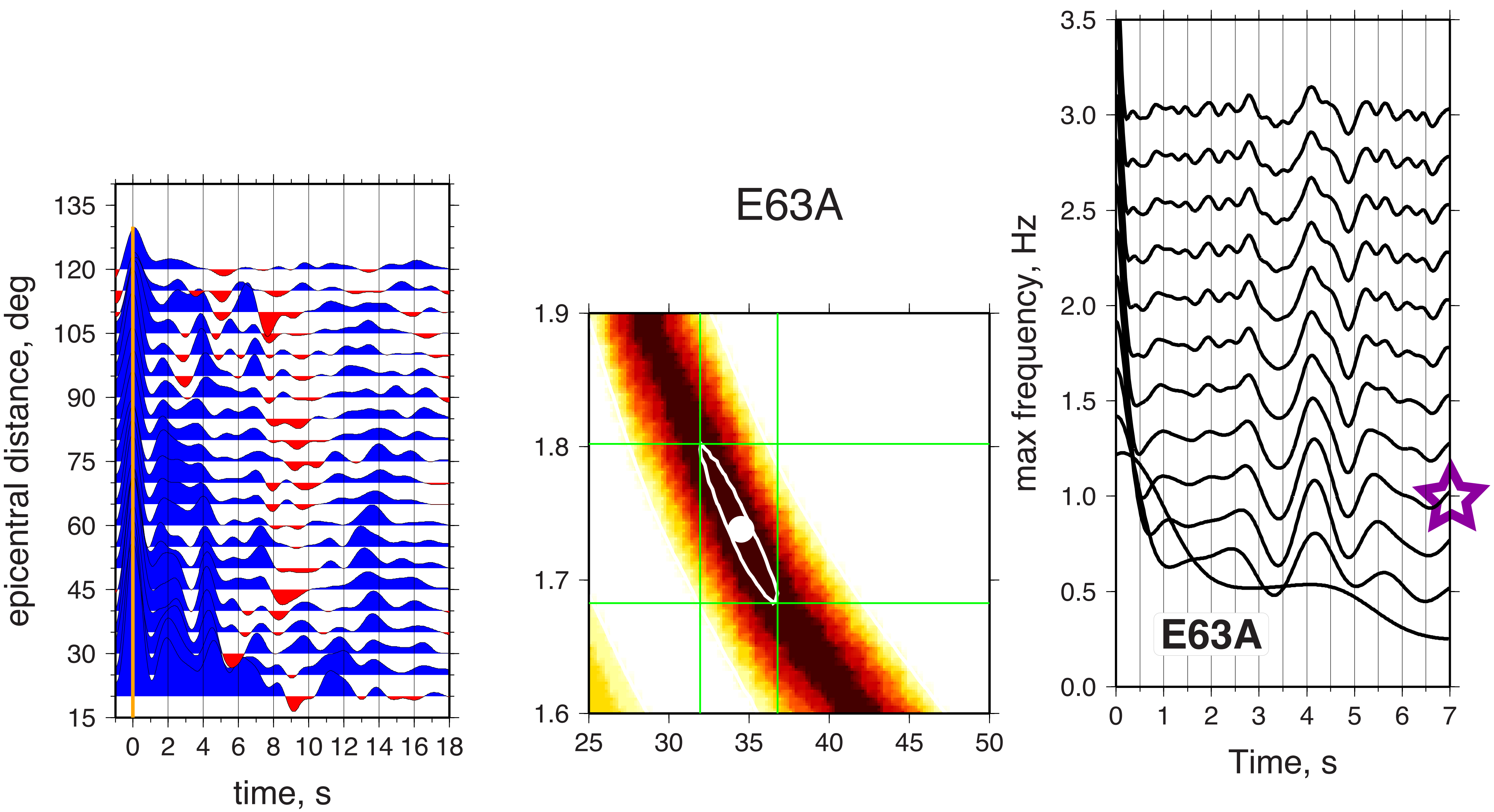
E63A
epicentral distance, deg
time, s
max frequency, Hz
Time, s
E63A

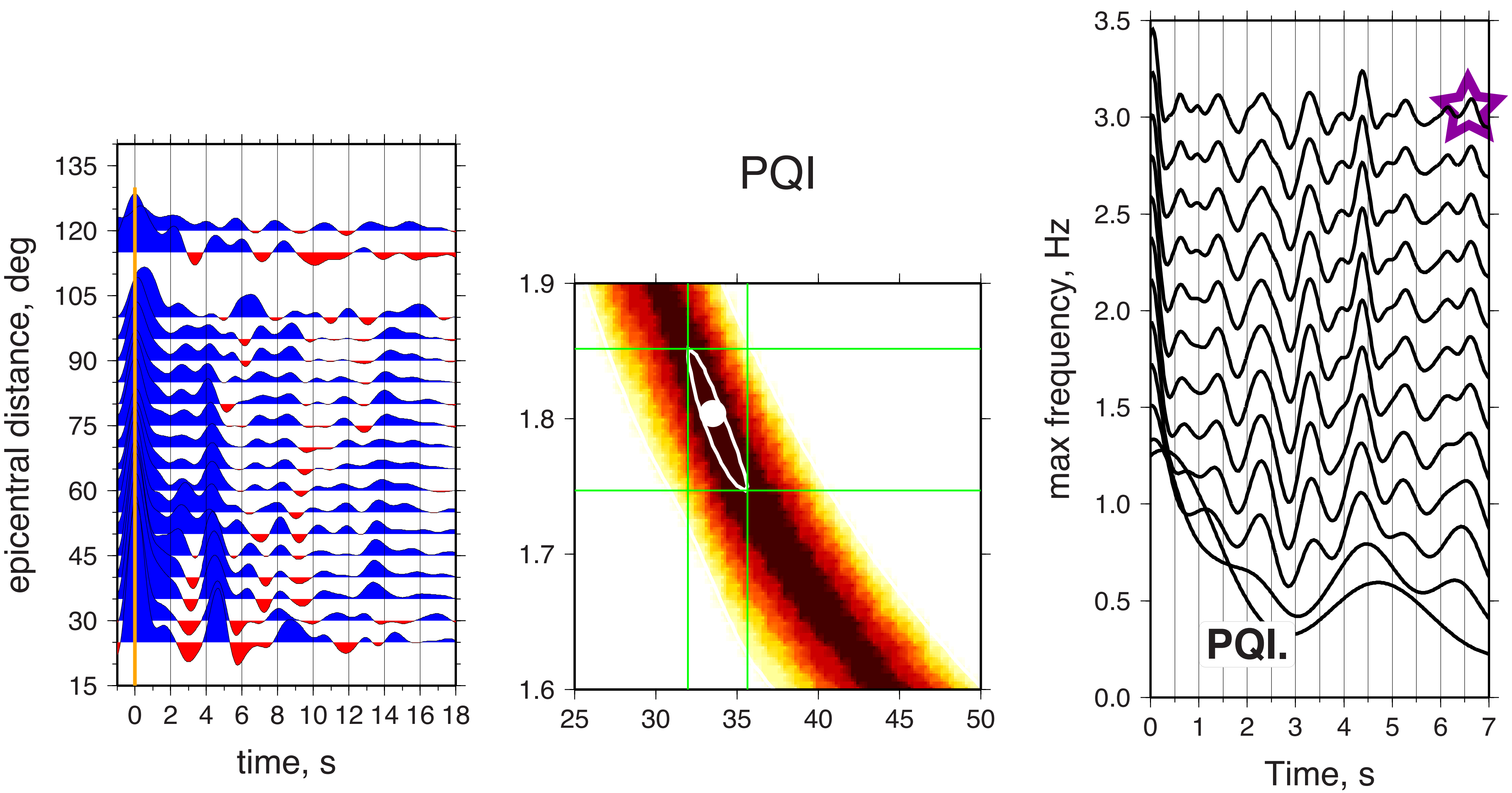

PQI
epicentral distance, deg
135
120
105
90
75
60
45
30
15
0
2
4
6
8
10
12
14
16
18
time, s
1.9
1.8
1.7
1.6
25
30
35
40
45
50
max frequency, Hz
3.5
3.0
2.5
2.0
1.5
1.0
0.5
0.0
0
1
2
3
4
5
6
7
Time, s
PQI.

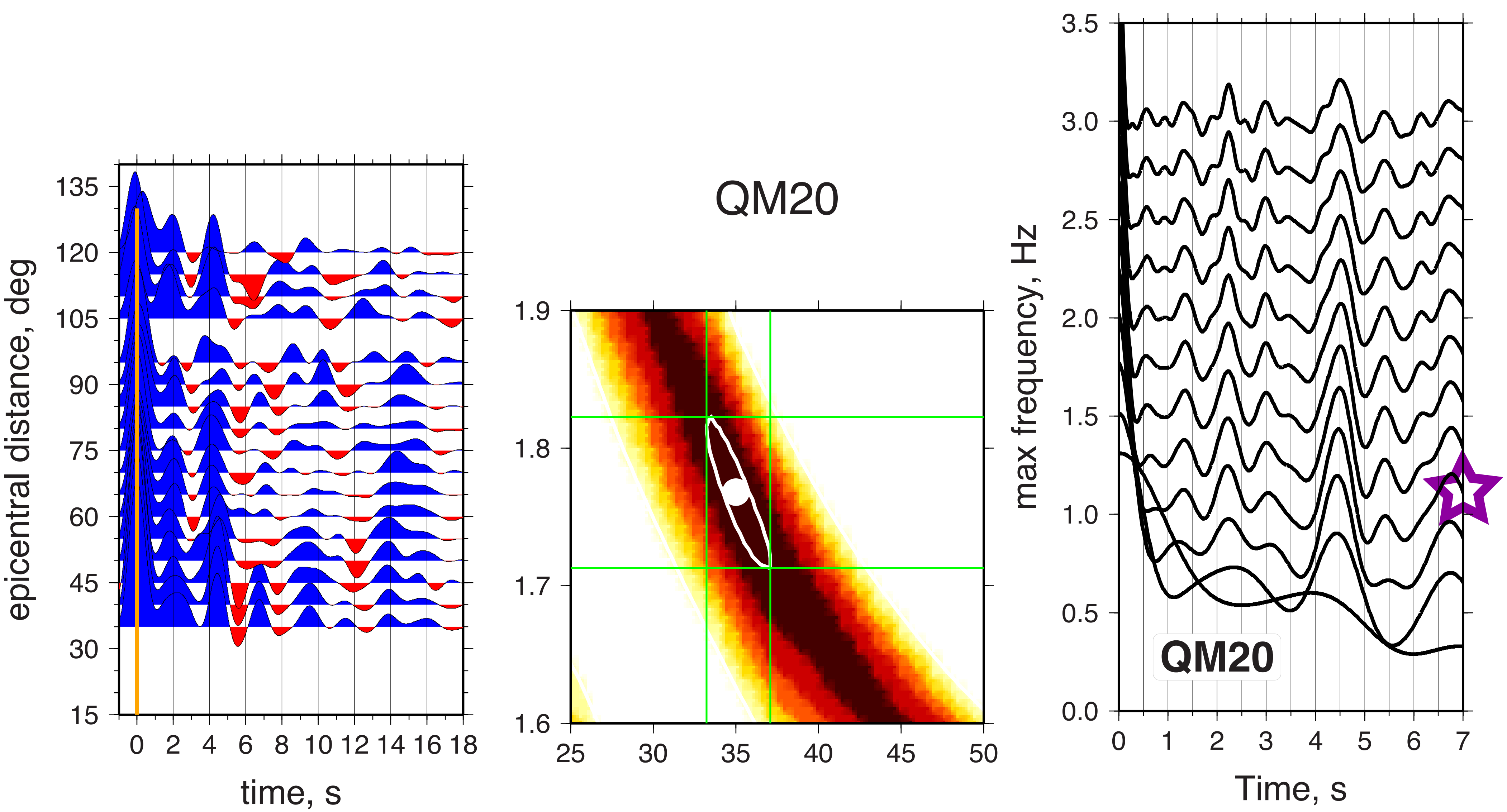
QM20
epicentral distance, deg
135
120
105
90
75
60
45
30
15
0
2
4
6
8
10
12
14
16
18
time, s
1.9
1.8
1.7
1.6
25
30
35
40
45
50
max frequency, Hz
3.5
3.0
2.5
2.0
1.5
1.0
0.5
0.0
0
1
2
3
4
5
6
7
Time, s
QM20

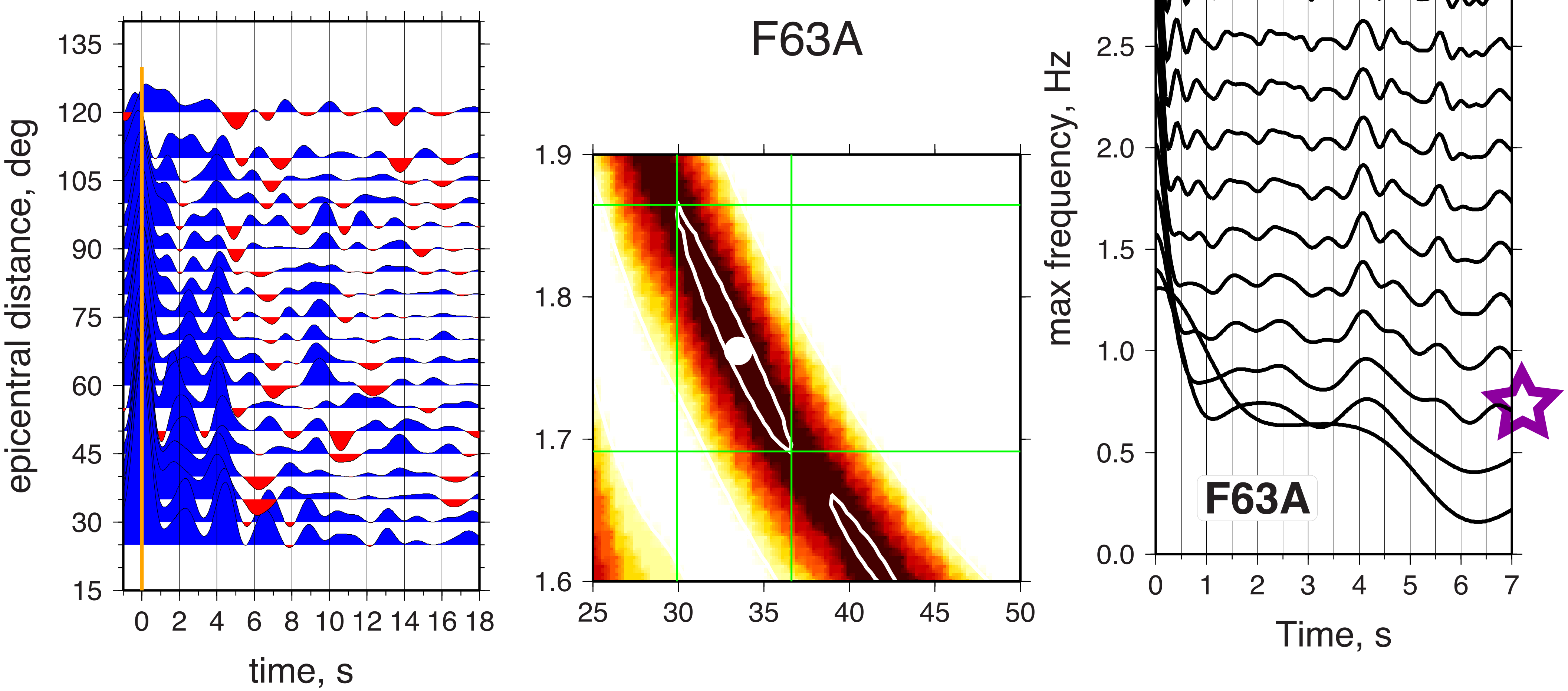

F63A
epicentral distance, deg
135
120
105
90
75
60
45
30
15
0
2
4
6
8
10
12
14
16
18
time, s
1.9
1.8
1.7
1.6
25
30
35
40
45
50
max frequency, Hz
3.5
3.0
2.5
2.0
1.5
1.0
0.5
0.0
0
1
2
3
4
5
6
7
Time, s
F63A

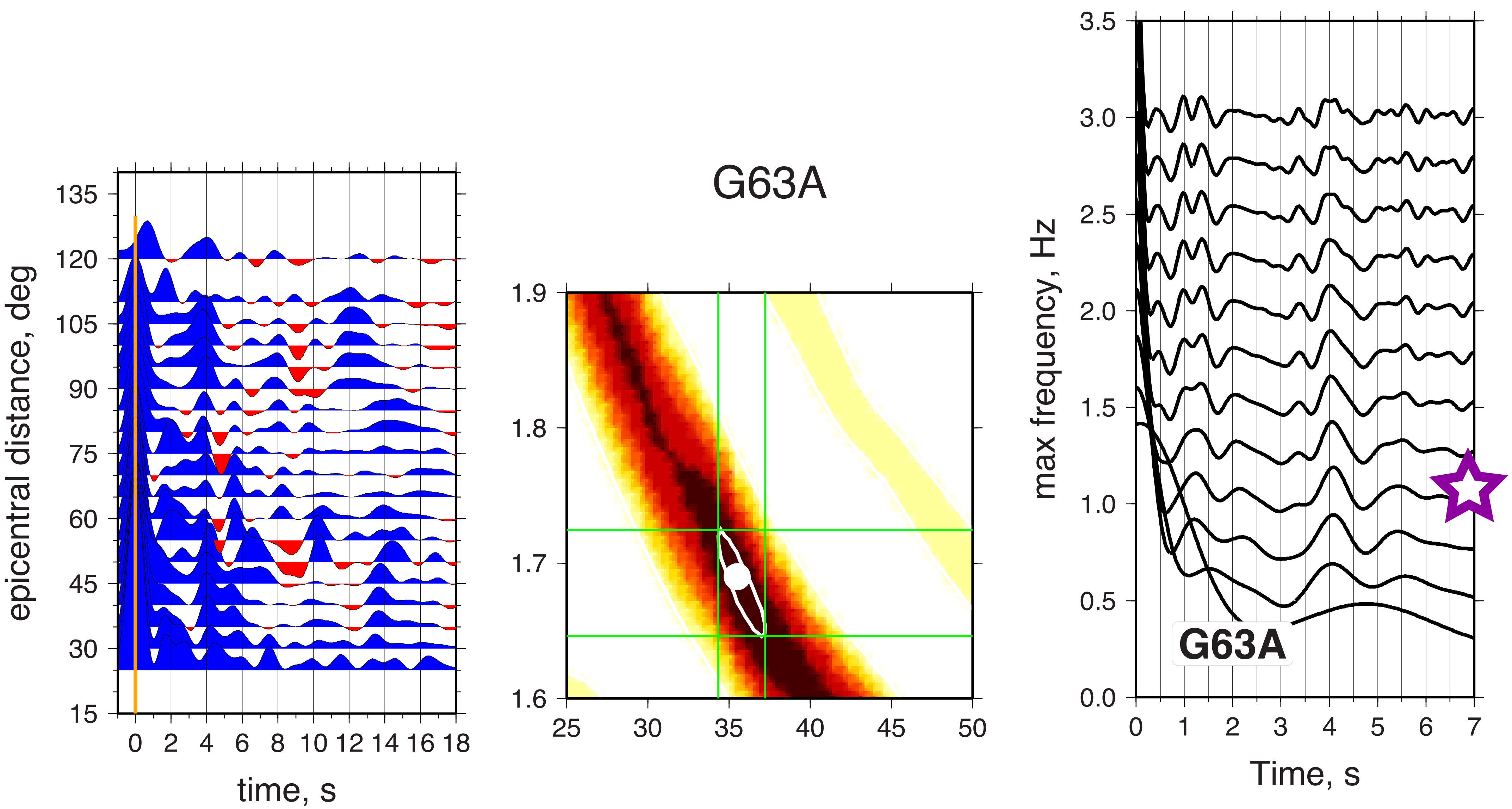
G63A
epicentral distance, deg
time, s
max frequency, Hz
Time, s
G63A

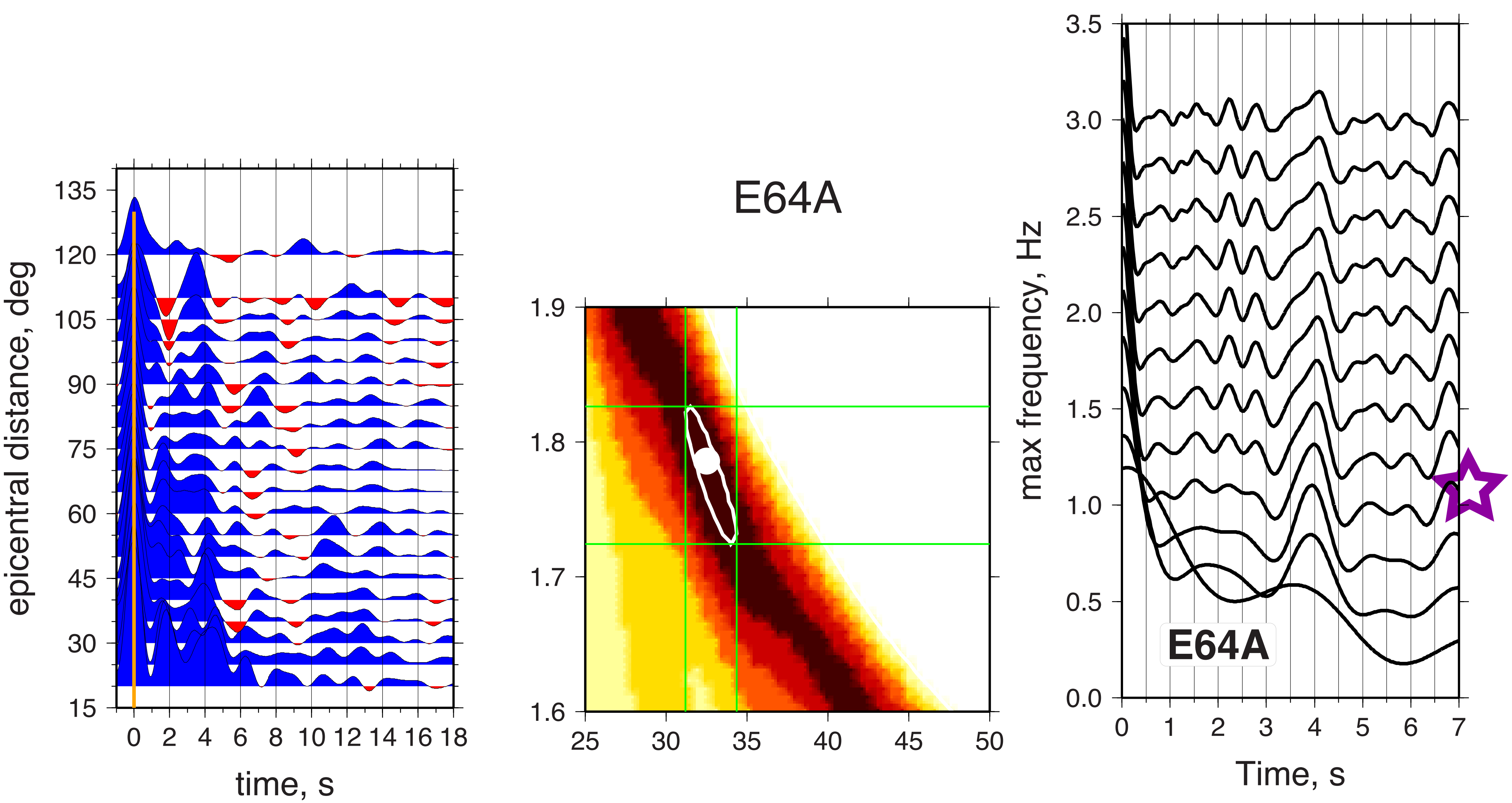

E64A
epicentral distance, deg
time, s
max frequency, Hz
Time, s
E64A

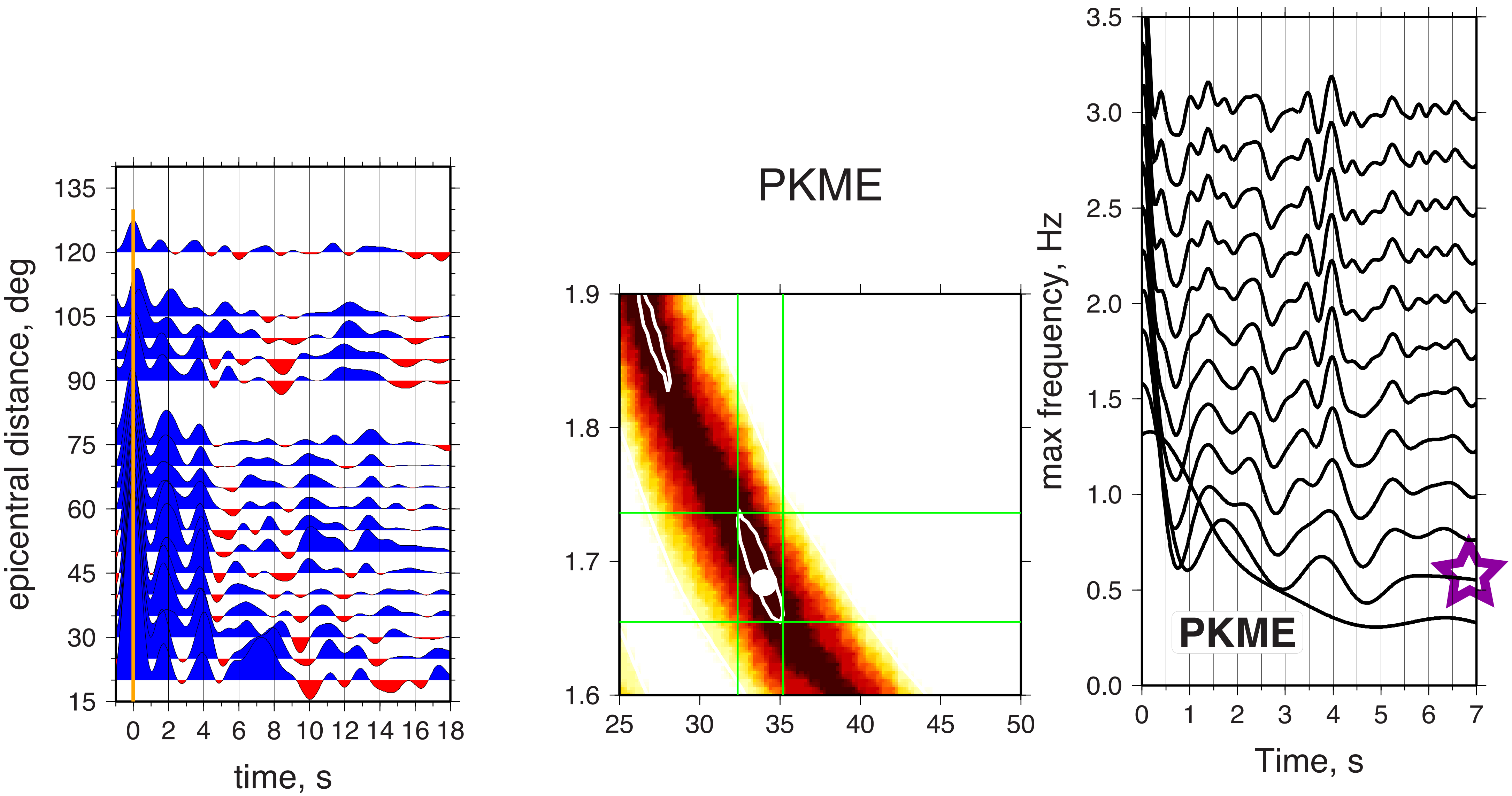

epicentral distance, deg
135
120
105
90
75
60
45
30
15
0
2
4
6
8
10
12
14
16
18
time, s
PKME
1.9
1.8
1.7
1.6
25
30
35
40
45
50
max frequency, Hz
3.5
3.0
2.5
2.0
1.5
1.0
0.5
0.0
0
1
2
3
4
5
6
7
Time, s
PKME

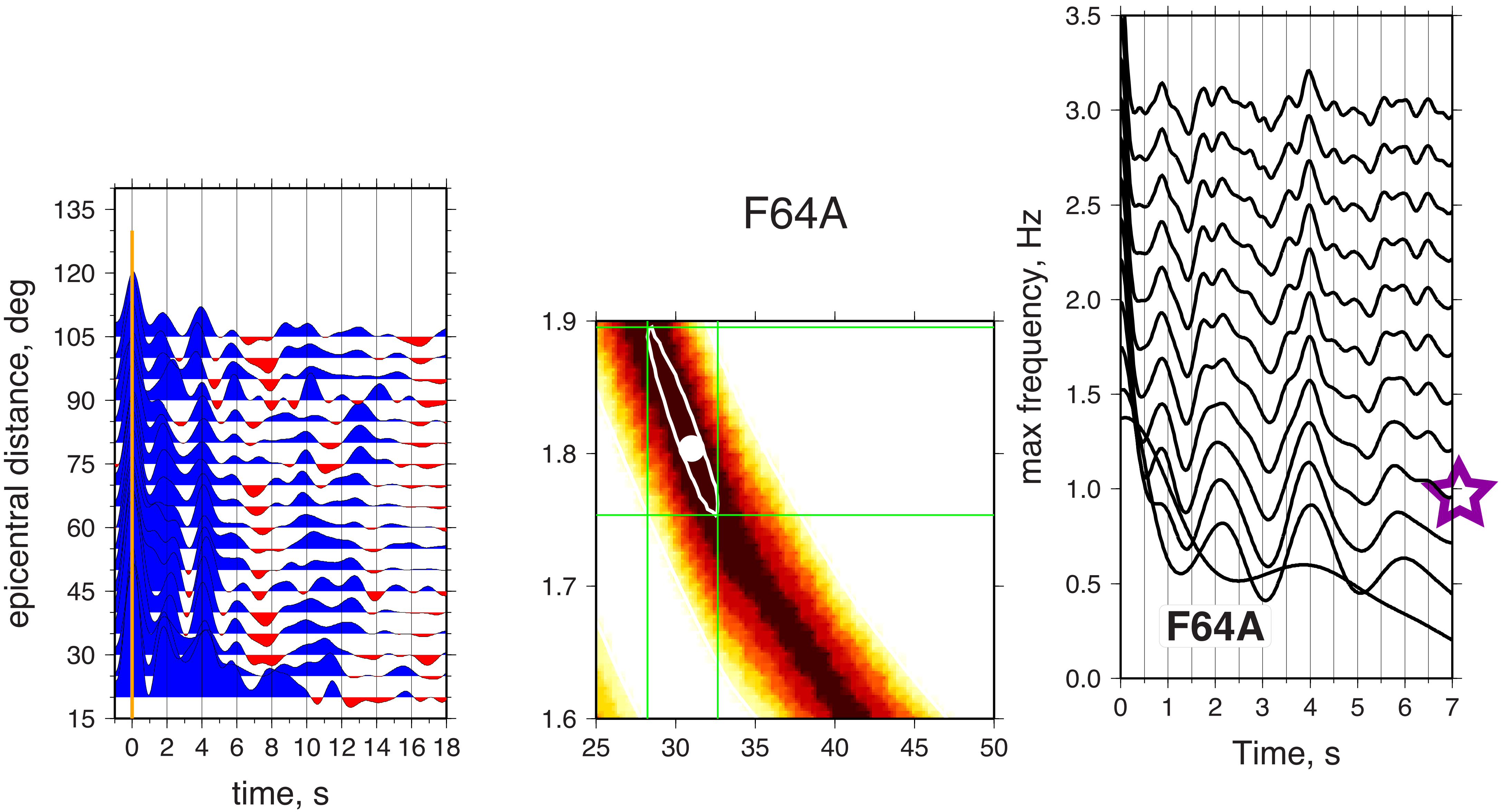
F64A
epicentral distance, deg
time, s
max frequency, Hz
Time, s
F64A

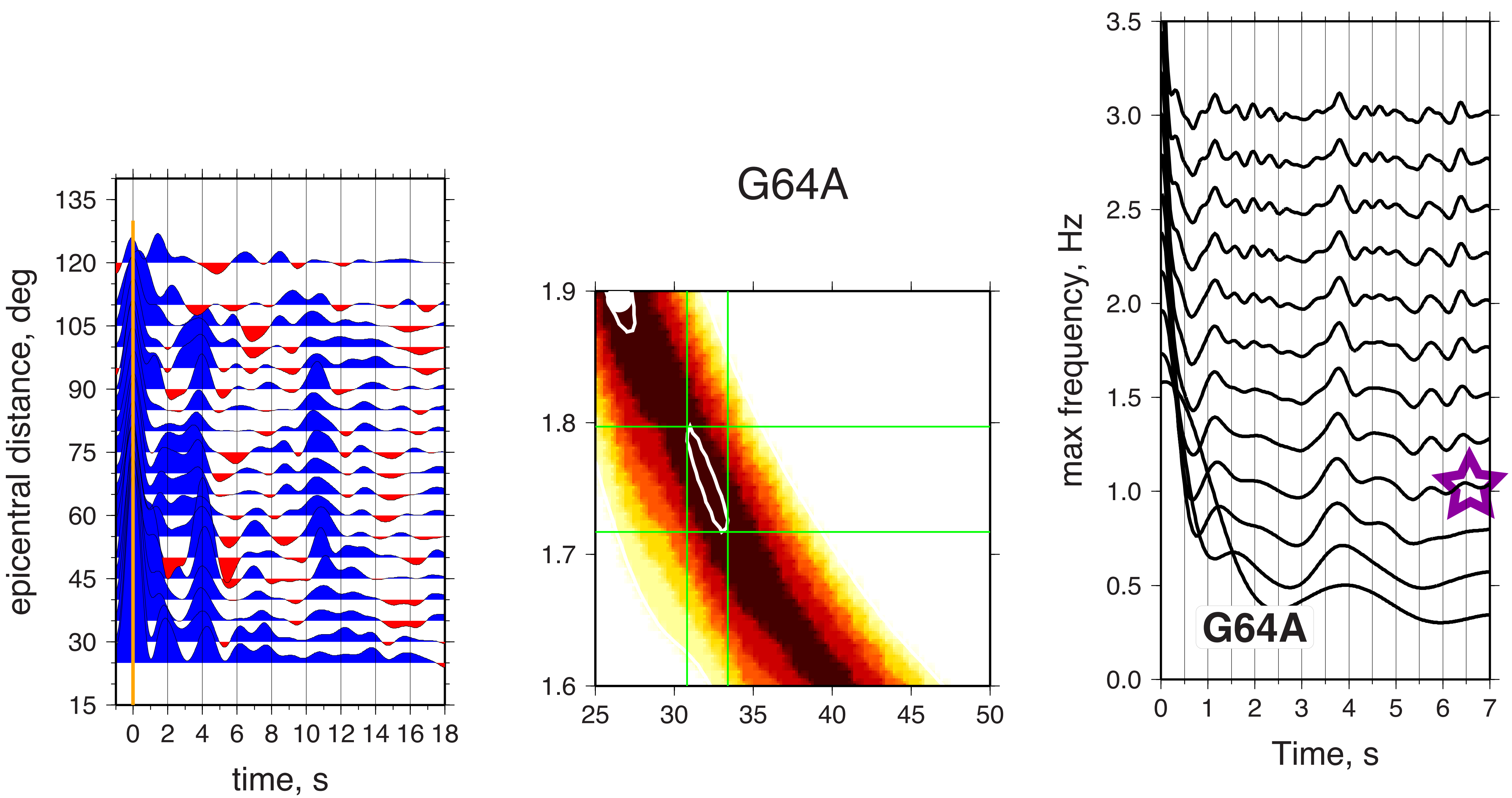

G64A
epicentral distance, deg
135
120
105
90
75
60
45
30
15
0
2
4
6
8
10
12
14
16
18
time, s
1.9
1.8
1.7
1.6
25
30
35
40
45
50
max frequency, Hz
3.5
3.0
2.5
2.0
1.5
1.0
0.5
0.0
1
3
5
7
Time, s
G64A

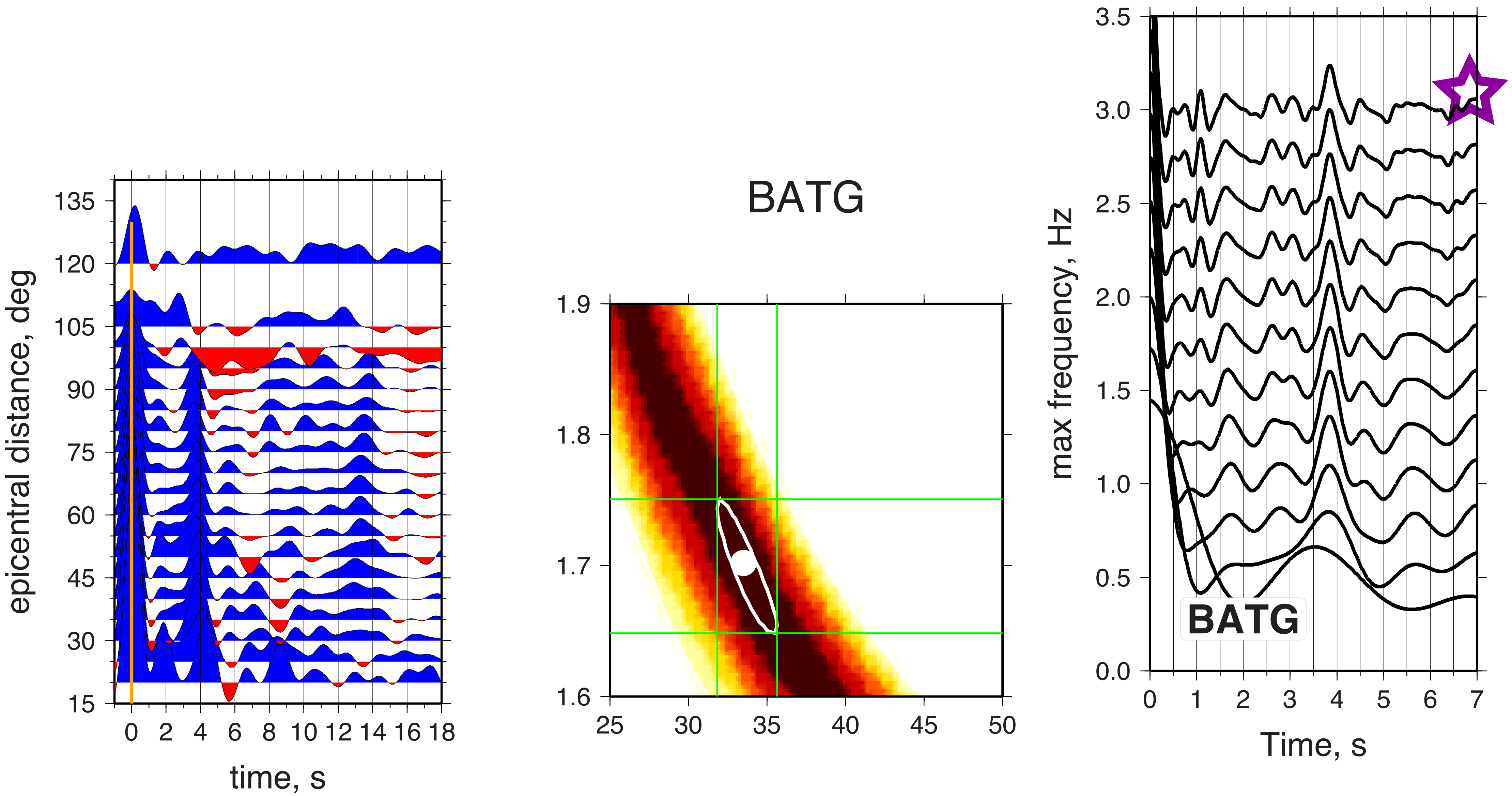

135
120
105
90
75
60
45
30
15
epicentral distance, deg
0 2 4 6 8 10 12 14 16 18
time, s
BATG
1.9
1.8
1.7
1.6
25 30 35 40 45 50
3.5
3.0
2.5
2.0
1.5
1.0
0.5
0.0
max frequency, Hz
BATG
0 1 2 3 4 5 6 7
Time, s

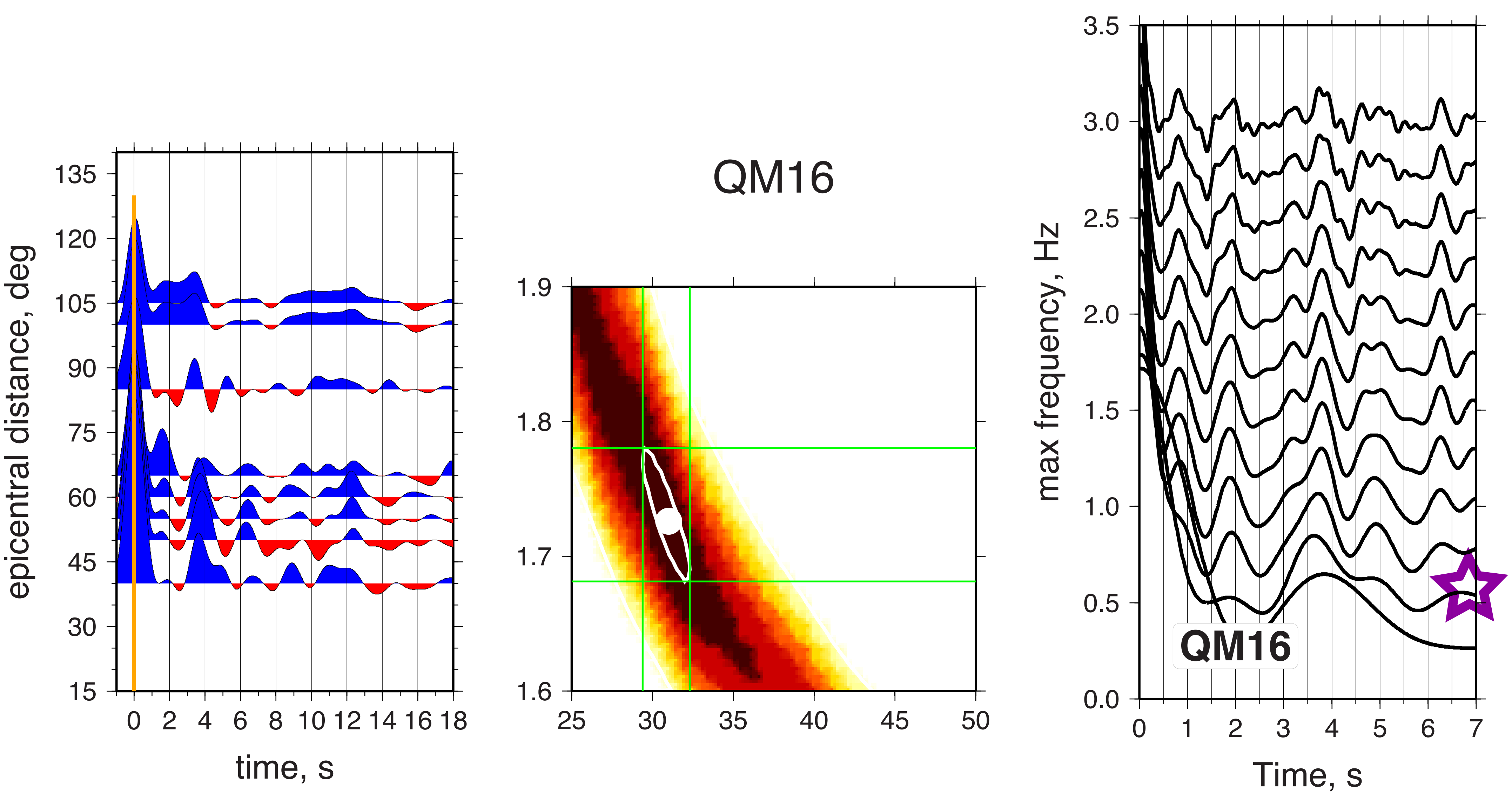
QM16
epicentral distance, deg
135
120
105
90
75
60
45
30
15
0 2 4 6 8 10 12 14 16 18
time, s
1.9
1.8
1.7
1.6
25 30 35 40 45 50
max frequency, Hz
3.5
3.0
2.5
2.0
1.5
1.0
0.5
0.0
0 1 2 3 4 5 6 7
Time, s
QM16

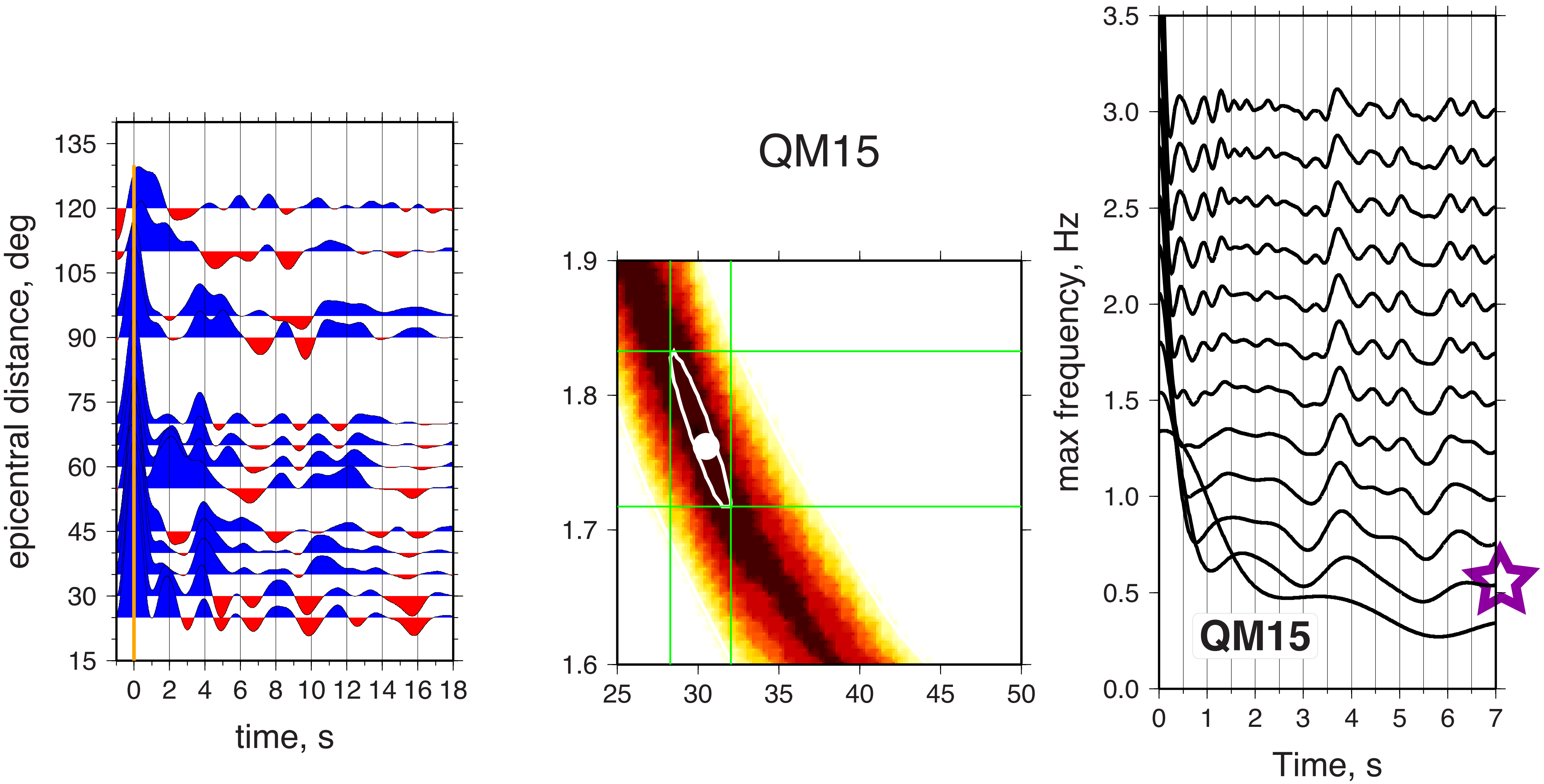

QM15
epicentral distance, deg
time, s
max frequency, Hz
Time, s
QM15

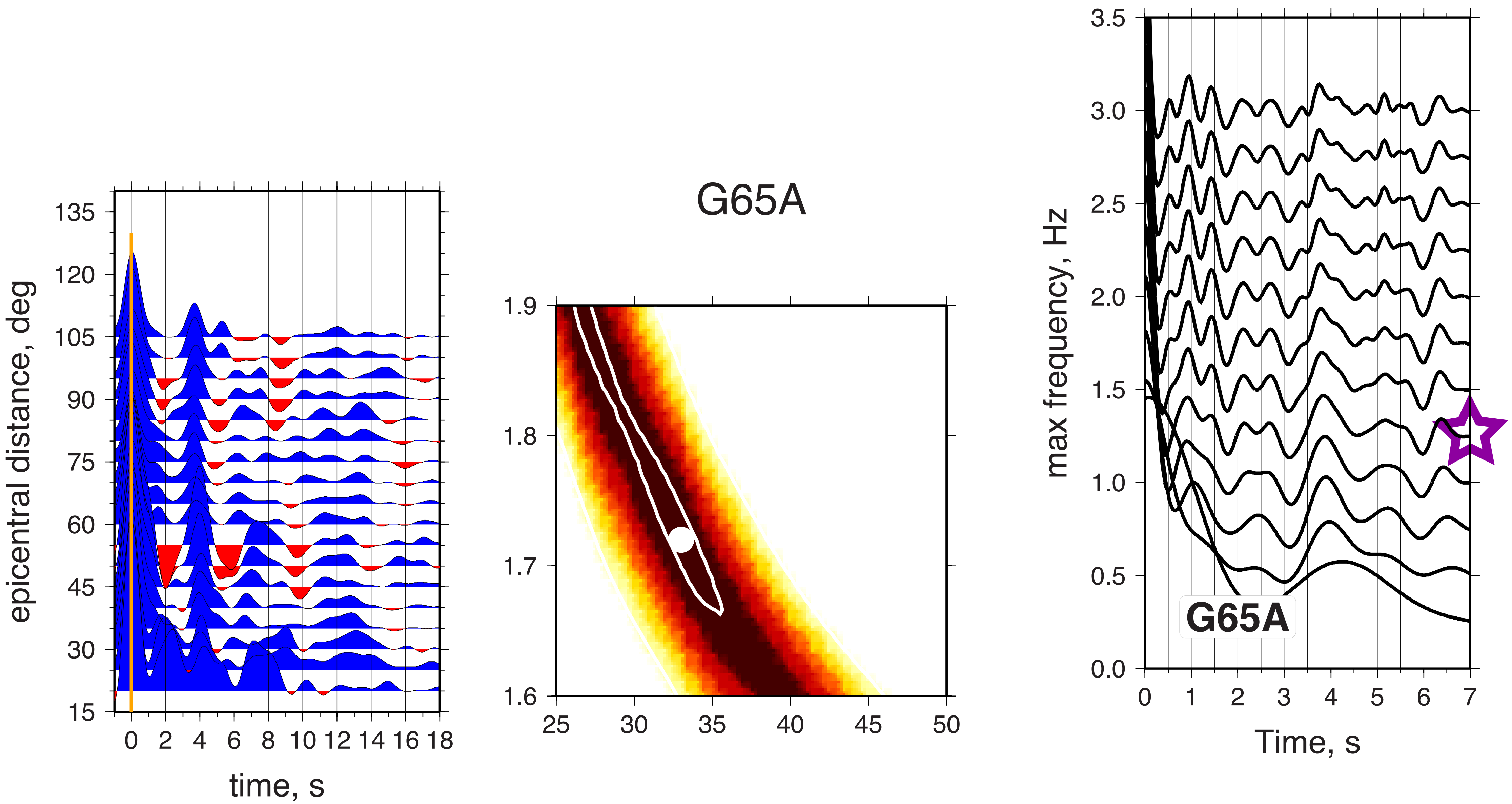

G65A
epicentral distance, deg
time, s
max frequency, Hz
Time, s
G65A

QM10_1_epi_0-360_5bins.rgrid scale

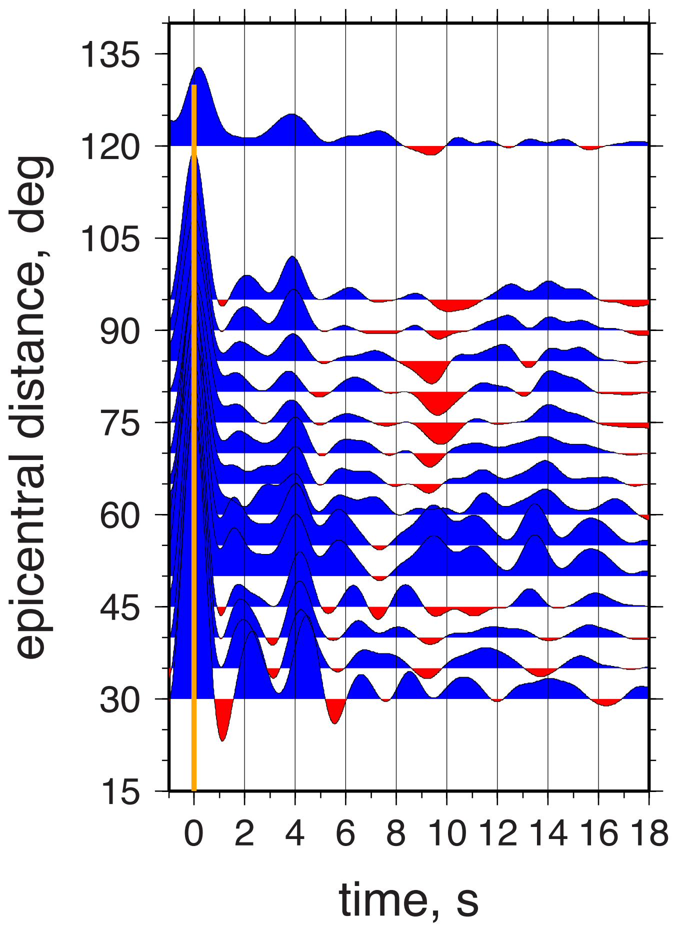

QM10

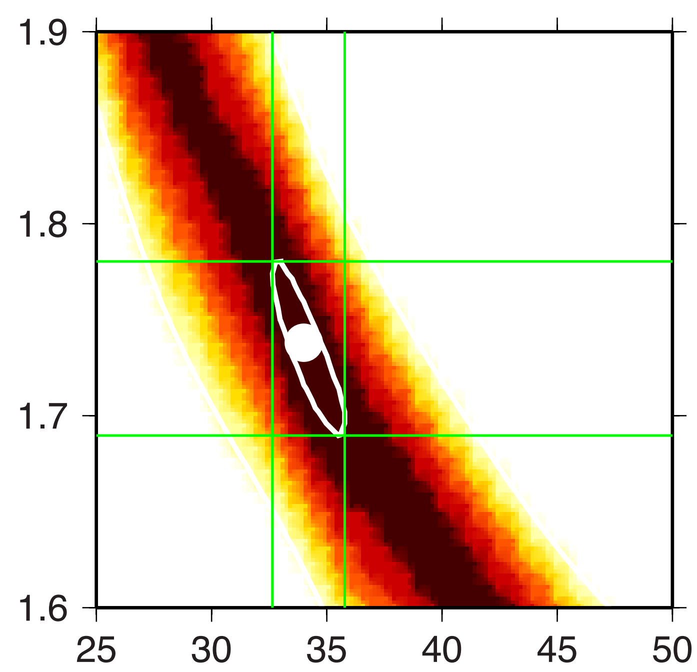

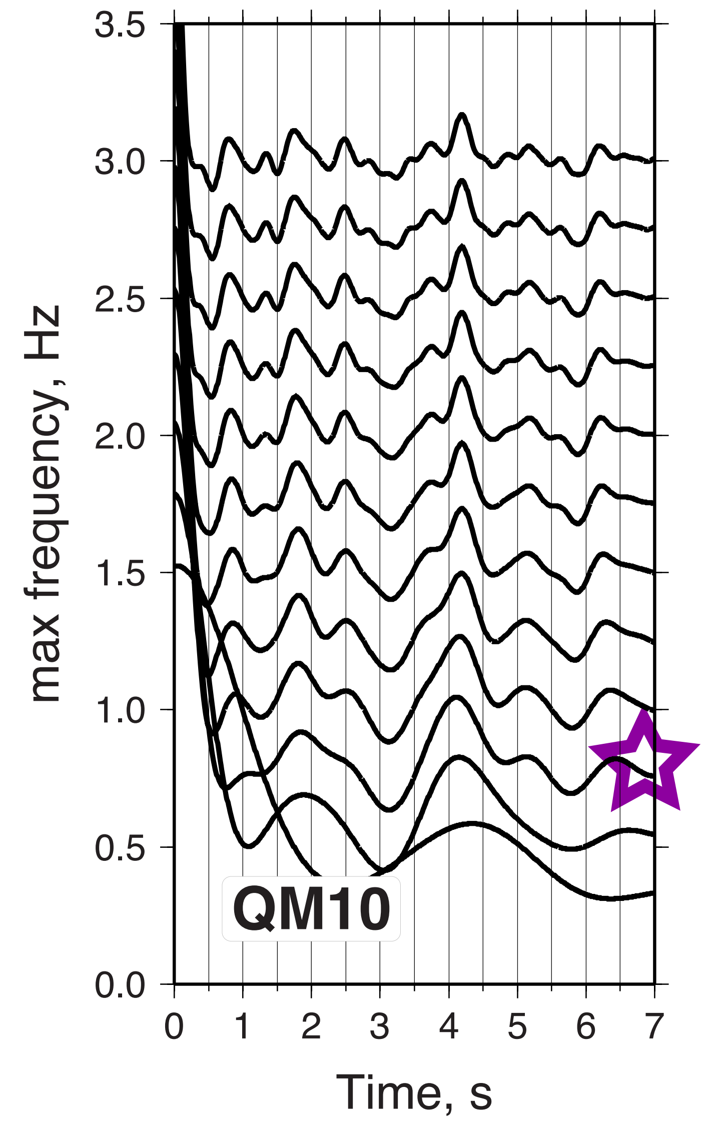

GBN_1_epi_0-360_5bins.rgrid scale

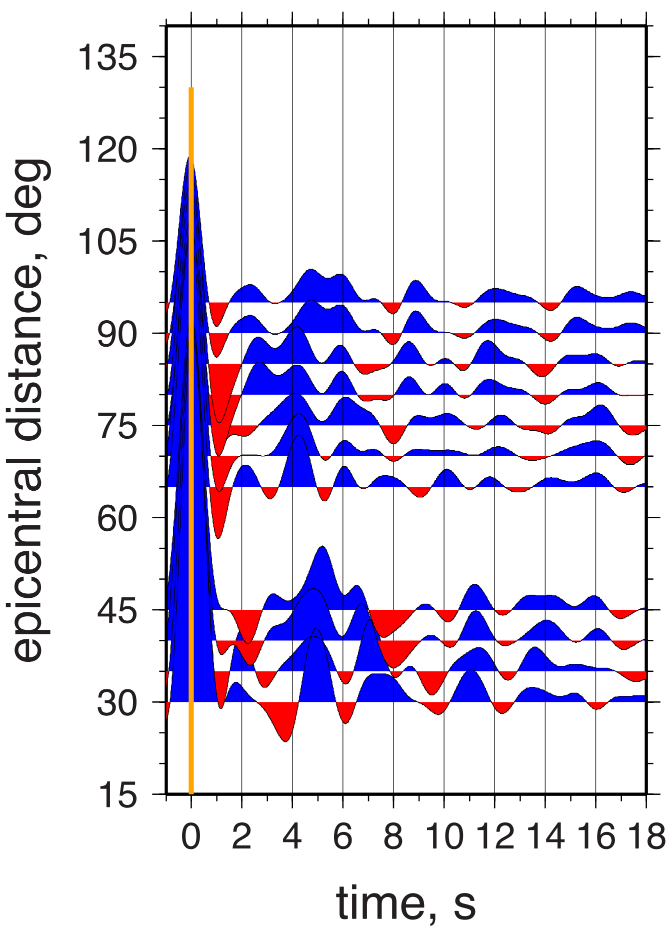

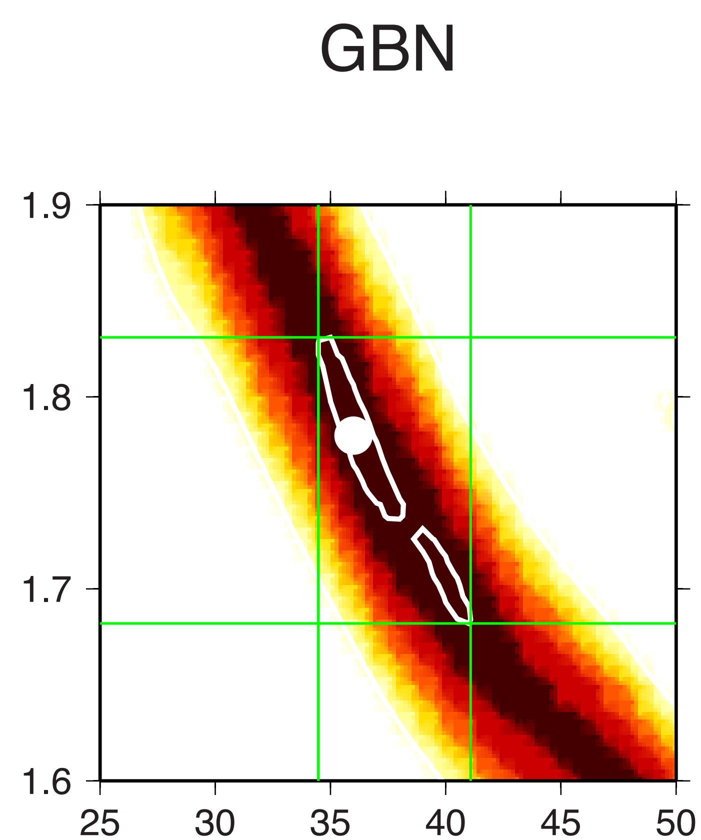

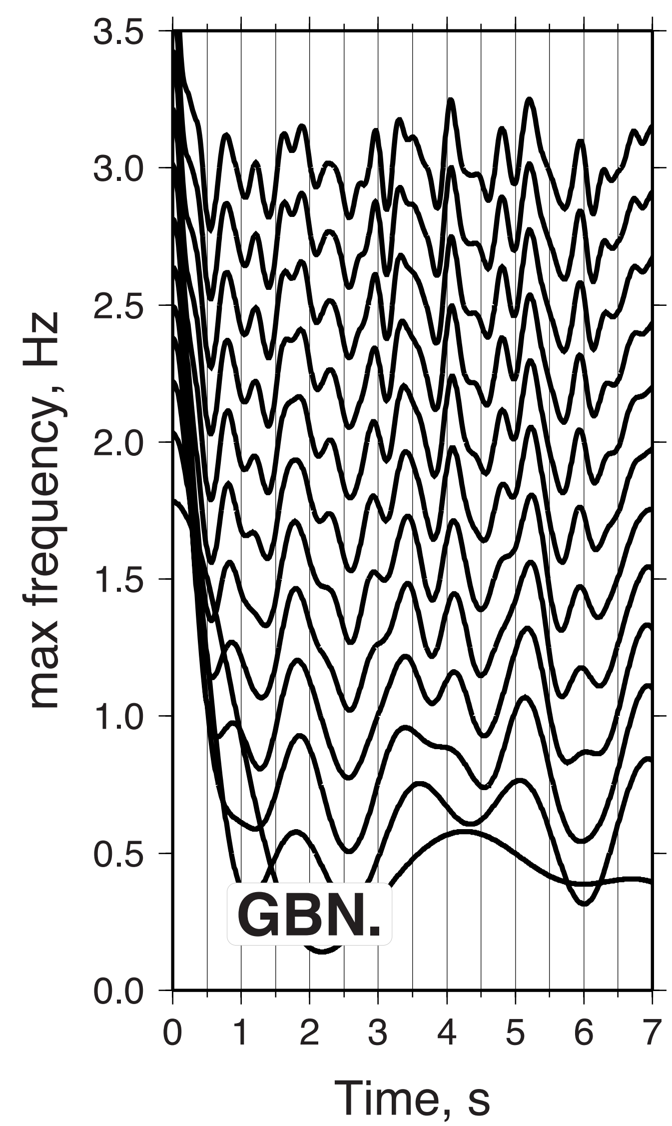

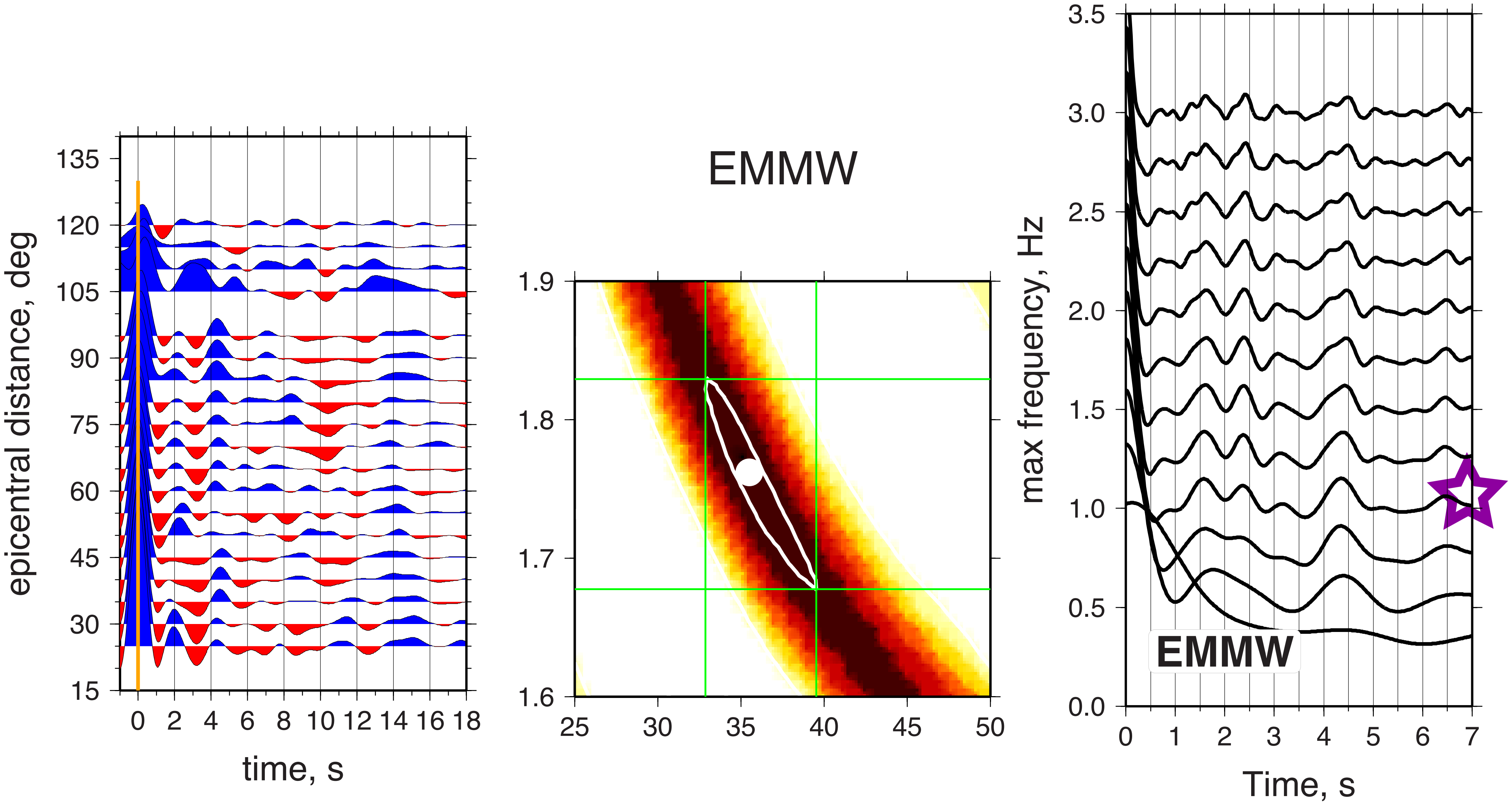

EMMW
epicentral distance, deg
135
120
105
90
75
60
45
30
15
0 2 4 6 8 10 12 14 16 18
time, s
1.9
1.8
1.7
1.6
25 30 35 40 45 50
max frequency, Hz
3.5
3.0
2.5
2.0
1.5
1.0
0.5
0.0
0 1 2 3 4 5 6 7
Time, s
EMMW

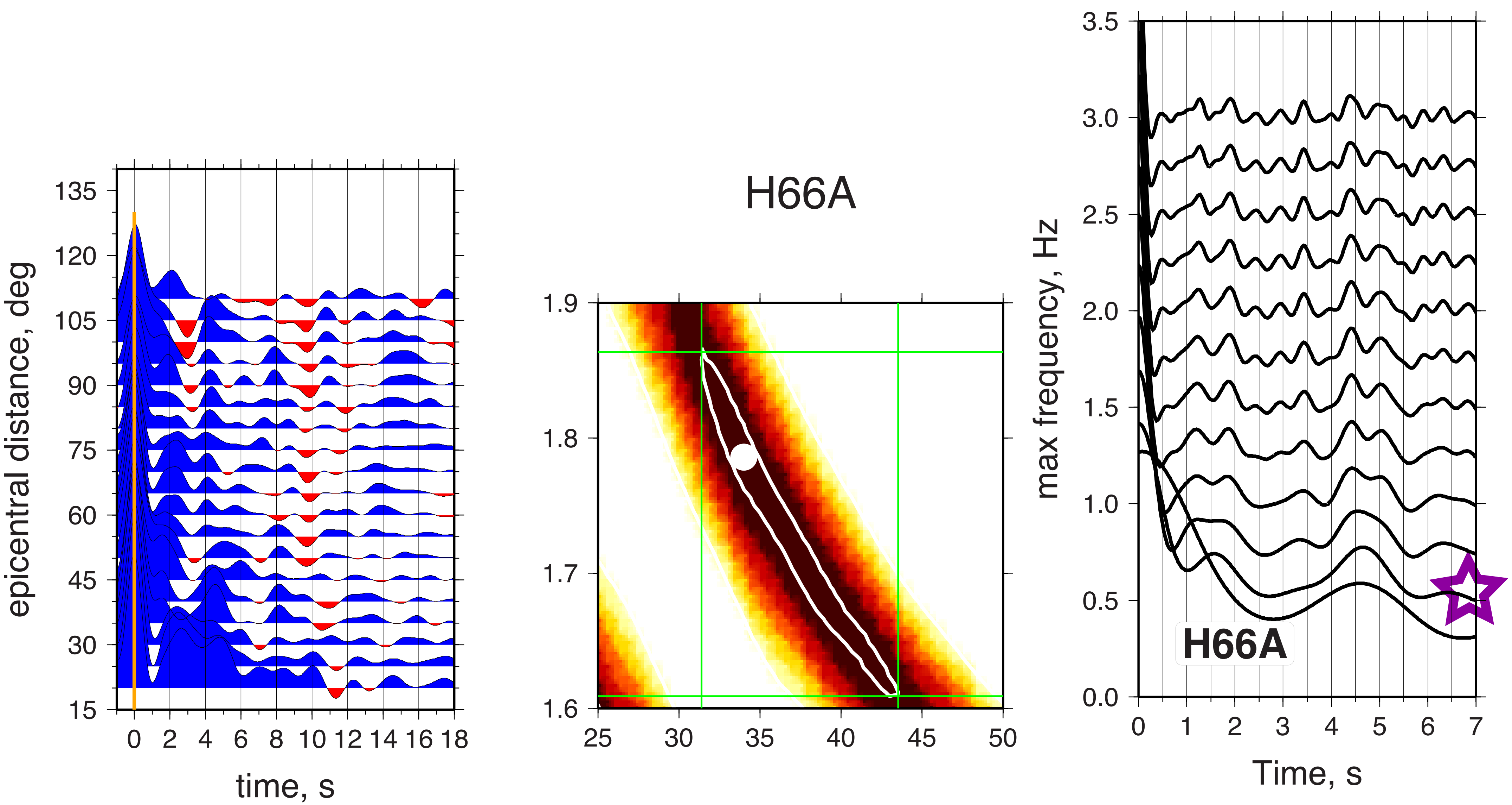

epicentral distance, deg
135
120
105
90
75
60
45
30
15
0 2 4 6 8 10 12 14 16 18
time, s
H66A
1.9
1.8
1.7
1.6
25 30 35 40 45 50
max frequency, Hz
3.5
3.0
2.5
2.0
1.5
1.0
0.5
0.0
0 1 2 3 4 5 6 7
Time, s
H66A

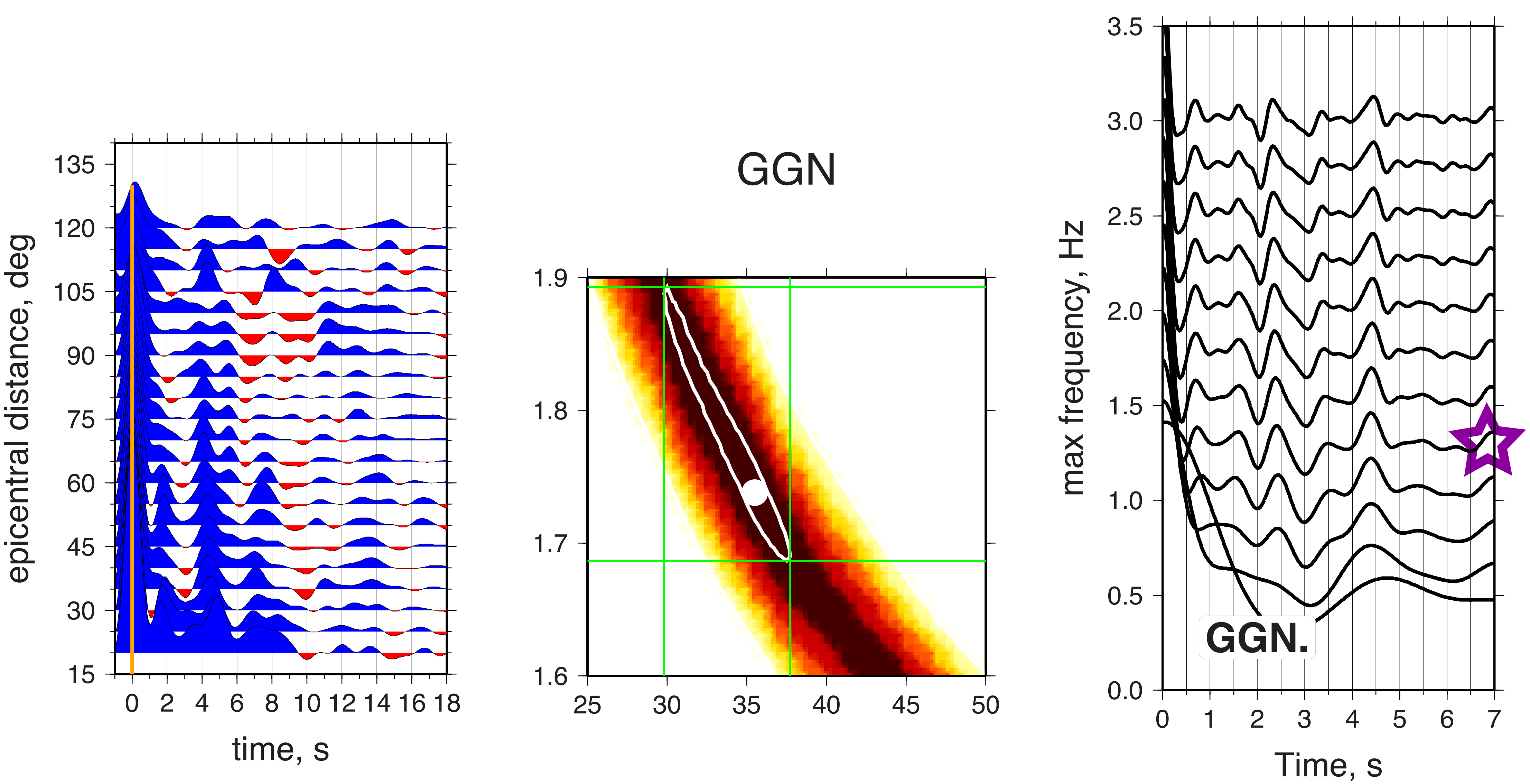
GGN
epicentral distance, deg
135
120
105
90
75
60
45
30
15
0 2 4 6 8 10 12 14 16 18
time, s
1.9
1.8
1.7
1.6
25 30 35 40 45 50
max frequency, Hz
3.5
3.0
2.5
2.0
1.5
1.0
0.5
0.0
0 1 2 3 4 5 6 7
Time, s
GGN.

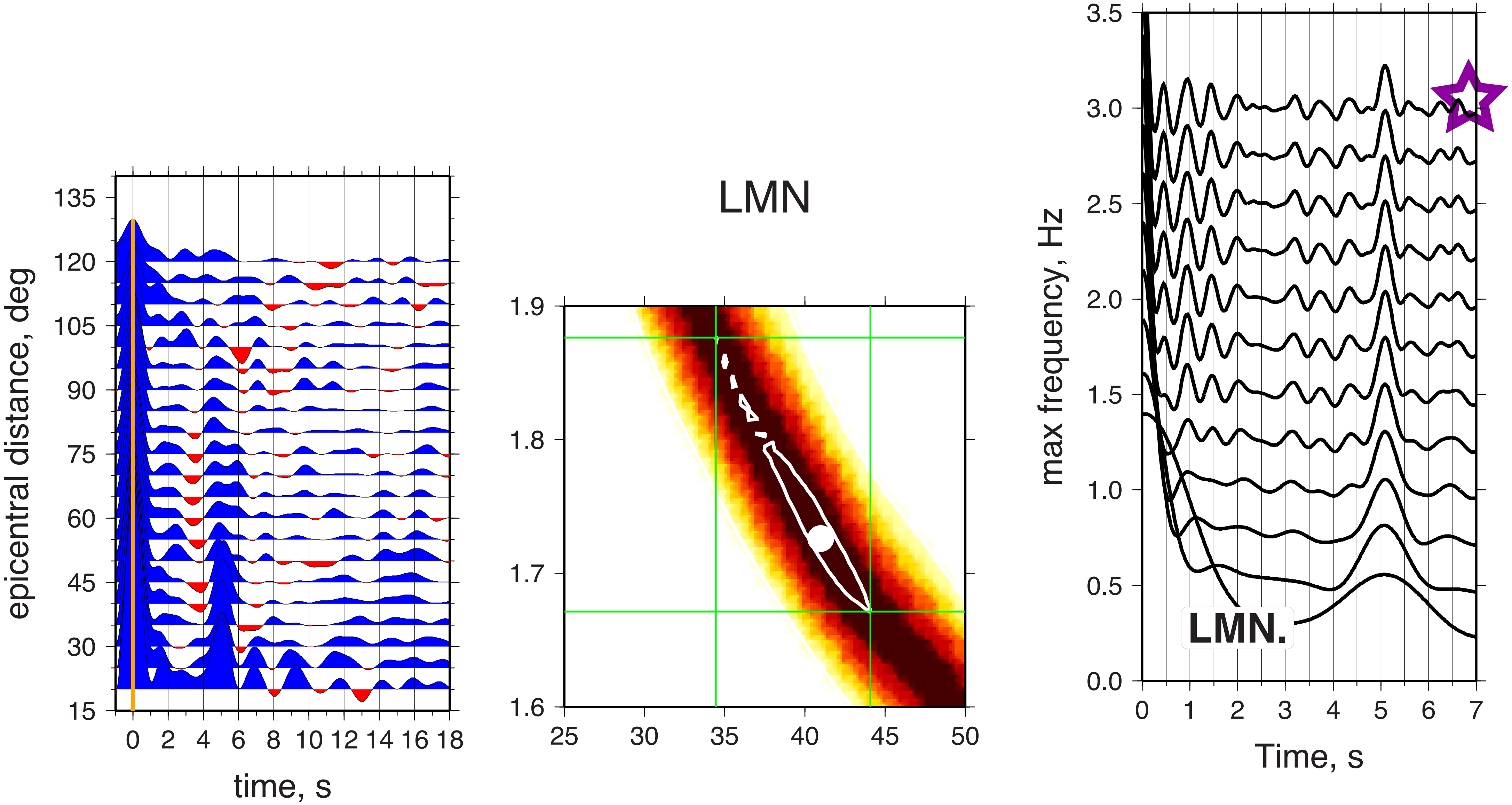
LMN
epicentral distance, deg
135
120
105
90
75
60
45
30
15
0 2 4 6 8 10 12 14 16 18
time, s
1.9
1.8
1.7
1.6
25 30 35 40 45 50
max frequency, Hz
3.5
3.0
2.5
2.0
1.5
1.0
0.5
0.0
0 1 2 3 4 5 6 7
Time, s
LMN.